TAMPEREEN TEKNILLINEN YLIOPISTO
TAMPERE UNIVERSITY OF TECHNOLOGY

Timo Vuorela

Technologies for Wearable and Portable Physiological Measurement Devices

Julkaisu 962 • Publication 962

Tampere 2011

Tampereen teknillinen yliopisto. Julkaisu 962
Tampere University of Technology. Publication 962

Timo Vuorela

Technologies for Wearable and Portable Physiological Measurement Devices

Thesis for the degree of Doctor of Science in Technology to be presented with due permission for public examination and criticism in Tietotalo Building, Auditorium TB109, at Tampere University of Technology, on the 13th of May 2011, at 12 noon.

Tampereen teknillinen yliopisto - Tampere University of Technology
Tampere 2011

ISBN 978-952-15-2560-5 (printed)
ISBN 978-952-15-2669-5 (PDF)
ISSN 1459-2045

Abstract

The study investigates technologies for portable and wearable physiological measurement devices. Physiological measurement is already an important field of research and is likely to become even more so in the future. An aging population in much of the industrialised world has led to increases in age- and lifestyle-related diseases. This increase places a greater burden on healthcare provision and healthcare costs for society a whole.

One way to offset this trend is developing and improving health monitoring applications. The benefits of such telemedicine and telemonitoring systems include earlier patient discharge from hospital since monitoring of recovery can be performed remotely via a data connection. Telemonitoring and alert applications also help the elderly to remain independent longer in the home environment and postpone the need for institutional care.

The study examines the technologies required in the implementation of portable and wearable physiological measurement devices. In such devices, as in all portable and mobile measurement devices, energy consumption is a critical design factor in ensuring the feasibility of the entire implementation. Here a novel method is presented for optimizing energy consumption caused by software running in a microcontroller or in a microprocessor. It has been shown that in low power 8-bit microcontrollers, savings of a few percent in energy consumption can be achieved by optimizing the software at the level of assembler instruction. The energy storage technologies utilized in current portable devices are investigated as well as methods for scavenging energy from external sources, such as the user or the environment.

A measurement device needs a communication link through which it can transfer the measurement results to a data terminal device such as a computer and a memory to store the results. An effective approach for a data link is to utilize wireless methods since wires readily impede the user during normal daily activity. The study presents the properties of the most common radio protocols utilized today. It also tests four different radio circuits and implements a radio link for a portable physiological measurement device with an ANT-protocol compliant radio. Various types of memory for measurement data storage are examined along with their suitability for the devices in question.

An important element in a physiological measurement device is an analogue front end that modifies the measured analogue signal to make it suitable for the analogue to digital converter. The signal can be modified in various ways such as filtering, amplification, and offset changes. The structure of the front-end block depends on the measurement signal and the interface of the analogue to digital converter. To understand the requirements of this front-end, some background is presented to the physiological signals that were measured with the devices implemented during the research. These signals include temperature, acceleration, body posture, bioimpedance, and electrocardiogram.

When body-generated electrical signals are measured, an interface such as an electrode is needed between the body and the electronics. The properties and placement of such interfaces are also briefly discussed.

Several prototypes are implemented to demonstrate the practicability of portable and wearable physiological measurement devices. These include two smart clothing prototypes, one for measuring and adjusting the user's thermal comfort and the other for measuring body impedance that can be used for determining water levels in the body. The study also describes the development of a device to measure the user's electrocardiogram, dynamic changes in bioimpedance, and acceleration on three axes.

Preface and Acknowledgements

This study was carried out from 2001 to 2011 in the Personal Electronics Group at the Department of Electronics, Tampere University of Technology, Tampere, Finland. I would like to thank the Department of Electronics for the excellent facilities.

I wish to thank my supervisor, Jukka Vanhala, for his support and encouragement. I am grateful for having had the opportunity to work in such a fascinating research field, especially the area of measuring physiological signals and physiological parameters.

Thanks are also due to the members of our textile and portable electronics team and colleagues in the Personal Electronics research group. I have greatly enjoyed your company and stimulating conversation, especially during the coffee breaks in “älkkäri”. I also wish to thank all my colleagues at the Department of Electronics, the Department of Automation Science and Engineering and the Department of Biomedical Engineering. You have provided an inspiring and creative environment for this work.

I am indebted to the reviewers, Fernando Seoane Martinez, PhD and Professor Petri Pulli for their constructive comments on the manuscript. I also wish to thank Alan Thompson, MPhil for the language revision.

This thesis was financially supported by the Department of Electronics, Graduate School in Electronics, Telecommunication and Automation (GETA), the Finnish Funding Agency for Technology and Innovation (Tekes), The European Space Agency (ESA), Academy of Finland, and Tamperelaisen Tutkimuksen Tukisäätiö. Their support is appreciatively acknowledged.

I also wish to express my gratitude to my family and friends for all their support throughout this research. I owe a special debt of gratitude to my uncle, who first introduced me to the world of electricity and electronics. Finally, my warmest thanks to my wife, Tuula, and our lovely daughter, Iida, for their love, encouragement, and support during all these years.

Tampere, 6.4.2011

Timo Vuorela

Contents

List of Publications

This thesis consists of an introduction section and nine publications [P1- P9]. The publications are listed below.

[P1] Timo Vuorela, Ville-Pekka Seppä, Jukka Vanhala and Jari Hyttinen. Wireless Measurement System for Bioimpedance and ECG. Proceedings of the 13th International Conference on Electrical Bioimpedance and 8th Conference on Electrical Impedance Tomography, IFMBE, August 29 – September 9, 2007, Graz, Austria, Vol. 17, pp. 248-251.

[P2] Timo Vuorela, Ville-Pekka Seppä, Jukka Vanhala, and Jari Hyttinen. Two portable long-term measurement devices for ECG and bioimpedance. Proceedings of the 2nd International Conference on Pervasive Computing Technologies for Healthcare 2008, Pervasive Health 2008, January 30 – February 1, 2008, Tampere, Finland, 4 pages.

[P3] Timo Vuorela, Jaana Hännikäinen, and Jukka Vanhala. Plaster like Physiological Signal Recorder – Design Process, Lessons Learned. Proceedings of the Ambience 08 Smart Textiles – Technology and Design. June 2 – 3, 2008, Borås, Sweden, pp. 89-96.

[P4] Timo Vuorela, Ville-Pekka Seppä, Jukka Vanhala, and Jari Hyttinen, Design and Implementation of a Portable Long-Term Physiological Signal Recorder, IEEE Transactions on Information Technology in Biomedicine, vol.14, no.3, pp.718-725, May 2010

[P5] Timo Vuorela, Kari Kukkonen, Jaana Rantanen, Tiina Järvinen, & Jukka Vanhala, Bioimpedance Measurement System for Smart Clothing. Proceedings of the Seventh International Symposium on Wearable Computers ISWC 2003, 21-23 October, White Plains, New York, USA, pp. 98 – 107.

[P6] Timo Vuorela, Jaana Hännikäinen, Katja Vähäkuopus, and Jukka Vanhala. Textile Electrode Usage in a Bioimpedance Measurement. Proceedings of the first international scientific conference on Intelligent Ambience and Well-Being, Ambience'05. ISBN: 952-15-1429-9. Tampere, Finland, September 19(Mon) – 20(Tue), 2005, pp. 147 – 154.

[P7] Timo Vuorela, Kimmo Surakka, Jukka Vanhala, and Hannu-Matti Järvinen. Instruction Level Energy Measurement of General-purpose Microprocessor: A Case Study AT90S8515 and Atmega8515. Proceedings of the sixth International Conference on Machine Automation, ICMA2006, June 7-8, 2006, Seinäjoki, Finland, 9 pages.

[P8] Kimmo Surakka, Tommi Mikkonen, Hannu-Matti Järvinen, Timo Vuorela and Jukka Vanhala, Towards Compiler Backend Optimization for Low Energy Consumption at Instruction Level, Proceedings of the Estonian Academy of Sciences, Engineering, Special issue on Programming Languages and Software Tools, 11/4 December 2005, pp. 347-357.

[P9] Timo Vuorela, Kari Kukkonen, Jaana Rantanen, Tero Alho, Tiina Järvinen, Jukka Vanhala, 2003. RF Data Link for a Smart Clothing Application. Adjunct Workshop Proceedings of 3rd International Workshop on Smart Appliances and Wearable Computing. Held at IEEE 23rd International Conference on Distributed Computing Systems, May 19 – 22, 2003, Providence Rhode Island, USA, pp. 7 – 12.

List of Abbreviations

μSD	Micro Secure Digital
μSDHC	Micro Secure Digital High Capacity
ADC	Analog to Digital Converter
Ag/AgCl	Silver / Silver Chloride
ALU	Arithmetic Logic Unit
ANT	A proprietary wireless protocolof Dynastream Innovations
BCA	Body Composition Analysis
BCM	Body Cell Mass
BF	Body Fat
BIS	Bioimpedance Spectroscopy
BIVA	Bioelectrical Impedance Vector Analysis
BT-LET	Bluetooth Low Energy Technology
CEPT	European Conference of Postal and Telecommunication Administration
CFR	Code of Federal Regulations
CNC	Computer Numerical Control
CMOS	Complementary Metal Oxide Semiconductor
CMRR	Common Mode Rejection Ratio
DC	Direct Current
DDS	Direct Digital Synthesis
DMFC	Direct Methanol Fuel Cell
DPM	Dynamic Power Management
DSP	Digital Signal Processor
DRAM	Dynamic Random Access Memory
DSSS	Direct Sequence Spread Spectrum
DUT	Device Under Test
DVS	Dynamic Voltage Scaling
EBI	Electrical Bioimpedance
ECC	Electronic Communication Committee
ECF	Extra Cellular Fluids
ECG	Electrocardiograph
ECM	Extra Cellular Mass
ECO	European Communications Office
ECW	Extra Cellular Water
EDR	Enhanced Data Rate

EEG	Electroencephalogram
EEPROM	Electric Eraseable Programmable Read Only Memory
E^2PROM	Electric Eraseable Programmable Read Only Memory
EN	European Standard
ETSI	European Telecommunications Standards Institute
FAT	File Allocation Table
FCC	Federal Communication Commission
FF	Foot to Foot
FFM	Fat Free Mass
FHSS	Frequency Hopping Spread Spectrum
FICORA	Finnish Communications Regulatory Authority
HF	Hand to Foot
HH	Hand to Hand
HRV	Heart Rate Variability
IA	Instrumentation Amplifier
IC	Integrated Circuit
ICF	Intra Cellular Fluids
ICG	Impedance Cardiography
ICW	Intra Cellular Water
IEEE	Institute of Electrical and Electronics Engineers
IO	Input Output
ISM	Industrial Scientific and Medical
LBM	Lean Body Mass
Li-Ion	Lithium Ion
LiPo	Lithium Polymer
MOSFET	Metal-Oxide Semiconductor Field Effect Transistor
MF-BIA	Multi-Frequency Bioimpedance Analysis
NiCd	Nickel Cadmium
NiMH	Nickel-Metal Hydride
NVM	Non Volatile Memory
OS	Operating System
PC	Personal Computer
PCB	Printed Circuit Board
PDA	Personal Digital Assistant
PE	Processing Element
PWV	Pulse Wave Velocity
RAM	Random Access Memory
RF	Radio Frequency
RFID	Radio Frequency Identification

RMS	Root Mean Square
RRI	RR Interval
RTC	Real Time Clock
SD	Secure Digital
SDHC	Secure Digital High Capacity
SDXC	Secure Digital Extended Capacity
SF-BIA	Single-Frequency Bioimpedance Analysis
SIG	Special Interest Group
SPI	Serial Peripheral Interface
SRAM	Static Random Access Memory
SRD	Short Range Device
TBF	Total Body Fluid
TBI	Total Body Impedance
TBW	Total Body Water
TDMA	Time Division Multiple Access
TUS	Tissue Under Study
UI	User Interface
USA	United States of America
USB	Universal Serial Bus
UWB	Ultra Wide Band
Wi-Fi	Wireless Fidelity
WLAN	Wireless Local Area Network
WMTS	Wireless Medical Telemetry Service
WSN	Wireless Sensor Network

List of Symbols

σ	Conductivity
α	Switching activity
ΔA	Change in cross sectional area
ΔG	Change in conductance
ΔV	Change in volume
η	Efficiency
λ	Wavelength of an electromagnetic wave
ρ	Resistivity
φ	Phase angle
ω	Angular frequency
$½V_{CC}$	Reference voltage, half of a supply voltage
A	Cross sectional area
a	Radius of a disk electrode
aU_F	Voltage of foot lead in Goldberg's ECG measurement setup
aU_L	Voltage of left arm lead in Goldberg's ECG measurement setup
aU_R	Voltage of right arm lead in Goldberg's ECG measurement setup
B_P	Susceptance in bioimpedance parallel model
BW	Body Weight
C	Nominal Current
$C_{1,2,3}$	Capacitors
C_L	Load capacitance
C_P	Capacitance in bioimpedance parallel model
C_S	Capacitance in bioimpedance series model
d	Propagation delay in CMOS inverter
$D_{1,2}$	Diodes
E_{base}	Instruction base energy
E_{ij}	Inter Instruction energy
$E_{overhead}$	Overhead energy of an instruction pair
E_{SW}	Switching energy
f	Frequency
g	Earth's gravity
G	Conductance
G(ω)	Conductance in parallel bioimpedance model
$G_{½}$	Conductance of a sphere electrode

GND	Ground potential
Ht	Body height
I_{av}	Average current
i_C	Load capacitor current
$I_{excitation}$	Excitation current in bioimpedance measurement
I_{meas}	Input current of measurement electronics in bioimpedance measurement
I_{SC}	Short circuit current
kbit/s	Kilobits per second
k_i	Weighting coefficient
l	Length
N_C	Number of clock cycles required to complete a task
N_i	Number of clock cycles required to execute instruction i
P_{SC}	Short circuit power
P_{SW}	Switching power
R	Resistance
$R_{1,2,3,4}$	Resistors
Rd	Destination register
r_f	Near field limit in radio frequency communication
$R_P(\omega)$	Resistance in parallel bioimpedance model
Rr	Source register
R_{ref}	Resistance of reference resistor
$R_S(\omega)$	Resistance in series bioimpedance model
R_{segm}	Resistance of a body segment
R_{sense}	Resistance of a current measurement resistor
R_{set}	Resistance of current setting resistor
Sm^{-1}	Siemens per meter unit of conductivity
T	Clock cycle duration
T_{high}	Higher absolute temperature
T_{low}	Lower absolute temperature
T_N	N-channel transistor
T_P	P-channel transistor
t_{sk}	Mean skin temperature
t_{ski}	Local skin temperature
U_{av}	Average voltage
U_I	Lead I voltage in Einthoven ECG measurement setup
U_{II}	Lead II voltage in Einthoven ECG measurement setup
U_{III}	Lead III voltage in Einthoven ECG measurement setup
U_{in}	Input voltage
$U_{measured}$	Measured voltage

U_{offset}	Offset voltage
U_{out}	Output voltage
V	Volume
V-	Negative voltage
V+	Positive voltage
V_{CC}	Supply voltage
V_{DD}	Supply voltage
V_F	Left foot potential
V_L	Left arm potential
V_R	Right arm potential
V_t	Threshold voltage
X	Reactance
X_P	Impedance of parallel capacitance
X_S	Impedance of series capacitance
Y	Admittance
Z	Impedance
$Z_{1,2}$	Electrode impedances
Z_C	Impedance of a current feeding electrode
$Z_{calculated}$	Calculated impedance
Z_{TUS}	Impedance of Tissue Under Study
Z_V	Impedance of a voltage measurement electrode

1 Introduction

Nowadays several physiological parameters such as heart rate, blood pressure and body composition are already monitored by a users themselves in non-clinical environments [Omron, Polar, Suunto]. These measurements produce a great deal of information about the body's behavior, motivating the user to keep fit, to lose weight and to follow a healthy life style. Typically, these measurements cover only a small time span of a day. Heart rate, for example, is measured only during an exercise session and blood pressure is monitored once or twice a day. However, continuous monitoring of these signals would increase the amount of data gathered and could help in various ways such as understanding the body's behavior during a recovery process after an exercise session, during sleep at night or after a medical operation.

In addition, continuous monitoring of physiological signals with small inconspicuous and portable measurement devices is an essential part of home health monitoring applications. According to Statistics Finland (Tilastokeskus), 26% of the Finnish population will be over the age of 65 years in 2030 [Tilastokeskus]. In Japan the figure for same age group has risen from 12.1% in 1990 and will be 27.8% by 2020 [Steg_05]. This, together with increasing living standards, means that in the near future there will be a much greater number of age- and life-style-related diseases. This will lead to a greater need for medical care and surveillance and thus an increased workload in hospitals and in health centers. One way to improve future health care systems is to develop supportive and preventive home health care methods and telemedicine applications. In these systems, patients are remotely monitored at home and any changes in their medical status are automatically reported to medical or healthcare personnel. It has already been shown that remote monitoring can help to reduce the hospitalization and nursing visits of the elderly [Rosa_09]. A major component in such monitoring applications is a physiological signal recorder or a smart sensor that measures the user's physiological signals. This can interpret the signals automatically or it can send the recorded data to a gateway, which forwards it to healthcare professionals. These same applications also enable the patient's early return to home from hospital after clinical treatment because the recovery process can be monitored remotely.

Monitoring of physiological parameters is not limited to home health monitoring applications. It can also be exploited to improve safety in dangerous occupations, such as fire fighters, and in different sport activities, such as motor racing. For example, in extreme temperatures, monitoring of body temperature could warn of critical conditions and in motor racing, information on a driver's physiological state could be acquired immediately after an accident.

Existing signal recorders for long-term measurements in non-clinical environments pose several challenges. Firstly, in order to save power and the amount of storage memory, monitors such as those for heart rate, do not typically record the full electrocardiogram (ECG) waveform. Instead they record only the interval between two consecutive heartbeats, a so called r-to-r interval. However, full ECG waveform recordings would

help in diagnosing many heart-related diseases, such as arrhythmias and myocardial infarctions [Schm_89]. Devices for measuring the full ECG waveform, such as the HCG-801 from Omron [Omron], can only record ECG for a short period after a user has manually started the measurement. Secondly, monitoring devices are quite expensive. Thirdly, gadget-type signal recorders may also feel slightly uncomfortable and are perhaps not as easy and intuitive to use as they should be. For example, the user manual for the author's own heart rate monitor takes about sixty pages to describe all the menus and functions of the wrist-worn device.

One solution to these problems is to utilize a wearable measurement device instead of gadget-type devices. A wearable sensor can take many forms such as a ring [Sokw_98], a necklace [Awad_99], a wristwatch [Vivago] or even fully integrated into clothing [P5, Hänn_07]. In this approach, the measurement system can be made less visible than a gadget and, with the help of careful integration the system, it can be made comfortable and easy to use. Although electronic components and some processing methods for integrating electronics into clothing [IsoK_05] and into wearable items [Sche_03] already exist, few of these are in the form of commercial wearable measurement applications. The adiStar Fusion Range textiles and shoes developed by Adidas and Polar are one step towards garment-integrated measurements [adiStar]. In the adiStar fusion shirt, textile electrodes required in heart rate monitoring are integrated into the shirt. The adiStar Fusion shoe has a place for a polar S3 stride sensor, which measures running speed, length, and step frequency [adiStar]. However, collaboration between these companies has recently ceased. One example of a wearable gadget-like measurement device is the Swim Distance Tracker [SDT], which tracks the distance a swimmer has covered in a pool. A more complex gadget-like measurement device is the Sensewear® Armband [SenseWear], which measures skin temperature, acceleration, galvanic skin response, and heat flux from the body. An example of wearable sensors is the Vivago wrist watch [Vivago], which monitors the user's sleep and activity.

However, wearable and portable measurement devices are still fairly uncommon. One reason for this might be the long and difficult development process. In order for a company to remain in the market and maintain customer interest, new products, or at least improved versions, should be released yearly or even more frequently. A delay in launching new products leads to loss in company revenue and the amount of loss depends on the length of the delay [Dens_08]. If every new measurement device must be designed from scratch, then this will inevitably lead to such delays. Furthermore, wearable measurement devices and wearable sensors must fulfill certain requirements like reliability, robustness, zero maintenance and fault recovery [Korh_03], which makes the design process even more challenging and time consuming. A lengthy design time increases the cost of devices and sensors and also decreases consumer interest in the products.

In the case of garment-integrated electronics, price is a major limiting factor. If all the electronics needed, such as those in an ECG measurement application, were to be permanently integrated into clothing, the price of the garment would rise significantly. High cost decreases the consumer's willingness to buy clothes that are worn daily even though the garments would have increased functionality. Another problem in garment-integrated electronics is the lifetime of the circuitry and the electronic devices. Nowadays a reasonable life span of consumer electronics, such as a cell phone, is at

least two years. In the case of a physiological measurement device, lifetime is an important feature and should be longer than that of a cell phone. However, it is not possible to wear normal clothes for such long periods on a daily basis because they will wear out. Fortunately, this challenge of garment lifetime can be overcome with a combination of a wearable gadget and garment-integrated electronics, as has been done in adiStar textiles. In these textiles only the sensing electrodes are integrated into the garment and the actual electronics are in the form of a gadget which is attached to the textile with an interconnection mechanism, such as snap fasteners. In this approach, the electronics can be transferred from one garment to another and electronic modules and clothing can even be purchased separately.

The challenge of a long development time is harder to overcome. Over time the functionality of measurement devices and sensors continues to improve. Many new properties and functions are implemented with software. However in wearable devices the amount of computation power and energy available for processing is often very limited. These constraints make the integration of software and hardware very challenging and increase the design time. In order to facilitate the development of physiological measurement devices and to improve their functionality and properties, this thesis examines the technologies enabling the development of portable and wearable measurement devices and also the implementation of some prototypes.

1.1 Scope and Objectives

This thesis presents portable and wearable physiological measurement device prototypes and technologies that enable the implementation of future real-life monitoring systems and applications. The study deals with the implementation process of a gadget-type portable signal recording device which can be worn on a belt under normal clothing. Two versions of wearable measurement system prototypes are also presented.

The main research question is whether the development of a portable or wearable physiological measurement device with sufficient operating time is feasible. This leads to the following specific problem; what are the most important design factors in the development process. These design issues are investigated through the development and implementation of several prototypes and basic research on enabling technologies.

Research methods utilized during this work involve iterative development and prototyping, combined with case studies that focus on specific measurement problems and design issues. This methodology was found to be suitable for this work due to its interdisciplinary nature. Implementation of physiological signal measurement devices involves a knowledge of many fields, including electronics, biomedicine, physiology, material science, and even textile technology. Due to its interdisciplinary nature, this work has required co-operation with scientists from diverse research fields.

The ultimate outcome of this study is the portable physiological measurement device implemented in the Wisepla project [Wisepla]. This device measures dynamic bioimpedance, electrocardiograph and acceleration along three axes. Sample rates in the device are relatively high, several hundred hertz per channel, and there is continuous twenty four hour operation without the need of battery recharge. The measurement

device in question is presented in publication [P4]. The whole development process, the design decisions and the corresponding lessons learned are presented in publications [P1] – [P4].

Clothing typically covers approximately 90 % of a user's skin. Therefore a convenient location for a measurement device measuring physiological signals is integration into the garments. This is examined in publications [P5], [Hänn_07] and [Kukk_01]. Publication [Kukk_01] presents a smart clothing prototype designed for improving the user's thermal comfort. The prototype consists of a temperature measurement unit that measures skin temperature at nine locations on the upper body and a heating unit that controls heating panels manufactured from conductive fabric. In order to store the measurement results and to control the effectiveness of heating, a personal digital assistant (PDA) device is utilized as a user interface. Publication [P5] presents a bioimpedance measurement system for measuring the user's bioimpedance during different activities, e.g. walking or bicycling. The main application of the system is measuring the user's fluid balance, which could enable detection of conditions such as dehydration during excessive exercise. The measurement system is integrated into a commercially available cell suit. To our knowledge this is the first attempt to integrate bioimpedance measurement into an item of clothing (not as a separate device), and to utilize textile electrodes to measure a moving subject.

In tissue, current is conducted by ions and in metallic wires, by free electrons. In order to measure bioelectrical signals an interface is needed, formed of electrodes, between the tissue and the measurement electronics. In clinical applications, commercial silver / silver chloride (Ag/AgCl) electrodes are utilized. The benefit of these electrodes is that they contain chloride, which is also present in the body so that the voltage changes over the electrode remain small. In Ag/AgCl electrodes a conductive gel is often utilized to improve contact and electrodes are attached to the skin with glue supplied from within the electrodes. A problem in Ag/AgCl electrodes is that the gel tends to dry in long term measurements and this adversely affects the measurement signals. The glue also irritates the skin. In clothing-based measurement systems, especially, a more clothing-like solution is needed. One approach is to utilize electrodes manufactured from a conductive yarn. The behavior of these so-called textile electrodes is studied in publication [P6]. Here the behavior of textile electrodes is compared with that of commercial Ag/AgCl gel-paste electrodes during light exercise. Behavior of both electrodes is found to be satisfactory. However, due to sweating, gel-paste electrodes required additional tightening with elastic bands.

An important design factor in wearable and portable measurement devices is a long continuous operating time. A long operating time means either that there is a large amount of energy available for the device or that the energy consumption of the device is low. This poses a problem because in mobile applications all the required energy must be portable. As a result large and heavy energy storages with high capacity are not an optimal solution. A more suitable approach is to design a device that consumes as little energy as possible. Many methods for decreasing energy consumption already exist, including a scaling of supply voltage or operating frequency, and selecting components with minimal energy consumption. A less common approach is to optimize the energy consumption caused by the use of software running in a microcontroller or in a microprocessor. This topic is studied in publications [P7] and [P8]. Both publications

deal with the measurement and analysis of instruction-level energy consumption on 8-bit microcontrollers manufactured by Atmel Corporation.

One module existing in most portable measurement devices is a data transfer channel between the measurement device and data terminal equipment or a user interface device. This channel is utilized for sending the measurement signals forward and in some applications also for configuring device parameters, such as sample rate and signal gain. The communication channel can be implemented using wires or using a wireless communication method, i.e., radio. There are many different radio techniques and protocols such as Bluetooth, ZigBee, ANT, and Wireless local area network (WLAN). All these techniques require a relatively large software stack to support the communication. Publication [P9] presents four different radios working on industrial scientific and medical (ISM) frequency bands below 1GHz. The implementation of these radio circuits is simple and the circuits in question contain only a small number of digital electronic circuits.

1.2 Thesis Outline

The thesis contains nine publications and an introduction. The publications present the main results of the thesis. They consist of the prototype design, prototype implementation, the evaluation of wireless data transfer methods, research on low power operation, and research on energy aware software optimization. The interconnection between the subjects and the publications is shown in Figure 1.

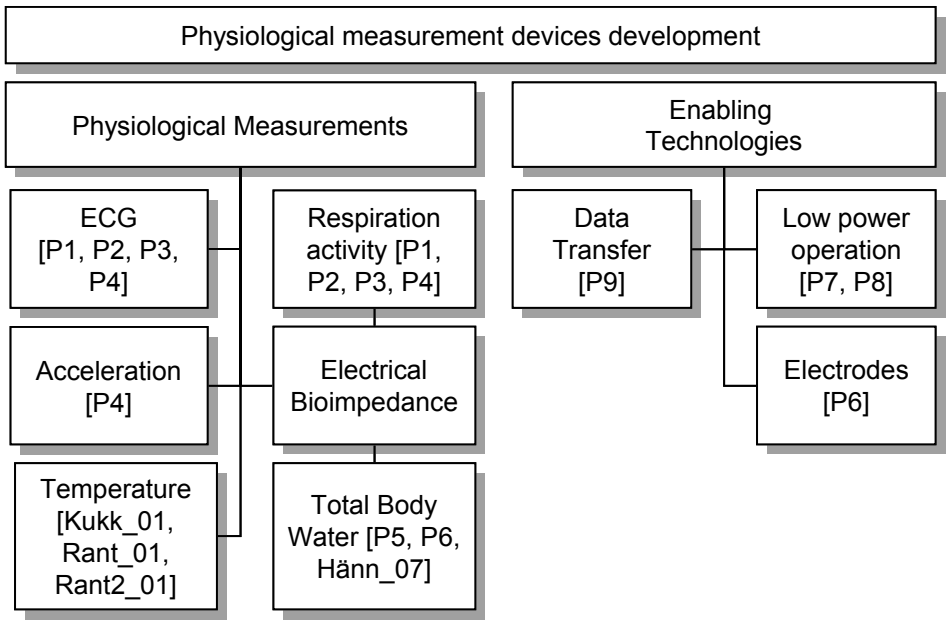

Figure 1. Schematic figure of interconnections between issues researched and presented in the thesis.

The introduction of the thesis presents the main findings of the publications and describes the application field. The introduction starts in Chapter 2 by presenting the general structure of a portable and wearable physiological measurement device. The chapter also discusses the design issues associated with the devices, including wireless communication, data storing, low power, operation and energy-aware optimization of software running in the microcontroller, energy sources and user centric issues such as usability. Chapter 3 presents the theoretical background and utilization of signals, which are measured with the measurement devices presented in Chapter 4. The final section of Chapter 3 deals with electrodes, which are important components in bioelectrical measurement devices. Chapter 4 presents the wearable and portable device prototypes designed and implemented at Tampere University of Technology during the research. These devices include two smart clothing applications; one for measuring and improving thermal comfort and the other for measuring the user's body fluid balance. The development process of a portable long term physiological signal recorder is also presented. Chapter 5 contains a brief summary of the publications and provides an explanation of the author's contribution. Chapter 6 presents the main conclusions of the study.

2 Requirements for Portable and Wearable Physiological Measurement Devices

2.1 General Structure

According to experience gained during the design and implementation of physiological measurement device prototypes at Tampere University of Technology [P1 – P5], [Kukk_01, Rant_01, Rant2_01] the measurement process can be divided into four stages. These stages are common to many portable measurement devices and also to other monitoring systems [Stoj_09, Bogo_09, Yang_05, Li_08]. These stages are sensing, signal conditioning, data storage and communication and/or user interface (UI). The measurement process is supported by essential energy storage and power supply functionality. A block diagram of this process and a general measurement device is presented in Figure 2.

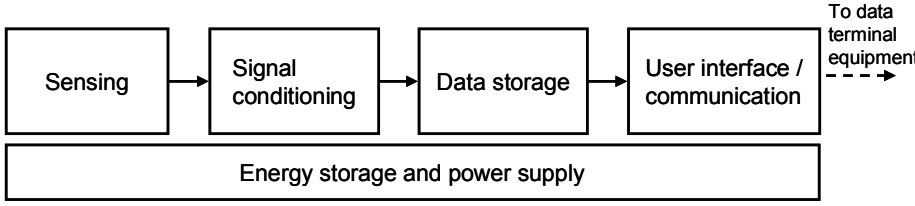

Figure 2. General structure of a portable measurement device

In many applications the first stage, sensing, consists of a single sensor such as an accelerometer, a temperature or a light sensor. However, this stage can also include other electronic components required to produce a measured signal such as current feeding in the bioimpedance measurement. The next stage, signal conditioning, is required to convert or shape the measurement signal into the final form. This stage can be either analogue or digital. In modern measurement applications it is assumed that signals are stored only in digital form. If the signal is not already digitized at the signal conditioning stage, then it will be done as the first task in the data storage block. Depending on the application, data can be stored for longer or shorter periods of time. The final stage in the measurement process is the communication or a UI or a combination of both. For example, in simple real-time monitoring applications, such as sporting heart rate monitors, the measured heart rate is typically only displayed to the user and then discarded without being forwarded to a personal computer (PC), for example. In clinical ECG monitoring applications, the measured data must be forwarded to medical personnel and stored for further analysis.

One way to facilitate the development of physiological measurement devices would be to implement a measurement platform that could be utilized as the starting point in design and in iterative prototyping of new devices. However, developing such a general platform suitable for multiple different measurements is a challenging task. As a result

of findings made while developing smart clothes and portable physiological measurement devices, a few requirements for the platform can be set. These requirements correspond quite closely to the measurement process presented in Figure 2. Firstly, it must be possible to attach both digital and analogue sensors to the platform. Secondly, applications may require additional memory, which means that an interface for a memory attachment is needed. This is challenging since embedded applications such as physiological signal measurement devices typically operate without an operating system (OS) or with a lightweight OS with reduced functionality. Therefore memory and file handling services are not usually available. Thirdly, a standard interface for communication with data terminal equipment or a remote UI is needed. Physical communication interfaces vary considerably from one application to another and, therefore, a preferable approach to standardize the interface is to utilize a software stack. The amount of computation power required varies according to the application. Therefore, in order to define the optimum platform, the amount of processing power must also be scalable. It must also be relatively easy to import the design from one processor or controller to another.

The software of the platform should provide at least a software wrapper component for analogue to digital converter (ADC). An important aspect in digitizing an analogue signal is that the conversion is as jitter-free as possible. This means that the time between consecutive conversions is constant. In a microcontroller environment this can be implemented with stable crystal oscillators and interrupt driven execution. Another commonly required software service is a real time clock (RTC), which is especially beneficial in long-term monitoring applications. Time stamped data helps in interpreting the measurements because signals can be compared to the time of day. If the application already contains an accurate crystal oscillator for timing the analogue to digital conversions, then this same crystal could be utilized for producing a clock service. However, if an RTC is implemented, then a method for adjusting the time is needed. This means that the measurement device needs either to have a communication channel to a remote UI or to have hardware UI that provides enough functionality for setting the time.

2.2 User Centric Issues

Wearable sensors must usually be robust and durable since their operating environments vary and users are not normally technical specialists. The maintenance required should be minimal and only involve actions such as charging or replacing batteries. Sensors should also have a “natural” look or they should “disappear” into the clothing to prevent user discomfort. Security is also an important aspect since many wearable devices contain radio communication. Any personal data transferred through the radio should be encrypted to prevent eavesdropping. [Korh_03]

An important issue in portable measurement devices is the cognitive burden caused for the user. For example, if performing a measurement requires the user to cancel an ongoing activity, like walking, then the cognitive load can be considered too big. Feedback from the device to the user is also important. During long term measurement in particular, it is helpful to know whether measurements are functioning properly or, for example, if the battery is flat. The user environment sets the requirements for the feedback. In a noisy urban area sound or vision feedback is less effective than tactile

feedback. This was observed during the development of the bioimpedance suit presented in [P5]. In the suit, user feedback is implemented by means of a vibration motor providing haptic feedback. Operation of the suit is described in more detail in section 4.2.

2.3 Low Power Operation

In portable and wearable applications the energy consumption of a device is one of the most important design factors because all the energy required to operate the device must be carried along with the user. If the energy consumption is low enough then either the size of the energy source or energy storage can be decreased or the operating time can be increased.

2.3.1 Energy Consumption Theory

The array of digital electronics in modern electronic devices is continually increasing. Most of digital components are implemented with Complementary Metal Oxide Semiconductor (CMOS) technology. A basic building block of the CMOS technology is an inverter, which is often used to illustrate the CMOS technology's energy consumption principles. The inverter consists of one n-channel and one p-channel Metal-oxide Semiconductor Field Effect Transistor (MOSFET) and its circuit diagram and output voltage in time domain are presented Figure 3.

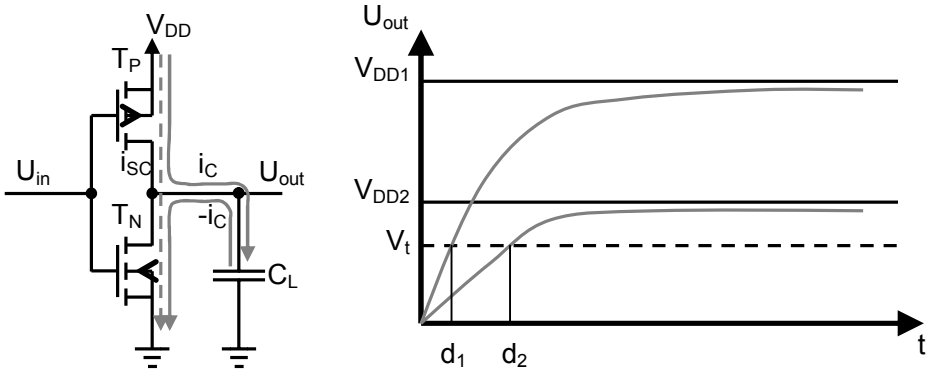

Figure 3. On the left a basic building block of CMOS technology, an inverter. On the right, the inverter's output when the input is switched from high voltage to low voltage, with two different supply voltages.

In Figure 3, the capacitor C_L represents the total input capacitance of the processing elements connected to the inverter output. When the inverter input is changed from low to high, the transistor T_P switches OFF and the transistor T_N switches ON. Now the current $-i_C$ starts to flow and discharges the load capacitance. When the input is switched from high to low, the transistor T_P is switched ON, T_N is switched OFF and current i_C starts to charge the capacitance from operating voltage V_{DD}. As can be seen from the graph on the right in the Figure 3, the supply voltage magnitude has a clear effect on output voltage. The logic gate (not shown in Figure 3) connected to the inverter's output changes its state when its input voltage reaches threshold voltage V_t. The delay from a change in inverter input voltage to the time when the output reaches

threshold voltage is marked d. If a lower supply voltage is utilized, then the delay increases because the load capacitance is charged with a smaller current.

The power consumption of a CMOS processing element (PE), such as the inverter, consists of static and dynamic parts. The static part is caused by leakage currents in the CMOS structure. For example, the transistors in the inverter are never totally switched OFF and a small leakage current always exists between drain and source terminals. The magnitude of leakage current is dependent on the semiconductor manufacturing process and cannot be reduced by an application designer. Leakage currents are usually negligible compared to the total power budget of integrated circuits (IC). However, with deep-submicron technologies and lower supply and threshold voltages, the significance of this current is increasing. Furthermore, in portable embedded applications processing elements are mainly in idle mode, which emphasizes the significance of leakage current [Maci_02].

Dynamic power consumption is caused by the switching activity of the processing element and is formed of two main components, switching power P_{SW} and short circuit power, P_{SC}. During switching, both transistors in the inverter are ON for a short period of time. During this time a current can flow from the supply voltage domain to ground, forming a short circuit pulse whose power can be defined as $P_{SC} = I_{SC}V_{DD}$. Short circuit power is usually less than 5% of the entire CMOS circuit's power consumption [Maci_02]. Switching power consumption is caused by charging the capacitive load in the inverter output. Switching power is usually the dominant factor in power dissipation and therefore extensive research is being done to minimize this component [Maci_02, Meht_97, Su_94, Kim_99].

It is worth noting that when the load capacitance is discharged, no energy is drawn from the supply voltage. Energy is only consumed when the capacitance is charged. The charging current can be calculated from equation (1) describing the capacitor current. In this equation, it should be noted that the output voltage U_{out} is not constant, but increases as the voltage in the capacitor increases and finally reaches value V_{DD}.

$$i_C = C_L \frac{\partial U_{out}}{\partial t} \tag{1}$$

The power consumption of a processing element during switching is then $P_{sw} = V_{DD}*i_C$. Further, the energy consumption during one clock cycle, which duration is T, can be calculated from equation (2)

$$E_{sw} = \int_0^T P_{sw}dt = V_{DD}\int_0^T i_C dt = V_{DD}C_L\int_0^T \frac{\partial U_{out}}{\partial t}dt = C_L V_{DD}^2 \tag{2}$$

The energy required for computing a particular task is then calculated by equation (3), in which N_C is the number of clock cycles needed in the computation of the task and α is the switching activity of the processing element during the task. The power consumption during the task can be calculated by dividing the energy consumed by the

computation time. This is presented in equation (4), in which f is the clock frequency of the processing element

$$E_{sw}^{task} = N_C^{task} \alpha C_L V_{DD}^2 \tag{3}$$

$$P_{sw}^{task} = \frac{E_{sw}^{task}}{N_C^{task} T} = \frac{N_C^{task} \alpha C_L V_{DD}^2}{N_C^{task} T} = \alpha C_L V_{DD}^2 f \tag{4}$$

Equation (4) is a familiar equation describing the power consumption of digital processing elements. In certain contexts the equation (4) is given in the form of average power consumption $P = \frac{1}{2}\alpha C_L V_{DD}^2$ [Maci_02, P7]. The difference between these equations is a coefficient ½. The purpose of this coefficient is to model the aforementioned phenomenon so that no energy is drawn from the power supply when the output switches from high to low. From equation (4) it can be seen that the most efficient way to decrease the power consumption is to decrease the supply voltage V_{DD}. However, as noted earlier, if the supply voltage is decreased, then the delay in processing elements increases, and the operating frequency must also be lowered. In portable devices in which the energy is usually being carried, energy consumption is more important than power consumption. From equation (3) it can be deduced that minimal energy consumption is obtained if the supply voltage is kept as low as possible. It can be concluded, therefore, that a portable device should operate with as low a clock frequency and supply voltage as possible. However, the amount of power required for completing computational tasks limits the lowest possible values of operating frequency and supply voltage.

2.3.2 Hardware Related Energy Saving Methods

The power and energy consumption optimization is a parameter that must be taken into account at every level of application design. For example, if the hardware is not designed to enable low power operation, then it is not possible to compensate this with software. Conversely, poorly designed software can waste more energy than is saved by hardware design. In hardware design the energy can be saved by selecting components that do not waste energy. This means, for example, utilization of low power versions of microcontrollers and high quality passive components such as capacitors with high equivalent series resistance.

Dynamic voltage scaling (DVS) is an energy consumption optimization method in which the processor's operating frequency and supply voltage are scaled according to computational needs [Schm_04]. This requires some additional electronics and software modules, which firstly enable changing the frequency and voltage values and secondly detecting when the values must be changed. In low power microcontrollers and microprocessors this is not yet a common technique. On the other hand, the scaling of clock frequency is already possible even in very simple microcontrollers. As can be seen from equation (3), scaling of clock frequency does not seem to decrease energy consumption. However, energy savings can be gained by using the various power saving modes, inbuilt in most microcontrollers and microprocessors. This means that a computing task is executed as fast as possible with a fixed supply voltage and the idle time between consecutive tasks is spent in as deep a sleep mode as possible, i.e. as

many blocks of the system as possible are stopped or powered down. This method is called dynamic power management (DPM) [Schm_04]. A problem with this approach is that wake up from deep sleep may take a relatively long time, especially if the operating voltage is low. Changing the clock frequency, however, is very fast. Therefore, if the idle time between consecutive tasks is short, it might be more energy efficient to scale down the operating frequency than to enter into sleep mode. An example of DPM is Enhanced Intel® SpeedStep® technology, which allows the system to dynamically adjust processor voltage and core frequency [Intel_04].

Both DVS and DPM require co-operation between software and hardware. Firstly software must be able to detect a situation when the energy can be saved through scaling the voltage and frequency or through shutting down processing elements. Secondly, the hardware must provide an interface that enables these operations. Further, the general functionality and architecture of the software must be designed so that energy is not wasted. This means that energy consumption must be taken into account at an early stage in the software development. An example of energy wastage in software is the generation of delays with loops executing a *no operation* (nop) command.

DVS and DPM are mainly utilized in processors that have a lot of computing power and heavy energy consumption. However, the workhorses of portable physiological measurement devices and ambient intelligence applications are small microcontrollers and microprocessors. In these applications the amount of energy is very limited and low power consumption is a crucial factor in operation and design.

Significant energy saving can also be achieved with the software functions. It is well known that if a microcontroller or microprocessor is programmed with a high level programming language such as C/C++, the compiler is unable to optimize the program as efficiently as the program writer. This is because the compiler cannot deduce the program's high level functionality and thus cannot, for example, optimize the register utilization as well as the programmer. In addition, numerous processor-dependent low power design methods can be utilized. One important and often overlooked issue is the handling of the processor's unconnected input-output (IO) pins. The correct handling of these pins is processor specific, but the general idea is to tie an unused pin to a predefined voltage so that unpredicted state changes can be avoided. In Atmel Corporations eight-bit AVR microcontrollers [Atmel], for example, the unused pins are tied to the supply voltage by enabling an internal weak pull-up resistor. One advantage of this approach is that the IO-pin is configured to be an input but it is still tied to a voltage supply. If the pin is now externally pulled low, the current flowing from the pin is relatively small. The internal pull-up is not available in all microprocessors. Texas Instruments' MSP430F1611 [Texas], for example, lacks this functionality and therefore unused IO pins should be configured to be outputs, which means that a pin is actively driven to a certain level. If an actively driven pin is externally pulled to an opposite voltage inadvertently, the generated short-circuit current can damage the system.

2.3.3 Software Related Energy Saving Methods

One way to achieve energy savings in embedded applications is to optimize the software according to its energy profile. This has been done in numerous research projects [Tiwa2_94, Chak_99, Russ_98, Oliv_03, Lee_01, Niko_03, Niko_05]. The main idea in energy driven software optimization is that different instructions in a

microprocessor's instruction set consume different amounts of energy. Furthermore, it is possible to implement certain operations with different instructions or instruction combinations. For example, in Atmel AVR microcontrollers [Atmel], clearing a register can be done with a clearing instruction (`clr Rd`), with an immediate and operation (`andi Rd,0`) or with subtraction operation (`sub Rd,Rd`). If the exact energy consumption of all instructions is known, then a compiler could automatically select an instruction with the lowest energy consumption.

In order to implement an energy aware compiler, energy consumption of all instructions in a target processor's instruction set must be known. This information can mainly be achieved in two different ways: simulation and measurement. Simulation can be done at different levels, such as on transistor, gate or behavioral level. At lower simulation levels, more accurate energy consumption results can be achieved but the simulation time also increases. A drawback in simulation is that a model of the target processor is required. Models of commercial processors are not widely available, which makes it impractical to use simulation with open source compilers. Numerous free source code behavioral level models of widely utilized compilers are available in the Internet [Opencores]. These models have the same functionality as the actual processor, but the internal implementation is different and so models cannot be utilized in accurate energy consumption simulation. Furthermore, low level implementation of a microcontroller core can be fine tuned during the controller's life span, which may have some effect on the energy consumption but leaves the instruction level functionality unchanged.

Analysis and optimization of energy consumption caused by the software at the instruction level were first proposed by Vivek Tiwari, Sharad Malik and Andrew Wolfe in 1994 [Tiwa_04]. Tiwari et al. have created a simple model for an instruction's energy consumption. This model consists of two parts that are easy to measure, utilizing a real processor and a multimeter. The first part of the model is instruction-related energy consumption (a so-called base cost), which is the amount of energy consumed each time a particular instruction is executed. In order to measure the base cost of an instruction, a processor is programmed to execute the instruction in an endless loop. The average current consumption and supply voltage are then measured. When the operating frequency of the processor is also known, the energy consumed by one instruction can be calculated. The second part of the energy consumption model is an inter-instruction effect. This is the amount of energy that is consumed when the instruction in execution is changed to another instruction. Inter-instruction energy is caused mainly by the switching activity in the processing elements when, for example, the operation code is changed. This energy is unique to every instruction pair in the processor's instruction set. If the base cost for instructions is known, then the inter-instruction energy can be measured by programming the processor to execute the instruction pair in an endless loop and carrying out the same measurements as for the base cost. The base cost of the instruction pair is calculated according to previously measured base cost and the result is subtracted from the measured instruction pair energy. The resulting overhead is then regarded as the inter-instruction cost.

As an example, let consider two instructions from Atmega8515 instruction set an addition of two registers, `add Rd,Rr` and addition with carry bit, `adc Rd,Rr`. In a 16-bit addition these two instructions are issued consecutively. First, a base cost for `add` and `adc` are measured to be 5.524 mA and 5.462 mA respectively. Execution time

of both instructions is one clock cycle. When executed as an instruction pair, the base cost can thus be calculated as (1*5.524 mA + 1*5.462 mA)/(1+1) = 5.493 mA. The measured cost for the pair is 5.624 mA, which yields an overhead of (5.624 mA – 5.493 mA) = 0.131 mA. The overhead now occurs after every clock cycle when the instruction in execution is changed. However, it is possible that the energy consumption in the situation when `add` is switched to `adc` is different from the situation when `adc` is switched to `add`. According to measurement results, it not possible to calculate the difference in these energies and so they are assumed to be equal. The current values utilized in this example are measured with an actual measurement setup and microcontroller, presented later in this chapter.

In order to measure instruction level energy consumption, a method is required for measuring the processor's operating current and supply voltage. The simplest way to do this is to utilize a current measurement resistor placed in series with the processor, as illustrated in Figure 4. Voltage over the sensing resistor R_{sense} can be measured with an averaging multimeter, for example. If a more accurate waveform is needed, then a differential measurement mode in an oscilloscope can be utilized. In our measurements an accurate instruction level understanding of the microcontroller's behavior was necessary and so the differential oscilloscope measurement is used. In order to identify which instruction is in execution, synchronization functionality has been implemented with the target microcontroller's one IO-pin. The program in the microcontroller is set into an infinite loop and at the beginning of every loop the synchronization pin is set from high to low. This signal is utilized in an oscilloscope to trigger the measurement.

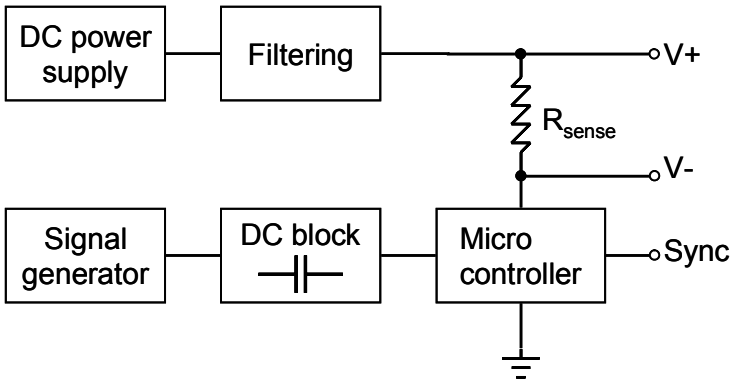

Figure 4. Measurement system for measuring microcontroller's instruction level energy consumption

In the first measurements a differential measurement mode of the oscilloscope was used. However, it became evident that the digitally formed differential signal contained twice as much noise as one measurement channel. As a result, the measurement setup was modified. In the modified setup the power supply voltage V+ acts as a reference voltage for oscilloscope measurement. The first oscilloscope channel measures the voltage over the resistor R_{sense} (V- – V+), the second channel measures the voltage between the measurement circuit's ground potential and supply voltage (GND – V+), the third channel measures the synchronization signal and the fourth channel measures the clock signal acquired from a signal generator. In order to implement this

measurement setup, the DC-power supply must be configured to float, i.e., the ground potential of the measurement board cannot have a galvanic connection to the power distribution network's ground potential. In this setup all the signal polarities are inverted but the amount of noise is far less than in differential measurement. Furthermore, the changing of signal polarity is a simple operation, for example, in a spreadsheet program or in Matlab.

Figure 5 presents a current signal, measured using the measurement system presented above and Atmel's AVR AT90S8515 microcontroller [Atmel]. The signal in the lower part of Figure 5 is a square wave clock signal produced with a signal generator. The upper signal is the current signal calculated from the voltage measured over the resistor R_{sense}. The clock frequency in the measurement was 1.7 MHz and the average current consumption of the microcontroller was 5.1 mA. The lines and numbers between the clock and the current signals indicate an instruction that is being executed. The instructions and corresponding numbers are presented in Table 1. As can be seen from Figure 5, current consumption is mostly below 5 mA and only at the edges of the clock signal does the current consumption increase. The increase in current consumption occurs because operations in the microprocessor are synchronized to the clock edges. The AT90S8515 has a two-stage pipeline so that when one instruction is in execution, the next one is fetched from program memory. The execution phase is divided into three stages so that on the first rising edge of the clock signal, the microcontroller's core fetches the register required in the instruction execution. On the second falling edge the actual operation in arithmetic logic unit (ALU) is performed and on the third rising edge a write back operation is executed [AT90S8515]. The pipelining in the controller core makes it difficult to analyze which part of the energy or current consumption is caused by which instruction. Particularly because on the clock signal's rising edge, two things (register fetch and write back) occur simultaneously.

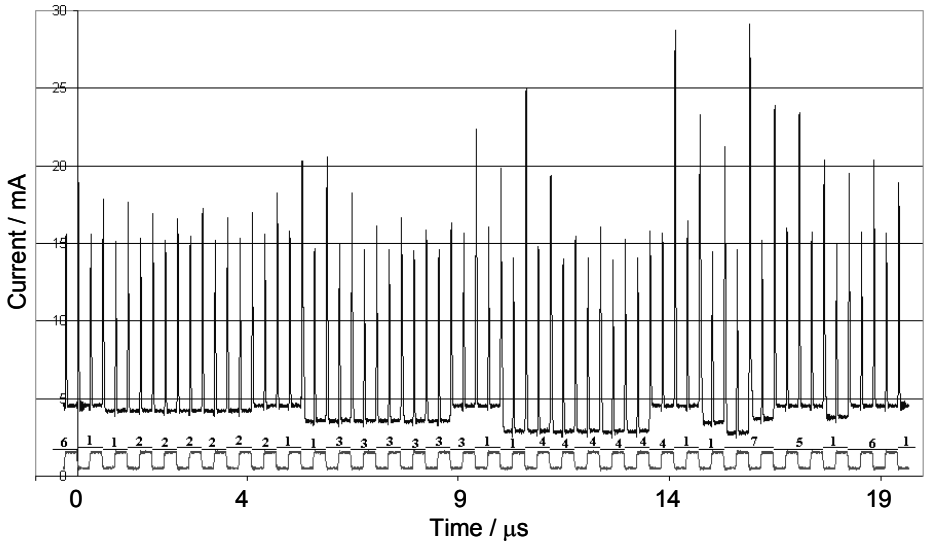

Figure 5. Instruction level current consumption of AT90S8515 microcontroller. The signal in the lower part of the figure is a clock signal supplied by a signal generator and the upper signal is the current signal.

Table 1. Instructions in Figure 5

No.	Instruction	Clock cycles	Binary code
1	nop	1	0000 0000 0000 0000
2	ldi r16,0x00	1	1110 0000 0000 0000
3	ldi r21, 0x55	1	1110 0101 0101 0101
4	ldi r31,0xff	1	1110 1111 1111 1111
5	sbi PORTD,5	2	1001 1010 1001 0101
6	cbi PORTD,5	2	1001 1000 1001 0101
7	rjmp	2	1100 1111 1110 0010

Figure 5 reveals an AT90S8515-related fact that the so-called basic level current consumption correlates very much with the instruction in the pipeline's prefetch phase. As can be seen, the current's base level is almost 5 mA when the no operation, *nop*, instruction is in prefetch and about three milliamperes when the instruction *ldi r31,0xff* is in the prefetch. Table 1 shows that the operation code of the nop is plain zeroes whereas the operation code of *ldi r31,0xff* is almost plain ones. In instruction three *ldi r21,0x55* there are nine ones and seven zeroes and the base level current consumption is between instructions one and four. It can therefore be concluded that the base level of the current consumption correlates with the amount of zeroes in the instruction's operation code, so that zeroes seem to be more expensive than ones. This is very likely to be a microcontroller-specific phenomenon and cannot be generalized. However [P8] presents many ways to utilize this phenomenon in energy consumption optimization. All methods are based on increasing the amount of one bits in the instruction operation code. For example, an operation code for an *and* operation of two registers (*Rd ← Rd • Rr, and Rd,Rr*) is *0010 00rd dddd rrrr* in which *d* refers to the destination register and *r* to another source register. If the operation is performed between registers r0 and r1, the operation code will be *0010 0000 0000 0001*. If the operation is performed with registers r30 and r31, the operation code is *0010 0011 1110 1111*, which results in ten one bits versus two one bits in the first opcode. As stated in [P8], a compiler backend has very limited scope for selecting the utilized registers, but it should be done at higher levels in the compiler. A similar correlation between energy consumption and operation code operands has been found by Nikolaidis et al. [Niko_02] in ARM7TDMI processor.

Because zeroes seem to be more expensive in terms of energy consumption in instruction, a hypothesis has been formed that in run time data zeroes are also more expensive than ones. Another hypothesis has been that utilization of registers with low addresses, i.e. 0 – 15, is more expensive than utilization of registers with higher addresses, i.e. 16 – 31. During the initial measurements it was also noticed that fetching instructions from one address consumes more energy than fetching from others. This phenomenon has been studied by using measurement programs executing no operation commands, *nop*, in continuous loops. The results of several measurements are presented in Figure 6. Instead of presenting the energy consumption of the whole instruction, Figure 6 presents only the energy of the first current peak, when an instruction located in the address given below the graph is in execution. For example, when the instruction stored into an address 0x007E is in execution, instruction from the

next address 0x0080 is in a prefetch stage. As can be seen from Figure 6, the energy of every sixteenth instruction is higher than the energy of other instructions. This is most likely caused by the page structure of the instruction memory. The hypothesis is that because the length of most instructions in AT90S8515 instruction set is sixteen bits, the instruction memory is divided into 32 byte pages. Activation of a new page consumes more energy than fetching an instruction from an already activated page. This provides a way to optimize energy consumption by locating a small, frequently executed loop within a single memory page.

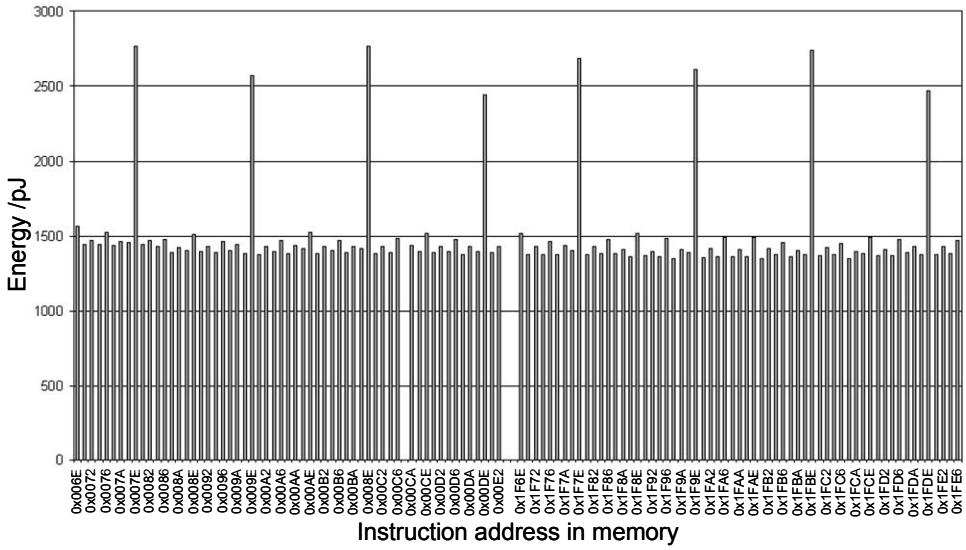

Figure 6. Energy of the first peak in instruction execution and fetch cycle when a no operation instruction is executed. In every sixteenth instruction the energy is considerably higher than in other instructions.

The three hypotheses above are tested with a benchmark program. The program simply calculates the sum of eight bytes and then forms an average by shifting the sum three times to right, which corresponds to an integer division by eight. The varied parameters in the programs are data, utilized registers and location of average counting loops in memory. Programs are set into an infinite loop and the average current taken by the microprocessor is measured with a multimeter. The results are presented in Table 2. Results from the benchmark test reveal that, contrary to the hypothesis, the ones in the runtime data consume more energy than the zeroes. However this is beneficial, for example, in loop counters in which the values handled are usually small. As expected, utilization of lower registers consumes more energy than utilization of higher registers. There are two reasons for this: firstly, utilization of higher registers increases the number of ones in the instruction's operation code and, secondly, the architecture of the AT90S8515 is optimized for the usage of a register with a higher address. For example, it is not possible to utilize all register-related instructions in a microcontroller's instruction set with sixteen lower registers. As expected, the location of the program in the instruction memory also affects current consumption. If the program is located so that at each execution of the loop the page border is exceeded, current consumption is greater than when the loop is located within one page. The difference in current

consumption between the best and the worst case is (7.510 mA – 6.733 mA) = 0.777 mA, which represents a reduction of ten percent. Despite the fact that 57% of this reduction is caused by the runtime data, the results show that simple software optimization can have an impact on software energy consumption.

Table 2. Average currents of benchmark programs executed in the AT90S8515 microcontroller and measured with a multimeter. Results show a difference between the worst and the best cases of about ten percent. [P7]

Upper registers	Data plain ones	Data plain zeroes
Looping over page border	7.220 mA	6.924 mA
Looping inside one page	7.034 mA	6.733 mA

Lower registers	Data plain ones	Data plain zeroes
Looping over page border	7.510 mA	7.070 mA
Looping inside one page	7.325 mA	6.880 mA

During the initial measurements it soon became apparent that manually measuring the instruction level energy consumption of every instruction in a microcontroller's instruction set is time consuming and laborious. As a result, the work was automated with the computer controlled measurement system presented in Figure 7. During the implementation of the automated measurement system, Atmel discontinued production of AT90S8515 microcontroller, so the target processor was also changed. The new microcontroller, Atmega8515 [Atmega8515], is almost identical to AT90S8515 and so the replacement made no difference to the implementation.

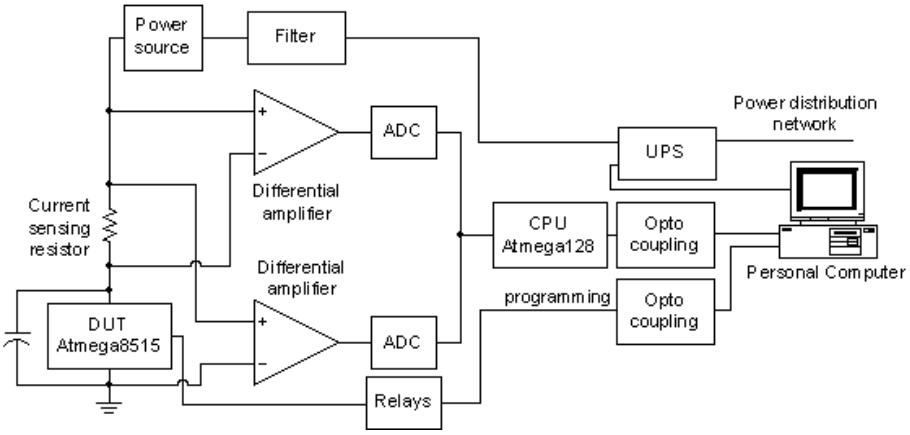

Figure 7. Computer controlled automated measurement system for instruction level energy consumption measurement.

The measurement principle for the instruction level energy consumption is similar to that used in the previous measurements. A current flowing into a microcontroller is measured as a voltage over a current sensing resistor. The main difference to the previous measurements is that an instruction level current waveform is not required, but an average current is measured instead. Therefore a relatively large number of power

supply filtering capacitors are placed in parallel with the device under test (DUT). The core of the measurement electronics is an Atmega128 microcontroller, which controls two analog to digital converters, measuring the voltage over the current sensing resistor and the supply voltage of the Atmega8515. The measurement procedure is controlled by means of a standard desktop computer running Linux operating system. Data connections between the measurement electronics and the computer contain a galvanic separation implemented with an optical coupler. This arrangement is designed to decrease the voltage noise and other disturbance caused by the computer. The desktop computer generates actual measurement programs according to a list of instructions stored into its memory and downloads programs to Atmega8515's memory through a serial programming interface. In order to prevent any current flow from the programming connection to the microcontroller during the actual measurement, the programming lines are switched off before the measurement with relays.

The actual measurement program in the DUT's instruction memory is set into an infinite loop, as before. In order to measure average energy consumption, the program is generated so that it fills the entire instruction memory of the DUT. This averages out the effect of instruction address, which has an effect on instruction energy consumption, as stated earlier. Whenever possible, the run time data is randomized so that its effect on energy consumption is averaged as well as possible. When the measurement program is downloaded into the DUT, the PC stays idle while the Atmega128 performs the measurements. The program execution in DUT and the measurements performed by Atmega128 are not in any case synchronized, which should increase the averaging effect on the measurement results. Both the current and voltage are sampled five hundred times at a resolution of 16-bits during a twenty milliseconds period. The DUT runs with a frequency of 4 MHz and its 8 KB instruction memory can store four thousand instructions. During the measurement period the program is, therefore, executed approximately twenty times, which should provide a good estimate of the average energy consumption of the instructions. After the measurement period, the results are transferred to a personal computer, which stores them and calculates the average values of the supply voltage and microcontroller current.

The Atmega8515 instruction set contains 130 instructions. However, it is not possible to measure all of these with the automated measurement system, and in some instructions the possible data and parameter values are limited. For example a store instruction, which stores data from a register to memory, cannot be allowed to store data into a stack pointer register or ALU's configuration register. Moreover, automatic test program generation for jump and branch instructions is challenging because their effect on the execution flow, and in the worst case the execution, resets or stalls the microcontroller. When these limitations are taken into account, there are 89 instructions that can be measured easily with the automated measurement system. From the measurements a Tiwari-Malik-model base cost is calculated for every instruction using equation (5), in which the I_{av} and U_{av} are the measured average current and voltage respectively, f is the DUT clock frequency and N_i is the number of clock cycles required to complete a particular instruction. The results of the measurements are presented in Table 3.

$$E_{base} = I_{av} U_{av} \frac{N_i}{f} \tag{5}$$

Table 3. Tiwar-Malik-model base cost energies for 89 instructions in Atmega8515 instruction set

	Instruction	Energy/nJ	Cycle
1	ser	5.099	1
2	sev	5.488	1
3	clt	5.491	1
4	cls	5.491	1
5	wdr	5.491	1
6	sei	5.491	1
7	clh	5.494	1
8	cln	5.494	1
9	cli	5.494	1
10	seh	5.495	1
11	clz	5.496	1
12	set	5.496	1
13	clv	5.496	1
14	lsr	5.556	1
15	clc	5.762	1
16	ses	5.785	1
17	sez	5.792	1
18	sen	5.797	1
19	bld	5.839	1
20	mov	5.839	1
21	lsl	5.867	1
22	clr	5.869	1
23	sec	5.886	1
24	or	5.887	1
25	sbr	5.888	1
26	and	5.889	1
27	mov	5.891	1
28	ori	5.892	1
29	andi	5.906	1
30	cbr	5.956	1
31	bst	6.011	1
32	asr	6.078	1
33	bclr	6.128	1
34	nop	6.159	1
35	swap	6.167	1
36	bset	6.182	1
37	ror	6.218	1
38	rol	6.224	1
39	cpi	6.339	1
40	inc	6.339	1
41	dec	6.342	1
42	cp	6.513	1
43	neg	6.570	1
44	cpc	6.573	1
45	ldi	6.624	1

	Instruction	Energy/nJ	Cycle
46	tst	6.697	1
47	com	6.776	1
48	subi	6.790	1
49	adc	6.792	1
50	eor	6.811	1
51	sbci	6.818	1
52	add	6.869	1
53	sub	6.883	1
54	sbc	6.942	1
55	ld x	11.779	2
56	st x	11.803	2
57	ld y	11.937	2
58	ld z	12.353	2
59	st y	12.451	2
60	ldd y+q	12.494	2
61	ld x+	12.543	2
62	ldd z+q	12.607	2
63	ld y+	12.621	2
64	ld –x	12.692	2
65	st –y	12.742	2
66	ld –y	12.842	2
67	ld z+	12.900	2
68	ld –z	12.963	2
69	sts	12.995	2
70	st z	13.026	2
71	mul	13.093	2
72	std y+	13.132	2
73	lds	13.143	2
74	sbiw	13.278	2
75	adiw	13.365	2
76	st –x	13.656	2
77	fmulsu	13.843	2
78	fmul	14.067	2
79	mulsu	14.214	2
80	mmuls	14.257	2
81	muls	14.364	2
82	lpm z	18.399	3
83	st x+	19.570	2
84	lpm z+	19.943	3
85	lpm	20.045	3
86	st y+	10.333	2
87	std z+	24.396	2
88	st z+	24.803	2
89	st –z	25.411	2

As it can be seen in Table 3, the energy consumption of the instructions with one clock cycle duration is between five and seven nJ. Instructions that require several clock

cycles to complete also consume more energy, though three cycle instructions are not the most expensive ones. The most expensive instructions are the ones storing data to memory with a Z pointer. This is an interesting result, since in Atmel AVRs there are three pointer register pairs X, Y, Z utilized in data load and store instructions. According to these results, utilization of Z pointer in store instructions is much more expensive than utilization of X and Y pointers. In general, it can be stated that instructions that store or load data to or from memory consume more energy than instructions that operate with registers. As a rule of thumb, data should be kept in registers for as long as possible and stored to volatile or nonvolatile memories only when necessary.

The inter-instruction currents of the Tiwari-Malik model are also measured and inter-instruction energies are calculated for the 89 instructions above. With 89 instructions it is possible to form 89 * 88 = 7832 instruction pairs. However, this amount can be reduced to half because the inter-instruction energy in pair `i-j` is regarded as identical to the pair `j-i`. The total amount of measurement performed with the automated system is then 7832/2 + 89 = 4005. The inter-instruction energy of instructions `i` and `j` is calculated with equations (6) – (8).

$$E_{base,ij} = E_{base,i} + E_{base,j} \tag{6}$$

$$E_{overhead} = I_{av,meas} U_{av,meas} \frac{N_i + N_j}{f} - E_{base,ij} \tag{7}$$

$$E_{ij} = \frac{1}{2} E_{overhead} \,. \tag{8}$$

Equation (6) produces the base energy of instruction pair `ij` according to measured single instruction base energies. Next, equation (7) is utilized to form an overhead energy, which is the difference between the base energy calculated with equation (6) and the actual measured energy consumption. Because in every instruction pair `ij` the change between instructions occurs twice, once from the `i` to `j` and once from the `j` to `i`, the overhead energy is divided by two to obtain the inter-instruction energy in equation (8).

Calculation of inter-instruction energies showed that most of them amount to less than ten percent of the base cost energy. Therefore, a relatively accurate estimate of the software's energy consumption can be acquired by summing up the instruction level base cost energies. Furthermore, 25 % of the calculated inter-instruction energies are negative.

Nikolaidis et al. [Niko_03, Niko_05] have also measured negative inter-instruction energies for ARM7TDMI processors. They explain negative energies with the pipelined architecture of the processor. However the measurement method utilized by Nikolaidis et al. is also a little different. In order to measure the energy consumption of one instruction in processors with a three-stage pipeline, Nikolaidis et al. surrounded the instruction in question with a reference instruction, whose energy consumption is known at every stage of the pipeline. In this method the measured base energy cost also

includes the inter-instruction energy consumed when the particular instruction is switched to the reference instruction. Therefore the base cost is likely to be too great and the inter-instruction energy calculations result in negative energies. Luo et al. [Luo_05] have created an energy model for ADSP-2189 digital signal processor (DSP) manufactured by Analog Devices. The authors discovered that if consecutive instructions in a DSP program are similar enough, the inter-instruction energy can even be slightly negative.

In the Atmega8515, the cause of this negative inter-instruction energy is likely to be different from those mentioned earlier. No clear reason for this has so far been found but the effect could be partly explained in terms of the observations made during the manual measurements. As shown in Table 2, the effect of the runtime data is approximately 5 % and the effect of utilized registers is approximately 1-2 % on the microcontroller current consumption. In the automatic measurement process the effect of runtime data and utilized registers has been averaged out through randomization. However, it is possible that the randomization effect is not equal in every measurement and this could lead to errors in the measurement results.

2.4 Energy Sources

A crucial component in a portable physiological measurement device is the energy source. Because all energy required during a measurement session must usually be carried along inside the device, the energy source should be small and lightweight. At the same time the energy source must contain enough energy to provide reasonable operating time for the application in question. In order to fulfill these two requirements the energy density of the energy source should be as high as possible.

The energy source must be able to supply enough energy for every operating mode of the device, i.e. the maximum available peak current must be sufficiently high. If the energy source is a rechargeable type, an important parameter is the amount of charge-recharge cycles. This parameter indicates how many times the energy source can be charged and recharged before its capacity starts to decrease significantly. In addition, the self-discharge current of the energy source should be as low as possible. Self-discharge is a problem, especially with some rechargeable batteries. For example, in Nickel-Metal hydride (NiMH) batteries the self-discharge rate can be as high as 30 % per month. Low self-discharge rates are required in applications in which operating times are long and need months or years without recharge. In such applications average current consumption is also low due to a low duty cycle, but peak currents can still be relatively high.

An important factor in design, especially in colder climates, is the operating temperature range of the energy source. During winter the temperature can fall several tens of degrees below zero. However, physiological measurement devices are usually carried near the body, which helps to keep the temperature of the device above zero. In serial production the cost of the energy source is also an important parameter, which should be as low as possible. At present, possible energy sources for wearable physiological measurement devices and portable devices in general are primary or rechargeable batteries, fuel cells, and energy scavenging or harvesting from environment.

2.4.1 Batteries

The energy sources of portable devices such as cell phones are usually implemented with rechargeable batteries. Their rechargeability reduces waste and provides a more economical solution compared to primary batteries. A common trend in portable and mobile devices is that as the technology evolves, more and more features are added to devices, which increases their energy consumption. This poses a problem with regard to primary and rechargeable batteries because their energy density is not evolving as fast as the increase in the devices' energy consumption. In [Star_03], Thad Starner presents improvements in laptop technology between 1990 and 2002. During this period improvements in disk capacity, central processing unit speed and available random access memory (RAM) have been more than a hundredfold. Over the same period improvements in the energy density of batteries has been only two or threefold. This data makes clear that the low energy density of batteries compared to the power requirements of portable devices is a major problem in portable devices. In 2004, Professor Yrjö Neuvo stated that the energy density of batteries increases by about ten percent annually [Neuv_04]. Over a period of twelve years this represents a threefold improvement, which is consistent with Starner's findings. Therefore the main priority in the design of a portable device should be the selection of battery. The rest of the device is then designed according to the battery properties since it is the component that will be the slowest to evolve during the design period [Star_03].

Today the three most widely utilized rechargeable battery technologies in portable devices are Nickel-Metal Hydride, Lithium Ion (Li-Ion) and Lithium-ion Polymer, commonly known as Lithium polymer (LiPo). The criteria according to which the battery selection is done differ from application to application, but a few common properties of these technologies are listed in Table 4. Formerly, Nickel-Cadmium (NiCd) batteries were widely utilized in portable devices such as battery-powered drills. The advantages of NiCd batteries are a high peak current and low cost. However, NiCd batteries are also relatively heavy and suffer from a so-called memory effect, which means that if the battery is not charged and recharged correctly, its capacity will decrease significantly. In addition, NiCd batteries contain cadmium, which is a toxic heavy metal. For these reasons alternative battery technologies are preferred in portable devices.

Table 4. Properties of the most common rechargeable battery technologies utilized in present portable devices. [Stoj_09]

	Nickel-Metal Hydride	**Lithium-Ion**	**Lithium-Ion Polymer**
Cell voltage	1.25 V	3.6 / 3.7V	3.7 V
Energy density	30 – 80 Wh/kg	100 – 160 Wh/kg	130 – 200 Wh/kg
Self discharge per month	30 %	5 %	1-2 %
Optimal load current	0.5 C	1 C	1 C
Charge – discharge cycles	500	1000	500

Nickel-Metal Hydride batteries have a higher energy density than NiCd batteries and they do not suffer from the memory effect. However, a drawback of NiMH batteries is a relatively large self-discharge current. The properties of Lithium-Ion and Lithium-Ion Polymer batteries are very similar. The difference between them is the electrolyte material. In Li-Ion batteries the electrolyte is in liquid form and in LiPo batteries in a hybrid form of solid and gel. A clear benefit in LiPo technology is that it enables the manufacture of very thin batteries. As can be seen from Table 4, the highest energy density of the batteries types is in the Lithium-Ion Polymer technology. The self-discharge of LiPo batteries is also the smallest, even if the value given in [Stoj_09] may be a little optimistic. In batteries manufactured with lithium technology, the optimal discharge current is equal to the nominal current (C), which is twice as much as the discharge current of the NiMH technology. However, the peak currents available from a LiPo battery, for example, can be several times the nominal current.

An important aspect in the design of a battery-operated device is the battery behavior under load. Firstly, the battery's geometry affects the maximum current supplied by the battery. According to our experience, coin-shaped batteries have a high capacity but low peak current. Larger peak currents can be gained from cylinder-shaped batteries. This is due to the size of the electrode surface area [Roun_04], which is larger in cylinder-shaped than in coin-shaped batteries. Secondly, a battery's recovery effect should be utilized whenever possible [Lahi_02]. The recovery effect is the battery's ability to recover during idle time when only a little or no charge is drawn. The reason for the recovery phenomenon is the accumulation of non-reacted charge carriers on the battery's electrodes during a high loading period. During an idle period these charge carriers have time to react with the electrode material and the battery's terminal voltage increases, in other words it recovers.

2.4.2 Energy Scavenging and Harvesting

Another possible way to source energy for portable devices is scavenging or harvesting energy from the environment or from the user. This area has been studied for many years and its significance has increased in step with the development of wireless sensor area networks (WSN). In a WSN, with hundreds or thousands of measurement nodes, batteries cannot be utilized as a power source because replacing them would be laborious. Therefore, if energy from a power-distribution network is unavailable, the only possibility is to design nodes to scavenge energy from ambient sources.

The main sources for harvesting energy are ambient radiation such as energy radiated by radio transmitters, or light from the sun or other light sources, temperature differences, and mechanical movements [Para_05]. An example of devices that harvest energy from Radio Frequency (RF) -radiation are radio frequency identification (RFID) devices such as those being implemented in the Wireless project at Tampere University of Technology [Wireless, Hein_06, Riis_07]. These measurement devices are designed to measure ECG but they have no onboard energy storage and operate solely on the energy drawn from an RF-signal from the reader device. A problem with such a system is the poor efficiency of the energy transfer. Efficiency can be increased with larger antennas, with stronger transmitters or with shorter transmission range. However, in portable applications this is not usually feasible because of size and energy constraints.

Another ambient energy source is the sun's radiation. Solar energy has been utilized in many applications, such as providing energy for a WSN node [Ragh_05]. A disadvantage with such a source is that it is not constant but varies a great deal according to time of the day, season, and location. In direct sunlight the power density of a solar cell can be as high as 15 mW/cm^2 [Ragh_05], but indoors under a 60 W desk lamp it drops to 0,6 mW/cm^2 [Stoj_09]. Therefore in order to utilize solar cells as an energy source, energy storage in the form of a rechargeable battery or a super capacitor is also required to back up the solar cell when the supply current is insufficient.

Energy generation from the human body has also been studied [Star_96, Star_04, Para_05, Para_06]. Human body expenditure varies from 81 W during sleep to more than 1600 W during strenuous exercise [Star_04]. If even a small amount of this energy could be scavenged, the energy problem of portable devices would be solved. However, the problem with this approach is the often rather poor efficiency of scavenging. Moreover, if too much energy is scavenged from the body, the scavenging process might become noticeable and distract the user.

Much research has focused on transforming the body's kinetic energy into electrical energy. For example, von Buren [vonB_03] et al. have estimated that a micro generator with a one gram proof mass could output power of 200 μW during walking. Kymiss et al. [Kymi_98] have tested piezoelectric materials and a rotary magnetic generator installed in footwear. Piezoelectric materials and the generator have produced an average power of a few tens of mW and a quarter of a watt respectively. Human powered magnetic generator-based flashlights have been available for a decade or so [Deve_16]. Newer versions of these flashlights as well as human powered cell-phone chargers and radios are marketed by companies such as Freeplay [Freeplay]. Freeplay's products are based on charging a device by means of a crank. Another commercially available example of utilizing the human body's kinetic energy is the wristwatches manufactured by firms such as Seiko [Seiko]. Operation of these watches is based on a moving mass, whose weight is a few grams. The mass is moved by wrist moments and rotates a generator that provides electric energy for the watch [Para_05]. Romero et al. [Rome_09] have tested a kinetic energy generator, based on electromagnetic induction similar to those in commercial wristwatches. The size of the generator is 1.5 cm^3 and it has been tested on different sites of the body. The authors report that the highest power, 3.9 μW, is harvested from the ankle.

One way to harvest energy from the human body is to utilize the temperature difference between the body surface and the surrounding air. The maximum efficiency of thermal energy scavenging can be calculated from the Carnot efficiency equation, $\eta = (T_{high} - T_{low}) / T_{high}$. According to this, the maximum efficiency of energy scavenging from a temperature gradient between body core temperature and room temperature is $\eta = (310.15\ \text{K} - 293.15\ \text{K}) / 310.15\ \text{K} = 0.055$ ➔ 5.5 % [Star_96]. According to Starner et al. human energy expenditure when sitting is 116 W. If all this energy could be utilized for thermal scavenging, 6.4 W could be gathered. However this would involve covering the whole body with energy scavenging devices and even then not all the energy could be retrieved because thermal energy is evaporated not only through the skin but also in other ways, such as respiration. Another problem is that if a part of the body is covered with a device, which tends to cool down the skin, the body will reduce blood flow to the area and thereby reduce the skin temperature. Paradiso et

al. [Para_05] have estimated that the energy available from a thermoelectric generator is about 60 $\mu W/cm^2$.

2.4.3 Fuel Cell

A promising energy technology for future mobile and portable applications is the fuel cell. The simplified operating principle of a fuel cell is to break a hydrogen molecule into two hydrogen ions and two electrons on a fuel cell anode. Inside the fuel cell the hydrogen ions travel to a cathode through an ion-porous membrane. Electrons are forced to travel from the anode to the cathode through an external electric circuit, which produces an electrical current. On the cathode, the hydrogen ions and electrons combine with oxygen molecules. This reaction produces pure water as a byproduct, which makes a fuel cell seems like an environment friendly way of producing electric current. It should be noted, however, that a fuel cell is not a primary energy source, but rather a method for transferring energy in the form of hydrogen. The amount of pollution produced depends on the methods used for producing the hydrogen [Knaa_10].

An obvious benefit of a fuel cell is a much faster recharge than secondary batteries, for example. For fuel cells, the recharge only involves filling the fuel tank. However, the fuel is also one of the most problematic parts in fuel cell technology. Pure hydrogen is highly volatile and explosive and requires specialized handling and storage. For example, refilling of a hydrogen tank involves grounding the tank to the same potential as the filling station to prevent sparks that could ignite the hydrogen. There is currently no such delivery system for hydrogen as there is for gasoline or electricity [Snel_09].

Another advantage of fuel cell technology over conventional primary or secondary batteries is that the cell voltage does not degrade during discharge. If enough fuel is supplied to the fuel cell, the cell voltage remains constant until the fuel runs out. However, the fuel cell cannot adjust its output power as efficiently as a battery or a capacitor. Therefore, a plain fuel cell is unlikely to be a suitable power supply for a mobile device. A better option is a hybrid system consisting of a fuel cell, a rechargeable battery and probably a super capacitor. In this arrangement the fuel cell is utilized to charge the battery that supplies energy for an application during high power peaks. If a small rechargeable battery with high output resistance is used, then a super capacitor can be added to provide energy for fast power peaks.

Due to the difficulty of handling pure hydrogen fuel cells, utilizing different fuels is likely to be commercialized first. A good candidate is a direct methanol fuel cell (DMFC) that uses liquid methanol as fuel. In addition to the hydrogen fuel cell, the DMCF also produces carbon dioxide, with water as a byproduct. Safety is also a concern with methanol. Even if methanol is naturally present in the human body, less than 100 ml of it can prove fatal if ingested and not promptly treated. Methanol is also a flammable liquid that burns with a faint blue, almost invisible flame, which may also pose safety risks. [Knaa_10]

In Europe, Japan and United States of America (USA) hundreds of million Euros have been invested in hydrogen and fuel cell research [Neef_09]. For example, in Finland the Finnish Funding Agency for Technology and Innovation (Tekes) has a fuel cell program that started in 2007 and is scheduled to continue until 2013. The Total budget of the program is 144 million Euros with Tekes contributing 50 million Euros [Tekes].

2.5 Communication

In a portable physiological measurement device an important requirement is a wireless data transfer link. Implementation of a pure data logging device with no external communication method during a measurement session is one option, but in this approach it is impossible to execute certain functions such as checking signal quality before measurements. Communication through wires is also possible, but during a measurement session wires impede the subject's normal activity. The most convenient communication method is, therefore, via an inductive or a radio frequency link. A wireless link can be either one-way, when only the measurement data is transferred from the measurement device or two-way, when configuration of the measurement device can also be performed.

An inductive link has been utilized in various applications such as implanted measurement devices similar to those implemented in the Wireless project [Wireless, Hein_06, Riis_07]. An advantage of an inductive link is that the energy required by the implant can be transferred at the same time as the data. The implanted device can, therefore, be manufactured without batteries, which are difficult to replace. However, in order to achieve high energy transfer efficiency, relatively large coils are required in both the external reader device and in the implanted measurement device [Yang_06]. This increases the implant's size and complicates the implantation process. A further problem is that the inductive link does not support high data transfer rates [Yang_06]. In the implant implemented in the Wireless-project, the highest sample rate is 237 10-bit samples per second [Hein_06]. Since every sample contains a six-bit header, the total maximum data transfer rate is 3792 bits per second. One limitation of inductively powered battery-free devices like RFID tags is that they cannot initiate data transfer [Yang_06]. This may pose a problem in certain applications such as those designed to signal an alarm if the subject's vital signs reveal a critical condition.

The most severe drawback of inductive data links is their short operating range. In general, the inductive coupling between the reader and the RFID device is possible in the near field, the upper limit of which is $r_F = \lambda/2\pi$ [Fink_03]. For example, for 13.56 MHz, the limit is 3.5 m. The range for inductive coupling can be increased with lower frequencies, but the size of coils used for communication increases at the same time.

A more convenient way for data transfer is to utilize radio frequency links. Radio links can be implemented in various ways and on different frequencies, depending on application requirements. However, in order to guarantee error free operation, the frequency and operating regulations must be taken into account. In Europe the operation of radio devices is governed by Electronic Communications Committee (ECC), which works under the auspices of the European Communications Office (ECO) and European Conference of Postal and Telecommunication Administrations (CEPT). The Local authority in Finland is the Finnish Communications Regulatory Authority (FICORA). In the USA the Wireless Telecommunication Bureau of the Federal Communication Commission (FCC) regulates the use of the radio spectrum [Yang_06]. An easy approach is to design the radio on license-free frequency bands, which are license-free provided the regulations concerning transmitting power and duty cycle are followed. Table 5 presents several license free channels with their parameters. The listing is not

exhaustive, but it does illustrate global variability. More information can be found in the standards presented in the far right column of the table.

In Europe the main frequency bands for license-free radio transmitters are around 434 MHz, 868 MHz and 2.4 GHz. The frequency channels below one gigahertz are intended for short-range devices (SRD) with the restriction that the audio and video applications are allowed, provided a digital modulation method is used. In North America the license free frequency bands are around 915 MHz (center frequency) and 2.4 GHz. In the USA a few frequency bands are also reserved for Wireless Medical Telemetry Service (WMTS).

Table 5. Frequency bands for low power, short range radio devices [ECO, CFR, Yang_06]

Start of band / MHz	**End of band / MHz**	**Max. TX power**	**Max. Duty cycle**	**Type**	**Region**	**Standard**
433.050	434.790	10 mW	-	SRD	Europe	ETSI EN 300 220
608	614	200 mV/m[i]	-	WMTS	USA	FCC CFR 47 parts 95.530, 95.639
868	868.6	25 mW	1 %	SRD	Europe	ETSI EN 300 220-1
868.7	869,2	25 mW	0.1 %	SRD	Europe	ETSI EN 300 220-1
869.4	869.65	500 mW	10 %	SRD	Europe	ETSI EN 300 220-1
869.7	870.0	5 mW	-	SRD	Europe	ETSI EN 300 220-1
902	928	50 mV/m[i]	-	ISM	USA, Canada	FCC CFR 47 parts 15.247, 15.249,
1395	1400	740 mV/m[i]	-	WMTS	USA	FCC CFR 47 parts 95.530, 95.639
1427	1429.5	740 mV/m[i]	-	WMTS	USA	FCC CFR 47 parts 95.530, 95.639
2400	2483.5	10 mW 50 mV/m[i]	-	ISM	Europe USA	ETSI EN 300 328 ETSI EN 300 440 FCC CFR 47 parts 15.247, 15.249
2471	2497	10 mW	-	ISM	Japan	ARIB STD T-66
5725	5875	25 mW 50 mV/m[i]	-	SRD	Europe USA	ETSI EN 300 440 FCC CFR 47 parts 15.247, 15.249

From Table 5 it can be seen that there is no single frequency band that could be utilized globally. The 2.4 GHz Industrial Scientific and Medical frequency band is a good candidate. This band can be utilized without a license in Europe, USA and in Japan, but it should be noted that the band limits slightly vary in different countries. A noticeable difference between Europe and USA on this frequency band is the maximum permitted

[i] Measured at distance of 3 meters

transmission power. If a radio transmitter is utilizing only a single channel, the maximum permitted power in Europe and in Japan is 10 mW and in USA about 0.75 mW (calculated at a field strength of 50mV/m), as presented in Table 5. This needs to be taken into account when designing a transmitter for global markets. In addition, if the transmitter utilizes multiple channels, as in frequency hopping, higher transmit frequencies are allowed. For example, FCC CFR 47 part 15.247 states that a transmitter on 2.4 GHz ISM frequency band in USA can output power up to one watt if Frequency Hopping Spread Spectrum (FHSS) or Direct Sequence Spread Spectrum (DSSS) techniques are used. Likewise, European Standard, ETSI EN 300 328 of the European Telecommunications Standards Institute (ETSI) specifies a maximum output power of 100 mW for devices on the 2.4 GHz band utilizing FHSS and DSSS.

The implementation of a cost effective wireless link requires that at least integrated transceiver ICs are utilized instead custom-designed multi-component radio circuits. Four different radio transceivers operating on license free frequency bands are tested in publication [P9]. The tested circuits are nRF401 form Nordic Semiconductors (formerly known as Nordic VLSI), XE1201 from Xemics SA (a business unit of Semtech Corporation since 2005), CC900 and CC1000 from ChipCon (a subsidiary of Texas Instruments since 2006). The tests involved measuring the range of radio links and the power consumption of radio circuits on different transmission power setups. An index number, the radio link's power consumption over the link's range, is calculated from the measurement results: the smaller the index, the more efficient the radio circuit. The results show that the most efficient radio circuit of the four ICs tested is the CC1000. Another benefit of the CC1000 is that it requires only a few external components, while impedance matching to a 50 Ω antenna can be implemented with only five passive components.

Of the circuits tested, the internal implementation of nRF401 is the simplest. This circuit contains only a few digital electronics and simply sends the data received from a serial bus to the antenna and vice versa. Even changing the transmitting power in nRF401 is simple to implement by changing a resistor connected to one pin of the IC component. XE1201, CC900 and CC1000 all contain a certain amount of inbuilt digital electronics and a connection for a digital control bus, which can be utilized, for example, to adjust the transmitting power through software. However, none of these circuits provides any support for network operation or packet orientated communication. For example, the ICs in question can have only one radio link open at a time so that if point-to-multipoint or star-like networks are needed, they must be implemented by the user with software. The lack of network support makes the circuits tested very suitable for point-to-point links, which are ideal when implementing a wireless connection between a portable physiological measurement device and a data terminal device.

Nowadays one way to speed up the design process and reduce implementation and development costs is to employ standardized wireless technologies, like Bluetooth and Zigbee. There are obvious advantages to standardized technologies such as Bluetooth. Since many cell phones and other portable devices like laptop computers already contain a Bluetooth interface, they can be easily used as a user interface or as a data terminal device for other devices. Table 6 presents the most common, currently available short-range communication protocols with their key properties.

Table 6. Comparison of RF-communication protocols [Adam_06, Lee_07, Bake_05, Yang_06, ANT, BTSIG]

	Wi-Fi	**Bluetooth**	**UWB**	**ZigBee**	**ANT**
IEEE specification	802.11a/b/g	802.15.1	802.15.3a	802.15.4	-
Frequency band(s)	2.4 GHz 5 GHz	2.4 GHz	3.1 – 10.6 GHz	868/915 MHz 2.4 GHz	2.4 GHz
Typical TX power	14 – 20 dBm	0 – 20 dBm	8 dBm	-25 – 0 dBm	-20 – 0 dBm
Maximum signal rate	54 Mbps	1 Ms/s[i]	11 Mb/s	250 Kb/s	1 Mbps [ii]
Range	100 m	10 – 100 m [iii]	10 m	10 – 100 m	1 – 30 m
Supported network topologies	(I)BSS[iv]	Peer-to-peer, star	Peer-to-peer	Peer-to-peer, star, tree, mesh	Peer-to-peer, star, tree, mesh
Maximum network size (nodes)	2007	8	8	>65000	2^{32}
Power consumption [v]	300- 600 mW BGW211	200 mW LMX9830	-	55-78mW CC2520	<40mW[vi]
Software stack	100 KB	256 KB	-	62 KB	2 KB

Wireless Fidelity (Wi-Fi) includes Institute of Electrical and Electronics Engineers (IEEE) standards for Wireless Local Area Networks (WLAN) [Lee_07]. Wi-Fi is mainly used to provide an internet connection for portable devices like laptop computers and cell phones. Devices can connect to the Wi-Fi network in two different modes. The first one is an infrastructure mode in which each device connects to an access point. The second one is an ad-hoc mode, in which devices are able to communicate directly between each other with peer-to-peer connections. Wi-Fi provides a high data rate and a long link range, though it consumes a lot of power. In portable battery-powered physiological recording devices a power consumption of 600 mW is many times too much.

Currently, the best known wireless protocol is probably Bluetooth, which is widely integrated in applications such as cell phones and portable computers. The Bluetooth specification was originally developed by a Bluetooth Special Interest Group (SIG). The original founders of the Bluetooth SIG were Ericsson, Nokia, IBM, Intel, and Toshiba. Bluetooth was designed to replace cables between computers and computer peripherals,

[i] The maximum symbol rate in the air is one mega symbol per second.
[ii] Maximum RF data rate for nRF24AP1. Maximum sustainable data rate 20 kbps.
[iii] Depending on the device class.
[iv] BSS refers to basic service set, in which devices connect to an access point (AP), i.e. base station. IBSS refers to independent basic service set, in which devices connect to each other in ad-hoc network.
[v] Estimated on 3V supply voltage.
[vi] Estimated maximum power consumption with maximum data transfer rates.

such as mice, keyboards, joysticks, and printers [Lee_07]. However, Bluetooth rapidly became a synonym for short-range radio communication. After the Bluetooth V1.1 specifications were finalized, the IEEE adopted and converted it into an IEEE standard, published in June 2002 [Yang_06]. Bluetooth operates on the 2.4 GHz ISM frequency band and provides relatively high data rates. The Bluetooth specification utilizes the frequency band as multiple 1 MHz channels, which restricts the maximum symbol rate on one channel to one mega symbol per second. However, with different modulation techniques the maximum data rate can be as much as 3 Mbit/s, as in the Bluetooth definition v2.0 + EDR (Enhanced data rate). Though the utilization of higher data rates increases the radio's peak power consumption, data transfer is also faster, resulting in decreased average power consumption.

Bluetooth technology continues to evolve. The next versions of Bluetooth aim for faster communication speeds and lower energy consumption. In April 2009 the Bluetooth SIG announced the release of the new Bluetooth high-speed specification, version 3.0 + HS. The maximum data rate of this version is approximately 24 Mbit/s and it is acquired by adopting the IEEE 802.11 radio protocol into the Bluetooth specification. The high-speed link is controlled with the usual Bluetooth radio link but data is transferred through a high speed "pipe" implemented with 802.11 [BTSIG, Hänn_09].

In late 2009, the Bluetooth SIG announced that part of the Bluetooth specification 4.0 is a Bluetooth Low Energy Technology (BT-LET). The Bluetooth specification 4.0 combines three technologies; "classic" Bluetooth technology, high-speed technology, and low energy technology. Low power Bluetooth is intended for devices such as watches, sporting heart rate monitors, and toys in which energy consumption is a critical factor. The main idea in the low energy Bluetooth is to allow implementation of two different kinds of device, dual-mode and single-mode. In dual-mode devices, the low energy function is integrated into an existing classic Bluetooth controller, which ensures compatibility with existing hardware. Single-mode devices include a lightweight link-layer that provides low power consumption. [BTSIG, Hänn_09].

One promising technology in recent years has been Ultra Wide Band (UWB) radio. This technology has been designed to be standardized as IEEE 802.15.3a. However, the group responsible for preparing the standard failed to agree on a choice between two technology proposals and the group was disbanded in 2006.

ZigBee is a communication protocol developed by the ZigBee alliance [ZigBee]. ZigBee applications communicate through Physical and Medium Access Control layers defined in the IEEE 802.15.4 standard. This standard enables ZigBee to operate not only on the 2.4 GHz frequency bands, but also on the less crowded sub-gigahertz 868/915 MHz frequency bands.

As mentioned earlier, a major difference between Bluetooth and ZigBee is that Bluetooth is designed to be a wireless cable replacement technology. Therefore it does not support any kind of automatic network formation [Yang_06]. Bluetooth specification defines two communication topologies; piconet and scatternet. A piconet is a net of a maximum of eight Bluetooth devices, in which one device operates as a master and the others as slaves. A scatternet is a collection of piconets, in which one Bluetooth device can participate in several piconets at the same time. A device in a

scatternet could be a slave in multiple piconets but a master in only one [Lee_07]. A problem with piconets is that if the master device becomes inoperative, the entire piconet collapses [Yang_06]. ZigBee's network layer supports star, mesh, tree, and peer-to-peer networks. A mesh topology provides multiple paths for a message to travel through a network and is thus more reliable than a star network.

A lesser known radio protocol operating on 2.4 GHz frequency band is ANT [ANT], developed by Dynastream Innovations Incorporated. ANT is designed for applications requiring ultra low power consumption. As can be seen in Table 6, the maximum power consumption with maximum data transfer rate is less than 40 mW for an AP1 chip or module. On lower transmission rates the power consumption decreases dramatically. Data on ANT link is transferred as 8-byte-long packets called messages. For example, on a message rate of one hertz, radio power consumption is about 450 μW. A message rate this low is adequate for simple applications like heart rate or temperature monitors. With newer AP2 chips or modules, power consumption decreases even further.

Integration of an ANT link into an application is designed to be very easy. This is achieved by encapsulating most of the communication stack required for the data link operation into an ANT radio chip. The host of an ANT link can therefore be implemented with a low-cost 4- or 8-bit microcontroller, which implements the session, presentation and application layers of the data link's software stack. This leads to minimal code size in the host microcontroller and, for example, a generic code supporting eight channels fits into a 16 Kbyte code space. Furthermore, a simple monitoring application with only one active link can be packed into a 2 Kbyte memory. [ANT].

A disadvantage of the ANT protocol is that it does not support frequency hopping. In certain environments this may reduce the reliability of links on crowded channels. However, an ANT radio can be configured to operate on 125 different 1 MHz channels so, if needed, a frequency hopping protocol or switching to a less crowded channel can be implemented on the application layer. A drawback in changing the frequency of a channel is that it must be closed and reopened and this restricts the hopping speed and increases energy consumption. The tolerance of ANT protocols of other transmitters on 2.4 GHz frequency band is relatively good even without frequency hopping. This tolerance is based on Time Division Multiple Access (TDMA) like adaptive isochronous network technology. As stated already, ANT radio uses small messages for transmitting data. The transmission timeslot for one message is very short, only 150 μs, and messages are sent at regular intervals. If interference from another transmitter is detected, the radio can adjust the timing of the slots and thus reduce the interference.

The ANT link is utilized in numerous commercially available applications. For example, Garmin [Garmin] has utilized ANT technology in bicycle computers and sport watches. Suunto [Suunto] has utilized ANT for connecting different measuring pods and belts to a sport watch. More commercially available applications utilizing ANT technology can be found on the technology's homepage [ANT]. ANT has also been utilized in the portable physiological measurement devices presented in publications [P1] – [P4].

2.6 Data Storing

In every measurement device, some amount of memory for data storing is required. The amount of memory needed varies greatly according to the device's functionality. If the measurement device is a simple data forwarder, which measures physiological signals and sends results to a data terminal or user interface device via a communication link, then a small amount of memory for data buffering might be sufficient. In long-term data logging devices, however, larger memories are required.

Memories can be classified into various categories. A main division is between read-only and read-write memories. Data content of a read-only memory can be written, for example, during the memory manufacturing process or only once, such as during microcontroller programming. Read-only memories are therefore suitable for storing constant data like a microcontroller's program in a portable physiological measurement device, but they cannot be utilized for storing run-time data. For data storing, a read-write memory must be utilized. Read-write memories fall into two main groups; volatile memories and nonvolatile memories (NVM). The difference between these is in unpowered data retention, i.e. whether the data is preserved when the supply voltage is switched off. Volatile memories, like Static Random Access Memory (SRAM) and Dynamic Random Access Memory (DRAM), lose the stored data when power is switched off. Nonvolatile memories, like Electric Erasable Programmable Read-Only Memory (EEPROM) and Flash memory, retain the data during a power down.

For a short term measurement, data-buffering volatile memories usually suffice. This is because many microcontrollers and microprocessors already have a small amount of volatile memory integrated on the same chip with the processor. Usually the integrated volatile memory is SRAM because data stored in SRAM does not require regular rewriting, as it does in DRAM. Consequently, current consumption in SRAM is lower than in DRAM, especially in idle mode. Moreover, SRAM is faster than DRAM. A drawback of SRAM is smaller cell density compared to DRAM: a one-bit memory cell implemented with SRAM technology requires more silicon area than the equivalent cell with DRAM technology. [Maci_02]

In data logging devices, a nonvolatile memory is preferred. NVM increases reliability because the measured data is not lost in the case of a power down or a reset. In portable and mobile devices, utilization of conventional hard drives based on a rotating magnetic disk is not an ideal option because these disks are very sensitive to movement. A more robust solution is to use nonvolatile semiconductor memories. Usually these memories are in the form of EEPROM or Flash. The basic structure and operation of both memories is similar and is based on a floating gate transistor. Flash is actually an EEPROM in which the whole memory, or a sub array within a memory chip, must be erased at one time. In contrast, EEPROM and, especially E^2PROM, enable erasure of one byte at a time. [Brew_08, Bez_03]

An advantage of floating gate memories is very low current consumption in idle mode. As the classification into non-volatile memories implies, no current is required for data retention. However, the leakage currents of interfacing and controlling electronics cause small idle mode energy consumption. Floating gate memories do have certain drawbacks. One is the relatively high current required during writing and reading

procedures. For example, the AT25DF641, a 64-Megabit flash memory manufactured by Atmel Corporation, has a standby mode current consumption of 25 μA, whereas the current consumption for reading and writing are 5-10 mA and 12 mA respectively. Another drawback is a long writing time. For the AT25DF641, writing a page of 256 bytes takes one millisecond. From the human perspective this is infinitesimal, but in the same time a reduced instruction set microcontroller operating at a clock frequency of 10 MHz can execute ten thousand instructions. Furthermore, an erase operation, required before new data can be written, takes almost one second in a worst case scenario [AT25DF641].

Due to leakage currents, the data stored in a non-volatile floating gate memory is not preserved forever. The minimum data retention time of a non-volatile memory is usually specified as ten years, which in a portable measurement device is often sufficient. Another issue to consider is the memory's endurance. Repetitive writing and erasing cycles are known to impair the performance of floating gate memories. However, the typical endurance of a flash memory is approximately 10^5 cycles, which in data storing applications, for example, is not a limiting factor because over ten years, the memory could be rewritten approximately 30 times per day.

NVM semiconductor memories are available as integrated circuits, which can be soldered on the printed circuit board (PCB), and as various types of removable memory cards, utilized in commercially available cell phones, digital cameras, and MP3-palyers. The advantage of IC-like memory chips is that they can be attached to the system during the normal manufacturing process. However, in portable physiological measurement devices, the computational power of a microprocessor or a microcontroller communicating with the memory is relatively low. This is also the case for the speed of the communication link between the device and a computer. If the amount of recorded data is large, low speeds pose a problem because transferring data from the memory takes a long time. An easy way to overcome this is to utilize a removable memory card. Depending on the application implementation, the memory card can be fairly easily removed from the device and attached to an external memory card reader, which can handle the data transfer rapidly. A drawback to this approach is that a file system, like file allocation table (FAT), must be utilized on the memory card. The file system requires slightly more computational power than one without a file system, which naturally increases energy consumption.

A very attractive type of memory card for portable applications are secure digital (SD) cards, particularly the smallest versions in the form of a micro secure digital card (μSD) and a micro secure digital high capacity (μSDHC) card [SDCARD]. The physical size of both cards is very small 15 x 11 x 1 mm. The SD cards are also asymmetric in shape so that they cannot be inserted incorrectly. The maximum capacity of a conventional SD is 2 Gigabytes (GB) and for SDHC 32 GB. The interface for a SD card can be implemented with three different signaling methods, one-bit or four-bit SD-mode signaling, or with serial peripheral interface (SPI) signaling [SDIO_07]. Because many microcontrollers and microprocessors contain hardware level support for SPI bus, this interfacing mode is an easy option for interfacing a SD card in portable applications. A drawback is that with μSD cards, the SPI is an optional interface. However, it now seems that the SPI interface is implemented in most μSD cards.

The next generation of the SD cards is a secure digital extended capacity (SDXC), which support memory sizes up to 2 Terabytes. The SDXC specification was released in April 2009 and Team Group Incorporated [Team] has already presented a 64GB SD card. It should be noted that previous SD card versions are compatible with SDXC host applications, but if SDXC card is formatted in former host devices, the card's capacity cannot be fully utilized [SDCARD].

Supply voltage range for SD cards is defined as 2.7 – 3.6 V [SDSpec_06]. This voltage range is also suitable for many portable devices because it can be easily produced with batteries such as two 1.5 V primary batteries or with a 3.6 V primary or secondary lithium battery. The current consumption of memory cards varies according to the manufacturer, but it can be even several tens of mA. This must be taken into account when designing a memory card based device. For example, some coin-shaped primary batteries cannot supply the high peak currents drawn by a SD card.

2.7 Decreasing the Amount of Components

As technology evolves, increasing functionality is added to single integrated circuit components. This makes it possible to implement electronic devices with fewer components and hence decrease the area required for the components on the PCB and often, also the power required by the circuit. An even greater advantage is that the design process takes less time, so products can be launched on the market earlier.

An example of component integration is the ADS1298 [ADS1298] component, manufactured by Texas Instruments. The ADS1298 is a complete analog front end for ECG and electroencephalogram (EEG) measurements. This integrated circuit contains all the required components for implementing simultaneous measurement on eight measurement channels. Power consumption is also low, only 1 mW/channel. IC is available in Plastic Quad Flatpack and in Plastic Ball Grid Array package. The packages measure 12 x 12 mm and 8 x 8 mm, with a PCB area of 144 mm^2 and 64 mm^2 respectively. For comparison, a one channel ECG measurement implemented with discrete components, as in [P1]-[P4], requires more PCB area and energy. For example, the ECG measurement electronics in [P4] require 21 passive components, three integrated circuits, one channel from the ADC integrated into a microcontroller and a PCB area of 225 mm^2.

Another integration example is the SensRcore™ Platform produced by ANT [ANT]. The platform includes an ANT-compliant radio and a baseband processor with firmware supporting simple measurement operations. Each drop-in SensRcore™ module can provide at least one radio link and four data channels, which can be either analog or digital. Operation of the module is controlled with a simple script, which is created using a software tool provided by the module manufacturer. The module measures 20 x 20 mm and the average current consumption is only 13 μA per measurement message. Utilization of the SensRcore™ module simplifies the development process because the module has already been certified to comply with the radio regulation standards.

3 Physiological Measurements

There are many types of physiological signals that can be monitored by means of portable devices. Classification of signals is challenging and can be done in various ways. One way is to divide signals into vital signs and other signals. Vital signs are measurements of physiological signals that enable the assessment to the most basic body functions. The standard vital signs are physiological signals monitored from a patient in a hospital environment and include blood pressure, heart rate, ECG, respiratory rate, and temperature [Aziz_06].

This section presents the basic theoretical background of the signals measured with the devices implemented in this work. These signals are temperature, acceleration, bioimpedance, and ECG.

3.1 Temperature

Humans belong to a group of homeothermal animals, meaning that the temperature of the human body is kept at a constant level that is usually higher than the ambient temperature. Because the heat produced in the body is lost to the environment from the body surface (e.g. the skin), the temperature of the parts nearest the body surface is lower than that of the central parts. The temperature of the skin varies a great deal according to the surroundings, whereas the temperature of the body core remains constant at around 37 °C. In other words, the shell of the human body is poikilothermic and the body core is homeothermic. However, the temperature of the body core also varies during the day. The maximum is achieved during the daytime and the minimum before morning. This variation can be as much as 1 °C. [Schm_89]

A temperature zone, inside which the body's heat production and heat loss are equal, is called a thermoneutral zone. At the highest temperature, the production of heat is greater than heat dissipation. The highest core temperature that a human body can tolerate for a short term is about 42 °C. A condition of extreme heat load, exceeding the body's capacity to lose heat is called hyperthermia. In prolonged hyperthermia, in which the temperature measured from rectum is above 39.5 °C – 40 °C, severe damage is caused to the brain and usually leads to death. This syndrome is called heat-stroke. Conversely, in temperatures below the thermoneutral zone, more heat is lost than can be produced by the body. Long exposure to low temperatures leads to hypothermia. If the body temperature falls to 26 – 28 °C, death can occur by myocardial fibrillation. [Schm_89]

The body mainly dissipates heat in four different ways; conduction, convection, radiation, and evaporation. Conduction occurs when the body is in contact with a firm substrate, such as a chair. If the skin is warmer than the surrounding air, the air layer near the skin is warmed, which causes it to rise and cooler, denser air flows in to fill the space. This phenomenon is called convection. Heat is also dissipated in the form of long-wavelength infrared radiation. Evaporation is caused by the evaporation of water

from the skin, usually in the form of sweating. [Schm_89] At room temperature, approximately 66% of the naked body's heat loss is caused by radiation, 15% by convection and conduction, and the rest by evaporation [Nien_93].

If the body cannot dissipate the heat caused by muscular activity or absorbed from the ambient environment during activity in warm environments or during strenuous exercise, human performance may be impaired [Nien_93]. The first symptoms of this inability to dissipate heat, called heat stress, are increased heart rate and increased body temperature. If heat is not dissipated and the body is not cooled down, symptoms like fatigue, light-headedness, or nausea may result. However, heat stress symptoms are highly individual and subjective, and may not be evident until unsafe levels are reached. Failure to detect excessive physiological strain can lead to heat illness and can be fatal in extreme cases [Obri_88].

3.1.1 Measuring Body Core Temperature

Monitoring body temperature during physical exercise or working in extreme temperatures could be utilized to prevent temperature-related symptoms. Body core temperature can be measured using several different methods. For instance, oesophageal temperature is measured with a temperature transducer inserted into the patient's oesophagus. Even though this measurement method is uncomfortable, it accurately reflects temperature variations in the blood leaving the heart. Rectal temperature is measured at the rectum, which is surrounded by a large mass of abdominal muscles with low thermal conductivity. Therefore rectal temperature is independent of ambient conditions. Intra-abdominal temperature is measured with a temperature transducer which is swallowed. Measured temperatures vary according to the location of the transducers inside the body. However, when taken in the stomach or the duodenum, the observed variations are similar to those in oesophageal measurement. Oral temperature is taken from the mouth beneath the tongue. It is important that the mouth is closed during measurement to prevent the ambient temperature affecting the measurement. Temperature can also be measured from the ear, either at the tympanic membrane or in the auditory canal. A relatively good estimate of the body's core temperature is achieved by measuring the temperature of urine during its discharge. However, such measurement must be taken either during discharge or immediately after it in order to prevent urine cooling. [ISO9886]

3.1.2 Measuring a Skin Temperature

Skin temperature varies greatly over the body surface. Therefore a distinction has to be made between local skin temperature measured at a specific point on the body surface and mean skin temperature measured over the entire body surface. Mean skin temperature cannot be measured directly and is estimated as a weighted average of local skin temperatures measured from predefined locations on the body surface. Measurement locations defined in international standard ISO 9886 [ISO9886] are presented in Figure 8. The skin temperature value t_{sk} is calculated using equation (9), in which k_i is a weighting coefficient and t_{ski} the local temperature. According to ISO-standard 9886, skin temperature can be calculated from all fourteen-measurement points or from a subset of four or eight points. When calculated from fourteen points, all have an equal weighting coefficient but if calculated from fewer temperatures, the weighting coefficients change. Standardized measurement locations and weighting

coefficients for different measurement setups are presented in Table 7. In conditions that are close to thermal neutrality, it is recommended to utilize the eight or fourteen point scheme. In these conditions it is possible to add additional measurement points such as from the fingers and toes. In warm conditions the four-point scheme can be utilized if the radiation temperature is symmetrical. Even though the skin temperature varies at different locations of the body, it provides a useful estimate of the body's thermal comfort.

$$t_{sk} = \sum k_i t_{ski} \tag{9}$$

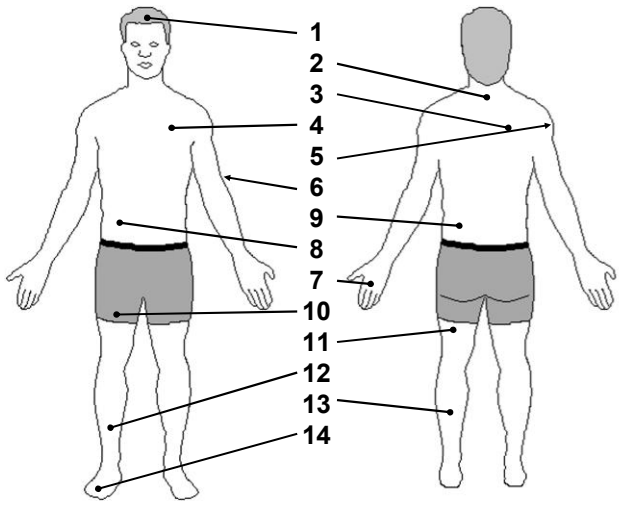

Figure 8. Measurement positions for measuring skin temperature, defined in the ISO standard 9886 [ISO9886].

Table 7. Measurement locations and weighting coefficients of skin temperature defined in international standard ISO 9886 [ISO9886].

	Sites	**4 points**	**8 points**	**14 points**
1	Forehead		0.07	1/14
2	Neck	0.28		1/14
3	Right scapula	0.28	0.175	1/14
4	Left upper chest		0.175	1/14
5	Right arm in upper location		0.07	1/14
6	Left arm in lower location		0.07	1/14
7	Left hand	0.16	0.05	1/14
8	Right abdomen			1/14
9	Left paravertebral			1/14
10	Right anterior thigh		0.19	1/14
11	Left posterior thigh			1/14
12	Right shin	0.28		1/14
13	Left calf		0.2	1/14
14	Right instep			1/14

The precision of the temperature gauge utilized in skin temperature measurement must be ±0.1 °C in the range of 25 °C to 40 °C. If the measurement is carried out in a cold environment, the precision range should be extended to 0 °C. The thermal capacitance of the gauge must be low, and 90% response time should be as short as possible, with a maximum limit of 0.5 min. [ISO9886]

3.2 Acceleration

Nowadays acceleration can be measured fairly easily with single-chip micro electrical mechanical system accelerometers. Acceleration is often divided into static and dynamic acceleration. Static acceleration is experienced when the acceleration sensor or the measurement object are motionless. In these cases acceleration is relatively constant and caused by gravity and a possible tilt position. Accelerometers can be utilized to measure direct accelerations for several reasons, such as studying the stress directed to the body in motor sports. Accelerometer data can also be utilized to produce indirect measurement of body-related signals such as calculating the number of steps taken [Sang_08] or to help in measuring the frequency of coughing [Jaeg_95]. Acceleration data can also be used to remove motion-related artifacts (e.g., from an ECG signal), and to detect postural changes during sleep [Kish_07].

3.3 Posture and Gesture

Measurements of body posture can be utilized for numerous purposes such as in fitness training and in rehabilitation after a surgery. They can also be used as preventive measurements such as monitoring back position when seated on an office chair [Matt_07]. Body posture can be measured using various techniques. Harms et al. [Harm_08] reported good results in posture recognition with a smart shirt containing accelerometers. Dunne et al.[Dunn_06] utilized a plastic optical fiber to measure spinal posture. A sensor made of the plastic optical fiber is stitched to the back of a garment near the spine. This setup provides a way to improve seated spinal posture. Mattmann et al. [Matt_07] used strain sensors to detected upper body postures. In their study strain sensors are manufactured from commercial thermoplastic elastomer which is filled with carbon black powder. With 21 sensors placed on the back of a close-fitting garment, the authors were able to identify between 15 sitting 12 standing postures. Tognetti et al. [Togn_06] have captured and classified body postures and gestures using conductive elastomer as a strain gauge. Sensors made of conductive elastomers have been integrated directly into a shirt and a glove made of Lycra fabric. Bachmann et al. [Bach_03] have tracked the human posture and position with sensors that contain accelerometers, gyroscopes and magnetometers. This application is to enable body tracking in immersive synthetic environments.

3.4 Electrical Bioimpedance

Electrical impedance is the ability of a given material to impede the flow of an electrical charge, i.e. current. Impedance consists of two parts; resistance and reactance. In Cartesian terms, impedance can be given as $Z = R + jX$, where resistance R is the real part of the impedance and reactance X is the imaginary part. The resistance part of the impedance is the material's ability to dissipate electrical energy whereas reactance is

the material's ability to accumulate and release electrical energy. In other words, reactance impedes a change of current. The term electrical bioimpedance in biomedical engineering refers to the way an organism or biological material impedes the flow of electrical charges when an electrical field is applied.

In order to measure impedance, an electrical alternating constant amplitude current (i.e. electrical excitation current) must be injected into the sample and the voltage generated by the current must be measured. The impedance can then be calculated with equation $Z_{calculated} = U_{measured} / I_{excitation}$. Impedance is usually presented as magnitude and phase angle $|Z|\angle\varphi$, where $|Z|$ is relation and $\angle\varphi$ the phase angle between voltage and current.

Bioimpedance is a preferred measurement method because it is non-invasive and causes no patient discomfort. Measurements can be made quickly and repeated at short time intervals. Bioimpedance measurement devices are also inexpensive, portable, and relatively easy to use [Ling_99].

3.4.1 Electrode Setup

Electrical bioimpedance can be measured with two, three, or four electrodes. In a two-electrode configuration, the same electrodes are utilized for feeding the excitation current and for measuring the voltage generated by the current, as can be seen on the left in Figure 9. Here Z_1 and Z_2 are impedances of the skin electrode interface and Z_{TUS} is the impedance of the tissue to be measured, (Tissue Under Study, TUS). The impedance value measured with the two-electrode setup is calculated with equation (10) and equation (11). As can be seen from equation (11), in the two-electrode measurement setup not only is the tissue impedance measured, but also the impedances in the skin electrode interface.

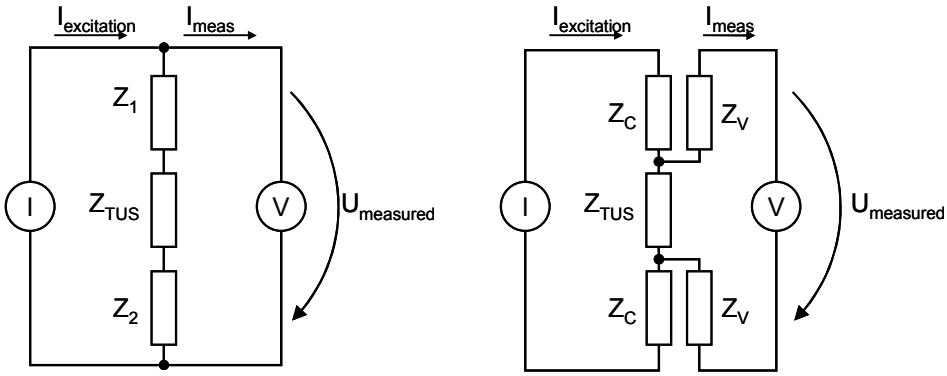

Figure 9. Two electrical bioimpedance measurement setups. On the left, a two-electrode setup and on the right, a four electrode setup. In the circuits, I is a constant amplitude excitation current generator and V is a voltmeter measuring the voltage generated by the excitation current. Z_1, Z_2, Z_C, and Z_V are electrode impedances and Z_{TUS} is the measured tissue impedance.

A problem arises with the electrode skin impedance, which is not stable and changes, especially during movement. Impedances Z_1 and Z_2 and are also clearly higher in magnitude than Z_{TUS} and therefore make it impossible to detect small changes in the

Z_{TUS}. This problem can be overcome with a four-electrode setup, also known as tetrapolar configuration, which is presented on the right in Figure 9. In this setup the impedance can be calculated from equation (12) and equation (13).

$$Z_{calculated} = \frac{U_{measured}}{I_{excitation}} = \frac{(Z_1 + Z_{TUS} + Z_2)(I_{excitation} - I_{meas})}{I_{excitation}} = \frac{(Z_1 + Z_{TUS} + Z_2)I_{excitation}}{I_{excitation}} - \frac{(Z_1 + Z_{TUS} + Z_2)I_{meas}}{I_{excitation}} \quad (10)$$

Because $I_{excitation} >> I_{meas}$

$$Z_{calculated} \approx \frac{(Z_1 + Z_{TUS} + Z_2)I_{excitation}}{I_{excitation}} = Z_1 + Z_2 + Z_{TUS} \quad (11)$$

$$(I_{excitation} - I_{meas})Z_{TUS} - Z_V I_{meas} - U_{measured} - Z_V I_{meas} = 0$$
$$U_{measured} = (I_{excitation} - I_{meas})Z_{TUS} - 2Z_V I_{meas} \quad (12)$$
$$U_{measured} = I_{excitation}Z_{TUS} - (2Z_V + Z_{TUS})I_{meas}$$

Because $I_{excitation} >> I_{meas}$.

$$Z_{calculated} = \frac{U_{measured}}{I_{excitation}} = \frac{I_{excitation}Z_{TUS} - (2Z_V + Z_{TUS})I_{meas}}{I_{excitation}} = Z_{TUS} \quad (13)$$

As can be seen from equations (12) and (13), with the tetrapolar measurement setup the effect of electrode-skin interface is minimized provided the current I_{meas} is kept low. Voltage over the tissue is usually measured with an instrumentation amplifier (IA), as illustrated in Figure 10. I_{meas} is mainly caused by the input bias currents of the instrumentation amplifiers, which are often in the range of pico or nano amperes.

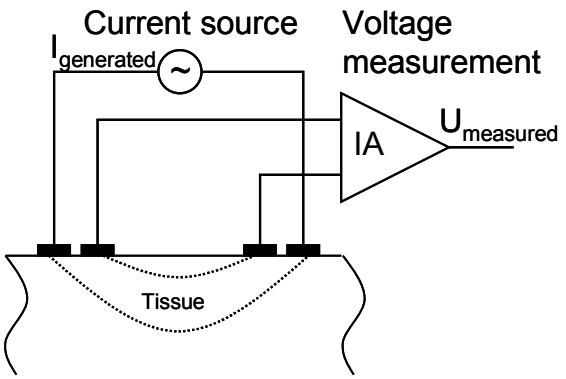

Figure 10. A typical four-electrode, tetrapolar, bioimpedance measurement setup. An alternating constant amplitude excitation current is generated with a current source. Voltage generated by the current flowing through the tissue is measured with an instrumentation amplifier.

3.4.2 Electrical Bioimpedance of the Human Body

In the human body there are numerous different cells, tissues and organs with membranes (e.g. cell membranes, lungs, stomach, etc.). A simple two-component model of a tissue consists of a resistor and a capacitor connected in parallel, as shown on the left in Figure 11. In this model, the conductance $G(\omega)$ models the outer cell environment's ability to constrain current flow and capacitor C_P represents the capacitance of the cell membranes. This model is useful for various purposes such as estimation of total body water (TWB) where the $G(\omega)$ correlates well with the water in the outer cell environment. However, measuring the $G(\omega)$ and C_P directly involves feeding a tissue with a constant amplitude voltage and then measuring the current caused by this voltage, as depicted on the left in Figure 11. In this measurement setup the measured admittance is directly proportional to the measured current, which enables easy calculation of $G(\omega)$ and C_P values. As stated, the constant voltage measurement poses a problem since the electrode-skin impedance is unstable and changes because of motion and other factors. A way to overcome this problem is to use constant amplitude current and measure the voltage induced by the current, which removes the electrode interface problem. This measurement setup is presented on the right in Figure 11. In idealized models, components $G(\omega)$ and $R_S(\omega)$ are ideal and independent of frequency. In reality, both elements are frequency dependent and this is represented by the omega symbol.

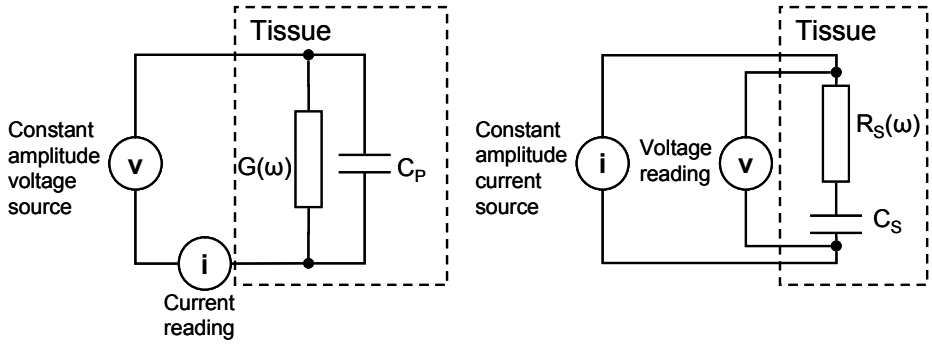

Figure 11. Constant amplitude voltage measurement setup on the left and constant amplitude current measurement setup on the right.

Many bioimpedance measurement devices represent impedance information as the modulus of the impedance and the phase angle between the current and voltage $|Z|\angle\varphi$. This presentation can be converted to serial model values with equations: $R_S(\omega) = |Z|\cos(\varphi)$ and $1/\omega C_S = |Z|\sin(\varphi)$. Likewise, the admittance of the parallel model $|Y|\angle\varphi$, measured with a constant amplitude voltage method, can be converted to corresponding parallel model values with equations $G(\omega) = |Y|\cos(\varphi)$ and $\omega C_P = B_P = |Y|\sin(\varphi)$. If necessary, values of the serial impedance model can be converted to values in the parallel model and vice versa through calculations presented in equations (14) – (19).

$$\frac{1}{Z} = \frac{1}{R_S(\omega) + 1/j\omega C_S} = \frac{R_S(\omega) - 1/j\omega C_S}{R_S(\omega) - 1/j\omega C_S} \frac{1}{R_S(\omega) + 1/j\omega C_S}$$
$$= \frac{R_S(\omega) - 1/j\omega C_S}{R_S^2(\omega) + 1/\omega^2 C_S^2} \tag{14}$$

Because $Y = G(\omega) + jB_P$, and because admittance is an inverse of an impedance ($Y = 1/Z$) on a defined frequency we can write

$$Y = G(\omega) + jB = G(\omega) + j\omega C_P$$
$$\equiv \frac{1}{Z} = \frac{R_S(\omega) - 1/j\omega C_S}{R_S^2(\omega) + 1/\omega^2 C_S^2} = \frac{R_S(\omega)}{R_S^2(\omega) + 1/\omega^2 C_S^2} - \frac{1/jC_S\omega}{R_S^2(\omega) + 1/\omega^2 C_S^2}. \tag{15}$$

Then, because conductivity is an inverse of resistance, $G(\omega) = 1/R_P(\omega)$ and comparing the real and imaginary parts in the equation (15), we can write

$$\frac{1}{R_P(\omega)} \equiv \frac{R_S(\omega)}{R_S^2(\omega) + 1/C_S^2\omega^2} = \frac{R_S(\omega)C_S^2\omega^2}{R_S^2(\omega)C_S^2\omega^2 + 1}$$
$$\Rightarrow R_P(\omega) = R_S(\omega) + \frac{1}{R_S(\omega)C_S^2\omega^2} \tag{16}$$

$$j\omega C_P \equiv \frac{-1/jC_S\omega}{R_S^2(\omega) + 1/C_S^2\omega^2} = \frac{jC_S\omega}{R_S^2(\omega)C_S^2\omega^2 + 1}$$
$$\Rightarrow C_P = \frac{C_S}{R_S^2(\omega)C_S^2\omega^2 + 1} \tag{17}$$

If we define that $X_S = 1/C_S\omega$ and $X_P = 1/C_P\omega$, then equations can be simplified to [Gudi_99]

$$R_P(\omega) = R_S(\omega) + \frac{1}{R_S(\omega)C_S^2\omega^2} = R_S(\omega) + \frac{1}{R_S(\omega)1/X_S^2}$$
$$= R_s(\omega) + \frac{X_s^2}{R_s(\omega)} \tag{18}$$

$$C_P = \frac{C_S}{R_S^2(\omega)C_S^2\omega^2 + 1}$$
$$\Rightarrow X_P = \frac{1}{C_P\omega} = \frac{R_S^2(\omega)C_S^2\omega^2 + 1}{C_S\omega} = X_S + \frac{R_S^2(\omega)}{X_S} \tag{19}$$

As mentioned above, the conductance in the parallel model as well as its inverse $R_P(\omega)$ are frequency-dependent. This can also be seen in equations (16) and (18). Therefore the series parallel model conversion is valid only for a defined frequency. Moreover, the conversion is not valid for DC-voltages or for very high frequencies. On DC frequencies, the impedance of series model is infinite and the impedance of parallel model equals the resistance of $R_P(\omega)$ or conductance $G(\omega)$. Similarly, at very high frequencies, the impedance of the parallel model is zero and the impedance of the series model equals resistance $R_S(\omega)$.

The conversion presented in equations (18) and (19) is utilized to calculate the segment's resistance required for TBW estimation in [P5], P[6] and [Hänn_07]. However, the two-component model is usually too simple for modeling the frequency dependency of measured variables [Grim_00]. A three-component model is, therefore, often preferred. The three-component model consists of two resistors and one capacitor or of two capacitors and one resistor. Selection of the utilized model depends on what is being modeled [Grim_00].

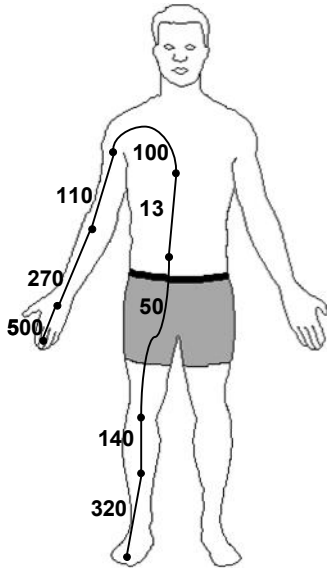

Figure 12. Resistances of different segments in the human body. On the hand 500 ohms is resistance measured from tip of one finger. Reproduced from [Grim_00].

Figure 12 illustrates the resistance of different segments of the human body. The values presented here are measured with a four-electrode measurement technique and they contain no skin contribution or current constriction. As shown in the figure, resistance is higher in the segments having a small diameter, such as the finger and upper arm. Conversely, resistance is lower in the segments with a larger diameter such as the abdomen and pelvis. If the living tissue is considered to be purely resistive, the resistance of the body segment can be estimated from the equation representing the resistance of a wire, $R = \rho l/A$, where R is the total resistance of the complete segment, ρ is its mean resistivity, l is the total length of the segment and A is its mean cross sectional area [Grim_00].

Bioimpedance can be utilized to measure many different quantities and signals in the human body. There are two major areas of bioimpedance applications: volume change-related measurements, called Impedance Plethysmography, and body composition-related measurements, called bioimpedance Body Composition Analysis (BCA).

3.4.3 Impedance Plethysmography

Let us consider a body segment whose resistivity is ρ and whose volume $V = Al$, where A is the cross sectional area and l its length. Resistance of the part can be estimated by the equation $R = \rho l/A$, and conductance by the equation $G = \sigma A/l$, where $G = 1/R$ and conductivity $\sigma = 1/\rho$. If the volume of the part changes because of an increase in the length and the cross-sectional area remains the same, conductance decreases. However, if the volume increases because of an increase in cross sectional area, then conductance increases. Therefore measured conductance does not necessarily change according to changes in the volume of the body segment [Grim_00]. However, in many applications an interesting parameter is not the absolute value of the segment's volume V but rather the change in the volume ΔV or the ratio $\Delta V/V$. Therefore, it is not necessary to know the absolute volume or absolute conductance values. This can be seen in equation (20), which assumes that the volume change is caused by change in the cross sectional area while the segment's length is constant. As equation (20) also shows, it is not even necessary to know the dimension of the segment

$$\frac{\Delta G}{G} = \frac{\sigma \Delta A/l}{\sigma A/l} = \frac{\Delta Al}{Al} = \frac{\Delta V}{V}. \tag{20}$$

Since it is not necessary to know the absolute value of the segment conductance in plethysmography, the measurement system can be simpler than others, such as the body composition measurement presented in the next chapter. To measure the absolute conductance value, the measurement system must be able to measure the static and low frequency part of the bioelectrical impedance. Though the low frequency and static parts of the bioimpedance signal are useful in certain bioimpedance applications, their accurate measurement involves fairly complex hardware, such as that utilized in the bioimpedance measurement suit presented in publication [P5]. For example, a reference method for system calibration must be implemented and signal amplification must be adjusted low enough to prevent saturation.

Measurement of volume changes using bioimpedance, is often associated with volume changes caused, for example, by beating of the heart. This is known as Impedance Cardiography (ICG). In ICG, the impedance of the thorax is measured with electrodes applied around the neck and chest [Kubi_70, Patt_89]. However, impedance plethysmography may also be related to other functions such as movements caused during respiration. [Grim_00]

Impedance plethysmography has been utilized in a number of studies such as that by González-Landaeta et al. [Gonz_08] to detect heart rate from plantar while standing on body weighing scales. This procedure is based on the fact that when a blood pulse wave travels through a blood vessel, the volume of the vessel changes and due to its high conductivity, the impedance of the vessel also changes. Together, these two effects

result in a change in the measured bioimpedance and enable the detection of heart rate. Cho et al. [Cho_09] have utilized the same principle for monitoring heart rate and pulse wave velocity (PWV) from the forearm. PWV is monitored by measuring the bioimpedance at two locations on the forearm. If the distance between these locations is known, the PWV can be calculated from the time difference between pulse wave detections. Blacher et al. [Blach_99] have shown that the pulse wave velocity closely associated with atherosclerosis can be used as an indicator and predictor of cardiovascular risk for patients with hypertension (high blood pressure). Panfili [Panf_06] et al. and Vondra et al. [Vond_06] have used bioimpedance for measuring cardiac-related signals. The objective is to continuously monitor cardiac output in terms of the amount of blood pumped by the right and left ventricles per unit time [Schm_89]. However, a recent study by Robert Patterson [Patt_10] shows that the change in aortic volume is not the main source of signal in ICG measurement. Measuring cardiac output with electrical bioimpedance methods is, therefore, made more challenging. Numerous physiological measurement devices have been implemented [P1 - P4, Mund_05, Naim_09] for using impedance measurement as a noninvasive method for measuring respiration rate. An advantage of bioimpedance respiration measurement is that it removes the need for devices to be inserted in the air passages [Bake_89], as is the case with a spirometer mask.

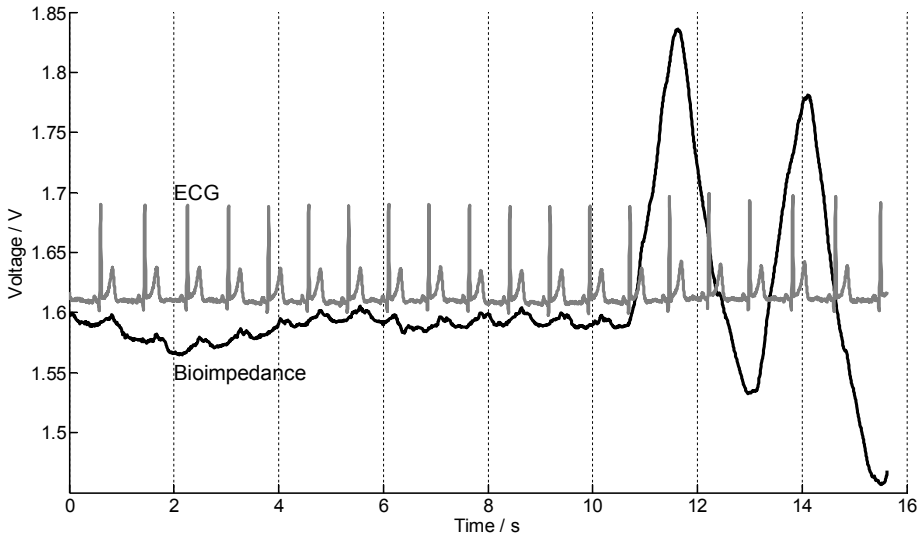

Figure 13. Bioimpedance and ECG signals measured from upper body. In the interval between zero and eleven seconds, the test subject is holding breath and the bioimpedance signal indicates the volume changes of the heart. After an eleven second time stamp, the subject is breathing again and heart volume changes in the bioimpedance signal are masked by volume changes of the lungs.

Figure 13 presents an example of impedance plethysmography, in which bioimpedance of the upper body is measured with a tetrapolar measurement setup. The measurement is carried out using the measurement device presented in [P4]. The electrodes are placed near the left and right armpit of the test subject, which is a suitable position for measuring lung volume changes caused by respiratory activity [Sepp_09]. The volume

changes of heart are also visible in this electrode setup. Concurrent with the bioimpedance measurement, as Figure 13 shows, the electrocardiograph signal is being measured. In the interval between zero and eleven seconds, the test subject has been holding breath and so the volume of lungs is almost constant. As the figure also shows, the impedance signal during this interval correlates well with the ECG signal. There is a notable increase in the impedance signal during the interval between the R-peak in the ECG signal and the end of the T-wave (see Section 3.5). During this interval, blood moves from the ventricles of the heart to the blood vessels and so the amount of blood in the heart decreases. A decrease in the amount of highly conductive blood in the heart results in an increase in measured impedance. As the amount of blood in the heart increases again during the interval between the T-wave and R-peak, impedance decreases. After holding breath, the test subject has started to breathe again, as can be seen in the impedance signal. During inspiration the lungs are filled with air, which decreases the amount of electrically conductive matter per unit volume [Nopp_97]. This is represented as an increase in the measured impedance. Similarly, during expiration the amount of air in the lungs decreases and the alveoli partly collapse, resulting in greater contact area between the alveoli walls [Nopp_97], which is represented as decreasing impedance. Because the impedance changes in the lungs caused by respiration are much greater than those in the heart, the heart rate is almost undetectable during this interval.

Seppä et al. [Sepp_10] have shown that impedance plethysmograpy can be utilized to monitor pulmonary flow. In this application, electrical bioimpedance measurement is known as impedance pneumography. Seppä et al. measured twenty subjects in three different positions and with five different electrode configurations. They found a close correlation of over 0.9 between impedance pneumography and the pneumotachograph reference signal.

3.4.4 Body Composition

Measuring body composition is based on the fact that the electrical properties of the body change according to the relative amount of body fluids and tissues [Beck_07]. Conductivity of blood and muscle is higher than that of other tissues such as fat and bone. According to Foster et al. [Fost_96], the resistivity of muscle is 2 – 10 Ωm while the resistivity of fat is 15 – 50 Ωm, which yields conductivities of 0.5 – 0.1 Sm^{-1} and 0.067 – 0.02 Sm^{-1} respectively.

Due to the capacitive nature of body cell membranes, the path of the measurement current depends on its frequency. At lower frequencies the current does not penetrate the cell membranes and flows mainly in the outer cell environment. At higher frequencies current also flows through the cell membranes, as illustrated in Figure 14. It is worth noting that the current through the cell membrane is a displacement current, i.e. no charges move through the cell membrane, but the current is caused by a time variable electrical field. This frequency dependency of the current path enables, for instance, estimation of the amount of extracellular fluid (ECF) and intracellular fluid (ICF) by measuring the bioimpedance at different frequencies [Grim_00]. In BCA, the terms intracellular water (ICW) and extracellular water (ECW) are employed to refer to ICF and ECF respectively. The sum of ECF and ICF is called Total Body Fluids (TBF) and the sum of ICW and ECW is called Total Body Water (TBW).

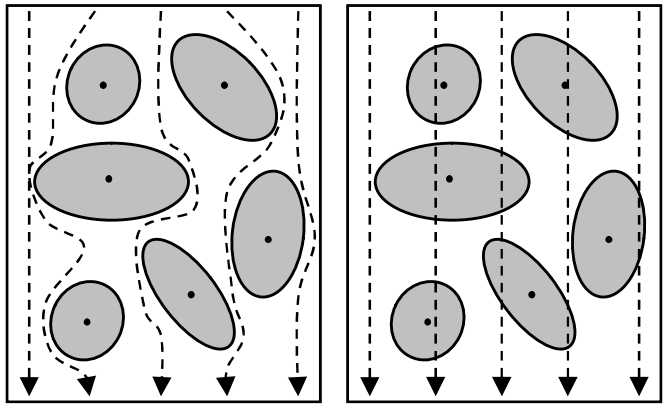

Figure 14. Left, low frequency current flow in a tissue. Right, high frequency current flow. Due to the capacitive nature of cell membranes, low frequency current flows in the outer cell environment and high frequency current also flows through cells [Grim_00].

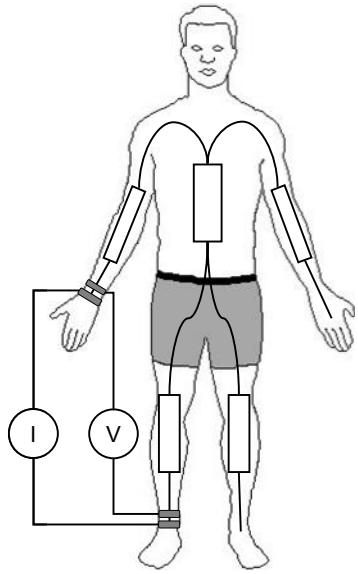

Figure 15. Hand-to-foot electrode placement in total body composition measurement and the components of the five–component mode.

In body composition measurement the body can be modeled as five segments: arms, legs, and trunk, as shown in Figure 15. Placement of the measurement electrodes differs according to which segment is monitored. Figure 15 presents a hand-to-foot (HF) measurement setup, in which electrodes are placed on the subject's hand and foot. In clinical measurements the hand-to-foot measurement setup is also known as wrist-to-ankle and it is a standard measurement for BCA [Kyle_04, Cox-02]. This setup enables measuring the sum of three segments: right arm, trunk and right leg. The setup is thus sometimes also known as right-side measurement. Other possible measurement setups

are foot-to-foot (FF) and hand-to-hand (HH), in which electrodes are placed at the extremes of these particular limbs. Cox-Reijven et al. [Cox_02] have compared measurement setups and conclude that hand-to-hand measurement correlates better with hand-to-foot measurement than the foot-to-foot measurement. However, if whole body measurements cannot be performed, FF and HH measurements can be utilized as alternatives. If only one of these segments (leg, arm or torso) is measured, the measurements are referred to as segmental.

Estimation of TBW with electrical bioimpedance usually relies on single-frequency right-side measurements at 50 kHz [Grim_00]. For example, according to Jaffrin et al. [Jaff_08] 50 kHz is too low a frequency for penetrating cell membranes. Therefore a measurement performed at this frequency does not accurately measure the inner cell environment. However, a 50 kHz measurement frequency has been utilized, for example, by Piccoli et al. [Picc_94] in bioelectrical impedance vector analysis (BIVA). In the BIVA method whole body resistance and reactance measured with a HF measurement setup are first standardized with the subject's height. Standardized measurements then form a vector on an $R - X_C$ plane. The vector is compared to reference ellipses measured for a healthy population. In practice the BIVA method can be utilized to indicate whether the subject has maintained normal hydration [Picc_95]. From a bioimpedance measurement the amount of water can be estimated with empirically derived equations. Lukaski et al. [Luka_85] have shown that the resistive part of the bioimpedance correlates better with the TBW than the reactive part. In addition, the correlation of resistance is as good as the correlation of complex impedance. As a result, plain resistance is often utilized in the equations instead of the complex impedance value. Equations (21) and (22) were derived by Kushner et al. [Kush_86] in a study with a group of 40 subjects, comparing right-side bioimpedance measurements with TBW values measured with a deuterium dilution method. Both equations are based on the assumption that the body is a homogenous cylinder having a constant diameter and a height equal to body height. This is not a real situation but the empirical equations do correlate well with the measured TBW values. In equation (21) the only parameter, in addition to impedance, is body height, Ht. Equation (22) also takes into account the body weight, BW.

$$TBW = k_1 \frac{Ht^2}{R_{segm}} + k_2 \tag{21}$$

$$TBW = k_3 \frac{Ht^2}{R_{segm}} + k_4 BW + k_5 \tag{22}$$

Kushner et al. [Kush_86] derived indexes $k_1 - k_5$, to be 0.714, 0.830, 0.556, 0.096, and 1.73, respectively. According to Kushner et al., equation (21) produces a correlation coefficient of 0.97 between the TBW values measured with dilution and bioimpedance analysis methods. When body weight is taken into account, the correlation coefficient increases to 0.99. The coefficients are valid for both genders, but Kushner et al. have also defined different coefficients for males and females. For males $k_3 - k_5$ in equation (22) are 0.396, 0.143, and 8.399, respectively, while for females $k_3 - k_5$ are 0.382, 0.105, and 8.315.

As mentioned earlier, electrical Bioimpedance enables BCA and it can be used to estimate several body composition parameters, such as TBW, ECW, and ICW. TBW is closely related to the body's Fat-Free-Mass (FFM), also known as Lean Body Mass (LBM). LBM can be calculated from the TBW with the following equation `LBM = TBW / 0.73` [Khal_95, Popa_06]. If FFM is known, then the amount of Body Fat (BF) can be calculated as follows `BF = BW - FFM` [Khal_95], where BW is body weight. Similarly, the Body Cell Mass (BCM) is closely related to the ICW [Jaff_08] and if the BCM is known, then the extra-cellular mass (ECM) can be easily calculated with the equation `ECM = BW - BCM`. The index ECM/BCM is an important parameter in assessing nutritional status and it should be less than one, in other words the body cells should contain more mass than the outer cell environment [Popa_06].

Measuring TBW can be done on single frequency provided the frequency is high enough for the measurement current to penetrate the cell membranes, as already stated. This measurement arrangement is known as single-frequency bioimpedance analysis (SF-BIA). In order to measure the parameters from both inner- and outer cell environments, the bioimpedance must be measured on multiple frequencies. A measurement arrangement utilizing at least two different measurement frequencies is called multiple-frequency bioimpedance analysis (MF-BIA). Typically an MF-BIA measurement utilizes two frequencies. The first of these is low (e.g. 5 kHz) and the second is high (at least 50 kHz). Another approach is called bioimpedance spectroscopy (BIS) and involves using multiple frequencies from 5 kHz to 1000 kHz. The BIS method is utilized in commercially available bioimpedance measurement devices such as the SFB7, manufactured by ImpediMed of Australia and the Hydra 4200 manufactured by Xitron Technologies, USA. [Eart_07]

Bioimpedance-based BCA has been employed in many research projects and in various applications. Edwardson et al. [Edwa_00] have implemented an impedance analysis device for measuring the ECW/FFM ratio. The device is a normal weighing scale with an additional hand-to-foot bioimpedance measurement and an analogue modem data connection. The target application of this device is to utilize bioimpedance measurement in the prediction of fluid overload in people having congestive heart failure. Murakami and Takanori [Mura_07] have utilized tetrapolar bioimpedance measurement to determine the thickness of subcutaneous fat. Vuorela et al. have implemented a bioimpedance measurement suit [P5], Lee et al. [Lee_03] devised a body fat measurement system based on a PDA–device. Medrano et al. [Medr2_07] developed a portable bioimpedance spectroscopy device for continuous monitoring applications, which measures the body impedance at one hundred frequencies between 5 kHz and 1 MHz. Body composition monitors are also available commercially. Omron, for example, has a product family of weighing scales, which in addition to measuring weight, also measure conditions such as body fat percentage and calculate Body Mass Index [Omron].

3.4.5 Other Bioimpedance Applications

Bioimpedance measurements can be utilized in various applications in addition to Impedance Plethysmography and BCA. For example, Yang et al. [Yang_05] have

designed an impedance measurement system for detecting tissue changes that could indicate a pressure ulcer. Majer and Stopjaková [Maje_08] present measurement equipment for monitoring the psycho-galvanic reflex of the human skin, which might be a useful stress indicator. Nakamura et al. [Naka_01] and Buyn et al. [Byun_03] have utilized a tetrapolar bioimpedance measurement system for body movement detection. Measurement of movement with bioimpedance methods could, for instance, replace still cameras and video cameras in the study of the mechanisms and techniques used by athletes. Halter et al. [Halt_07] have measured the bioimpedance of the human prostate with an implemented measurement probe in the detection of prostate cancer. According to their measurement results, normal prostate conductivity and permittivity are higher than in malignant tissue.

3.5 Electrocardiogram

Electrocardiography is the recording of the electric potential generated endogenously by the muscular activity of the heart on the surface of the thorax [Malm_95]. Because the heart operates like a single fist-size cell, its action potentials are relatively large. Changes in this potential are spread throughout the body by conductive liquids and can be measured relatively easily at all points on the body surface. However, the electrodes utilized in measuring ECG are normally connected to a few standard points which form so-called standard leads. The recorded voltages are relatively small; a few millivolts. [Nien_93]

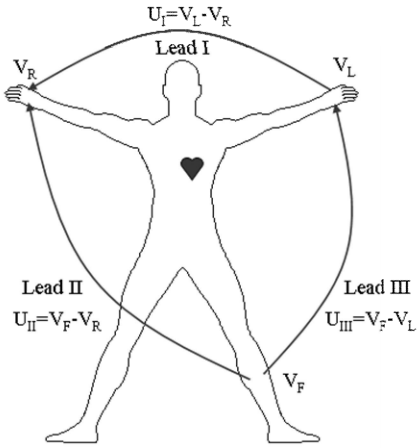

Figure 16. Einthoven ECG measurement setup. V_L,V_R, and V_F are potentials of left arm, right arm and left foot, respectively. U_I, U_{II}, and U_{III} are voltages on the lead I, II, and III, respectively. Simplified from [Malm_95].

Figure 16 presents the ECG measurement setup as developed by Willem Einthoven. This setup consists of three measurement points on both arms and the left leg. One measurement lead in ECG measurement is defined as a difference in potential between two measurement points, i.e. voltage. The leads presented in Figure 16 are known as standard limb leads, and they form the so-called Einthoven triangle [Malm_95].

Einthoven leads are bipolar in that they have one positive and one negative pole. Another measurement method is to use unipolar leads. In unipolar measurement, a recording electrode is placed on a specific site on the body and the potential is measured with respect to a reference electrode. Figure 17 presents unipolar limb leads - also known as Goldberger leads. This measurement setup employs the same electrode positions as the Einthoven setup. However the signal is measured as the voltage between one limb, e.g. right arm (aU_R), and a reference electrode, which is formed as a voltage division of the other two limbs. Due to their different measurement setups, Einthoven and Goldberger leads view the heart from different angles and therefore produce slightly different signals [Schm_89].

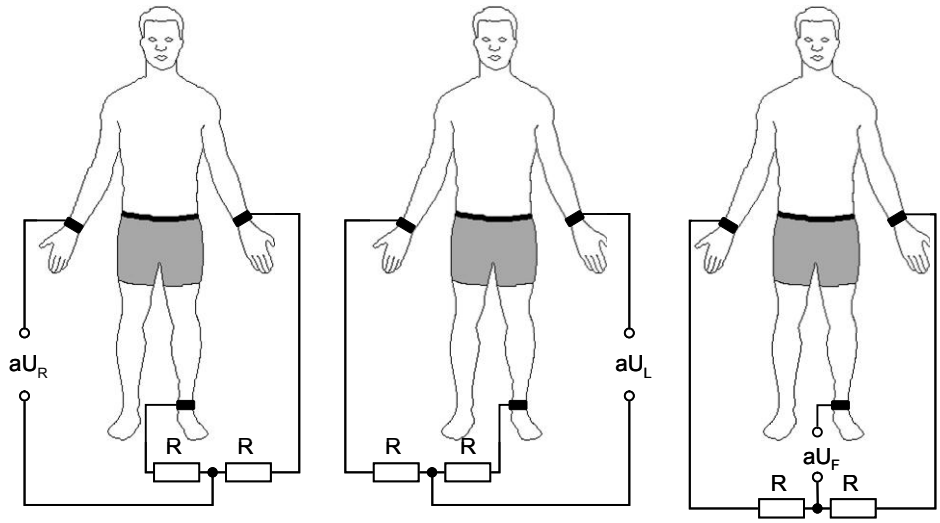

Figure 17. Goldberg's ECG measurement leads. aV_R is the voltage between right arm and voltage division of left arm and left leg. aV_L is the voltage between left arm and voltage division of right arm and left leg and aV_F is the voltage between left leg and voltage division of left and right arms.

During exercise, for example, the ECG signal is distorted due to errors caused by motion artifacts produced mainly by muscular activity, respiration and electrode movements. Motion artifacts caused by muscular activity can be reduced by repositioning the electrodes from the body extremes closer to the heart. For example, electrodes from the right and left arm can be moved to the right and left shoulder respectively and the electrode from the left leg can be moved to the hip [Malm_95]. Heart rate detection can be also implemented with two electrodes located on the user's chest. This setup is used in various commercial heart rate monitors [Polar, Suunto].

Figure 18 presents a theoretical ECG signal. Deflections in the signal are marked with letters of the alphabet starting with P. Depending on the position of electrodes used to measure the biopotentials, different segments of deflections in the signal are more or less visible. The small U-wave, for instance, is not usually visible in an ECG signal.

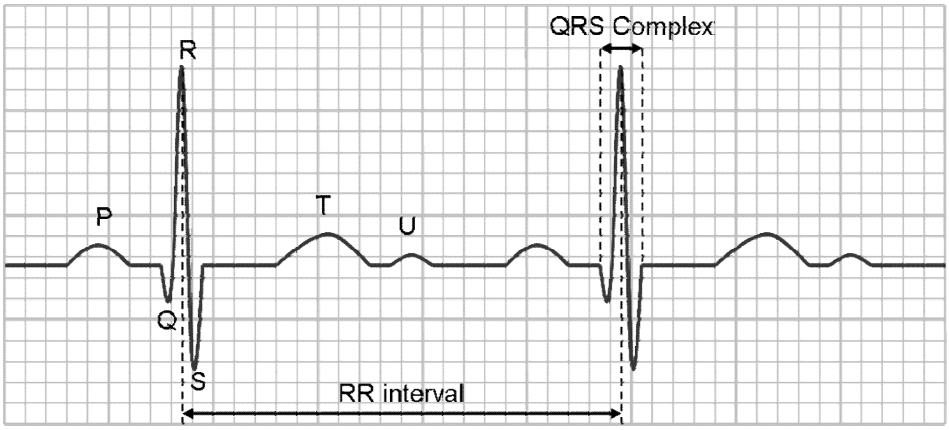

Figure 18. Theoretical ECG signal waveform. Simplified from [Malm_95].

The ECG signal can be exploited in diagnosis in various ways. A full waveform ECG can be utilized in the detection of many cardiac diseases. A simple application of ECG analysis is the calculation of heart rate. Due to the periodic operation of heart, the heart rate can be calculated in several ways such as measurement of the interval between two consecutive R peaks in the ECG signal. Because the R peak is the most visible peak in the ECG signal, it is relatively easy to detect, even during movement when a lot of motion artifacts are present in the signal. The time between consecutive R peaks is the RR interval (RRI) and this value can be exploited to calculate other physiological parameters such as heart and respiration rate.

A more general term for RR interval changes is heart rate variability (HRV). HRV describes variations in both the instantaneous heart rate and in the RR intervals. In order to perform HRV analysis on an ECG signal, a few requirements must be met. Firstly, a fiducial point, usually the R peak, in the ECG signal must be clearly marked and so the sampling rate of the ECG signal must be high enough. The optimal range is 250-500 Hz, or even higher [Mali_96, Pinn_94, Merr_90]. However, if interpolation[8] algorithm is utilized in the mathematical analysis, then even a sample rate of 100Hz may behave satisfactorily. Secondly, the interval analysis of the recorded ECG signal must be performed carefully in order to eliminate the effect of ectopic beats, arrhythmic events, missing data, and noise. [Mali_96]

An example of HRV analysis is presented in Figure 19. Here the upper curve represents the heart rate calculated from the ECG signal with a simple R-peak detection algorithm. This is presented in greater detail in section 4.3.3. The lower signal is the bioimpedance measured at the thorax. In this setup the measured bioimpedance changes in synchrony with the pulmonary inspiration and expiration and therefore describes respiratory activity rather well. It should be noted that the scale of the y-axis is the heart rate and the bioimpedance signal is scaled to be visible in the figure. In addition, the bioimpedance signal describes only the changes of the thorax impedance caused by respiration and its absolute value is meaningless. Figure 19 shows that each time lung

[8] Interpolation is a mathematical method of constructing new data points within the range of a discrete set of known data points. Interpolation is a specific case of curve fitting, often utilized in engineering. The principle in curve fitting is to construct a function that fits closely to the data points.

volume changes, it also causes changes in heart rate. During the interval from 63 s to 88 s the test subject has been holding breath, which can be seen in the flat bioimpedance signal. During this interval the heart rate also stabilizes slightly.

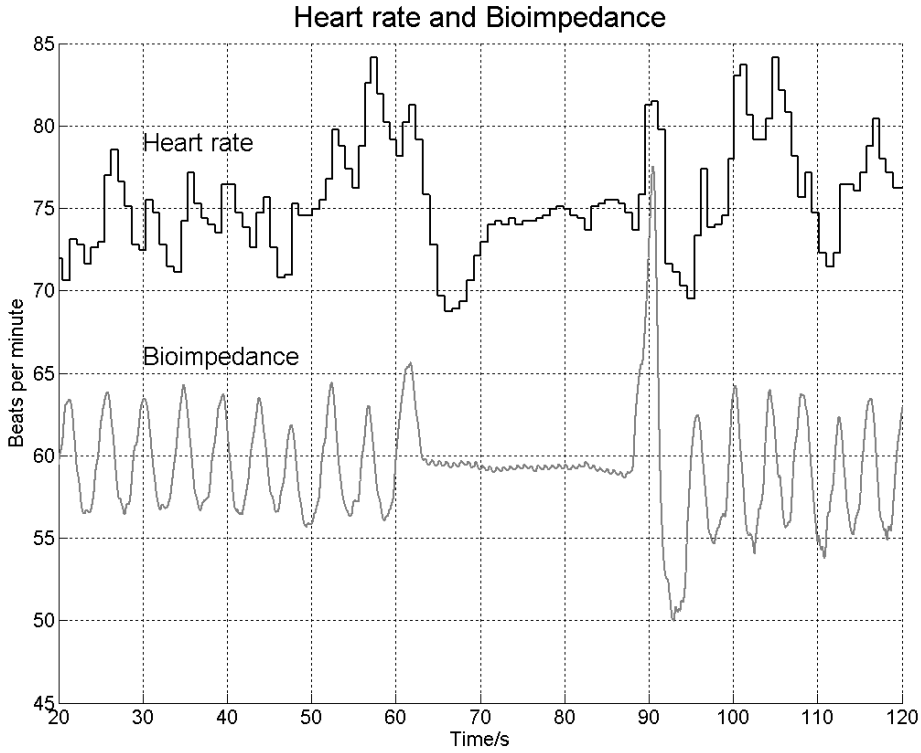

Figure 19. Correlation between respiration and heart rate. The upper curve represents heart rate calculated from ECG signal. Lower signal represents bioimpedance measured from thorax. From time 63 s to 88 s the test subject has been holding breath.

HRV analysis can be done either in the short term or in the long term. Short-term measurements are normally performed in a controlled laboratory environment and take from five to fifteen minutes. Short-term measurements can, for instance, be utilized to monitor the effect of clinical maneuvers by performing the measurement before and after the procedure. Long-term measurements usually last for 24-hours and are performed during the patient's normal daily activities. Long-term measurements produce useful data for risk predictors in cardiovascular disease. Analysis on HRV can be done either in the time domain, in spectral or frequency domain, geometrically or nonlinearly [Klei_05].

More complicated parameters of cardiac performance can be calculated from the HRV signal. For instance Rusko et al. have demonstrated in [Rusk_03] that excess post-exercise oxygen consumption can be predicted from the analysis of RRI. Pulkkinen et al. have evaluated in [Pulk_05] five different methods for estimating energy expenditure from the HR signal. The best results are obtained with an algorithm, which first

calculates the respiration rate and on-off dynamics according to RRI and then utilizes these results in energy expenditure estimation [Pulk_05].

3.6 Electrodes

Electrodes play a crucial role in biopotential and bioimpedance measurements. In metallic wires, electrical current is carried by electrons moving in the opposite direction to the applied electric field. In biomaterials and biological tissue the amount of free electrons is minimal and therefore electrical current is created by the movement of ions, i.e. the current in the metallic leads is electronic while the current in tissue is ionic. An electrode is a transducer that transforms current conducted by electrons into a current conducted by ions. The properties of the electron ion-interface are highly frequency dependent. They are also non-linear, as well as time invariant [Grim_00].

The electrodes utilized in biopotential measurements can be classified as either polarizable or non-polarizable. In the polarizable electrode there is no net transfer of charge across the metal electrolyte interface, whereas in the non-polarizable electrode this transfer is possible. Real electrodes are neither totally polarizable nor non-polarizable but their properties lie between these idealized limits [Gedd_89]. However, some practical electrodes can approach these theoretical limits. Electrodes manufactured from noble metals such as platinum behave like polarizable electrodes. Widely utilized Ag/AgCl electrodes approach the characteristics of non-polarizable electrodes [Neum_95].

In physiological measurements electrodes are utilized in two different roles, recording and stimulating. For example in electrical bioimpedance (EBI) measurement, stimulating electrodes are utilized to feed the excitation current into a tissue, whereas recording electrodes pick up the voltage generated by the excitation current. It should be noted that even though in some applications an electrode can function in both roles, injecting current and recording voltage, at least two electrodes with a galvanic connection between them must exist in all applications.

When a metal electrode comes into contact with an electrolyte containing ions of the metal, an ion-electron exchange occurs. This exchange causes charges to accumulate at the electrode-electrolyte interface causing a voltage, known as half cell potential, over the interface. In non-polarizable electrodes, charges can move freely across the interface and no charge is accumulated, leading to zero half-cell potential. In biopotential measurements, a primary source of motion artifacts is mechanical disturbance in the electrode-electrolyte interface, which disrupts the distribution of charges and causes the voltage over the interface to change. In a recording electrode, this change in half-cell potential is detected as motion artifacts. Therefore in recording electrodes, non-polarizable electrodes are preferred, especially in applications in which the measured information is on low frequency bands, as in ECG and EEG [Neum_95].

In stimulating electrodes, electrode conductance is an important design consideration. As explained in section 3.4.1, the tetrapolar measurement method can be used to minimize the effect of electrode-skin interface impedance in electrical bioimpedance measurement. However, if the impedance of current injecting electrodes is very high, a high voltage is required to produce a constant current in a tissue. In portable devices it is

particularly challenging to produce high voltage due to the battery-provided supply voltage. Conductance of a disk electrode can be estimated from the equation $G_{1/2} = 4a\sigma$ [Grim_00], where a is the disk radius and σ is the disk conductivity. As can be seen from this equation, the conductivity of a disk electrode increases as the electrode radius increases. In addition, a large electrode area increases electrode capacitance which decreases electrode impedance. As a result, electrodes with large radii or circumferences are preferred for current injecting.

In the simplest applications, biopotential recording is done using a single electrode pair and a negligible current. Because the current through the electrode is almost zero, the voltage caused by the impedance of the electrode-skin interface can be considered insignificant compared to the measured biopotential. However the electrode area still influences the measurement. The larger the electrode area, the larger is the averaging effect of the electrode. [Grim_00] This leads to lower spatial resolution that can be exploited in portable and mobile measurements to decrease movement artifacts.

Since electrodes have an important role in physiological measurements, they have been studied in numerous research projects. Puurtinen et al. in [Puur_06] have measured noise and impedance of textile electrodes of different sizes and with different preparations. The authors report that impedance of skin-electrode interface decreases as the size of an electrode increases. Further, the noise levels of dry electrodes are markedly higher than in electrodes moistened with water or covered with a hydrogel. Marquez et al. [Marq_09] compared the suitability of conventional Ag/AgCl electrodes and textile electrodes for electrical bioimpedance measurement. Their results show that utilization of textile electrodes instead of gel-paste electrodes does not significantly influence the bioimpedance measurement. Moreover, an abrasive-conductive paste utilized to improve the electrode-skin contact is likely to cause more notable differences than the electrode material. A comparison between commercial Ag/AgCl electrodes and custom-made textile electrodes in bioimpedance measurement has also been carried out by Vuorela et al. [P6]. They conclude that both electrodes behave similarly in TBW measurement, though in clothing applications textile electrodes are easier to use. Medrano et al. [Medr_07] have implemented a theoretical model for the skin electrode interface of textile electrodes, based on real measurements carried out with textile electrodes. They also measured the impedance of electrode-skin interface in textile electrodes as being several times higher than in conventional bioimpedance spectroscopy electrodes. However, Medrano et al. report that textile electrodes can be utilized in tetrapolar bioimpedance measurement if the current through the voltage recording electrodes is kept low.

Several authors have investigated optimal electrode placement in bioimpedance and ECG measurements. Pola and Vanhala [Pola_07] report that due to differences in body shape and direction of the heart's electrical axis, it is difficult to determine an optimal electrode setup that is suitable for all human subjects. A commercially available thoracic hydration monitor ZOE [ZOE] utilizes a different electrode setup to measure the status of fluids in a subject's thorax. In ZOE measurement, electrodes are placed at the top and bottom of the sternum. However, Beckmann et al. [Beck_07] have studied the optimal placement for electrodes in bioimpedance spectroscopy measurement for detecting water in the lungs. According to their finite element simulation, the best locations are very close to the armpits. Seppä et al. [Sepp_09] found the same electrode

setup suitable for impedance pneumography (i.e. respiration monitoring) by comparing the bioimpedance signal with the signal acquired from a spirometer. Lozano [Loza_97] has shown that bioimpedance measurement is very sensitive to electrode placement. If care is not taken when placing or replacing the electrodes, the changes in measured impedance caused by electrode placement are easily greater than actual changes in impedance.

4 Measurement Devices Developed at the Department of Electronics

This section presents the wearable and portable measurement devices implemented at the Department of Electronics of Tampere University of Technology. All the devices presented are prototypes and are therefore unsuitable for commercial production without redesign and optimization for an industrial manufacturing process. The timeline of developed measurement devices is presented in Figure 20. The vertical axis in the figure shows the physiological signals or parameters measured by the devices and the horizontal axis is the time.

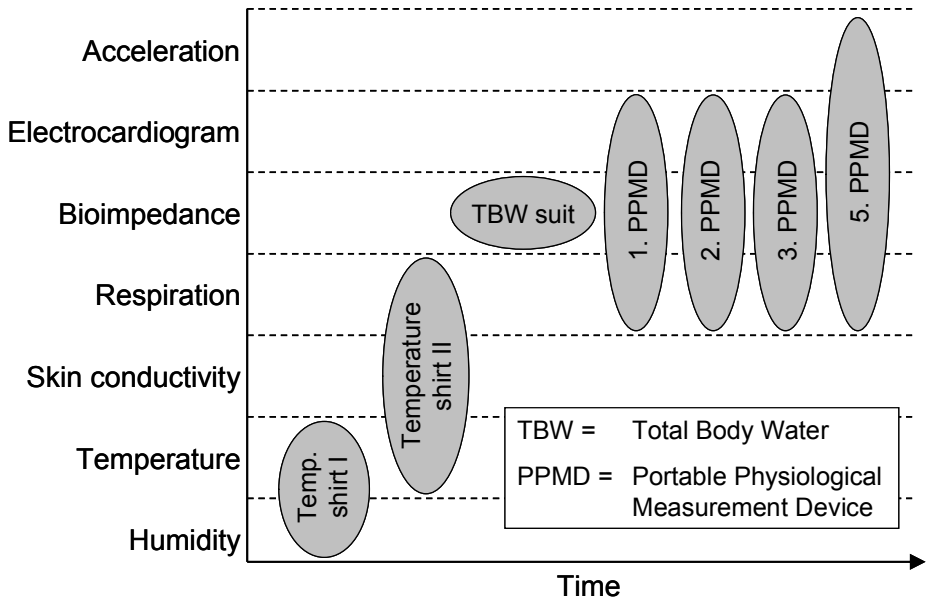

Figure 20. Roadmap of physiological measurement devices developed at the Department of Electronics.

4.1 Temperature Measurement and Electrical Heating Shirt

As technology evolves, it becomes possible to improve the functionality of a traditional garment by integrating additional electrical or electronics functions. To demonstrate the integration of electronics into textile materials and test whether human thermal comfort can be improved with electronics, two smart-clothing outfits were implemented. The term “thermal comfort” refers to whether a person feels too warm, too cold, or thermally comfortable. The thermally comfortable state is when there are no thermoregulatory mechanisms, such as shivering or sweating, and blood flows through the peripheral

circulation of the body at an intermediate rate [Schm_89]. According to this definition thermal comfort can be improved in two main ways, by heating or cooling. In Finland low temperatures, especially in winter, are a major discomfort factor. As a result, the prototype presented in this section and in publications [Kukk_01, Rant_01, Rant2_01] is designed to keep the user warm by means of electrical heating.

The textile platform for the measuring and heating prototype is an undershirt, manufactured from Thermostat and polyester. Heating is implemented with twelve resistive carbon fiber panels located around the upper body. In the first phase of the implementation, the heating panels were attached to the undershirt with Velcro, thus allowing panel replacement and repositioning. On the basis of preliminary test results, the twelve locations presented in Figure 21 were chosen for the final implementation. In order to measure heating effectiveness and control of the heating panels, nine digital 1-wire temperature sensors (DS1820, Maxim-Dallas Semiconductor, California, USA) are attached to the shirt. The location of the sensors was selected according to the international standard ISO 9886 [ISO9886], presented in section 3.1.2. In addition to eight sensor locations defined in the standard, one additional sensor (A) is placed on the user's right hand. The purpose of this sensor is to enable the monitoring of temperatures of both upper body extremes, i.e. the palms. The working hypothesis is that because there are large temperature variations over the skin, a temperature reading from one hand may not correlate with that from the other. Accuracy of the selected temperature sensors is ±0.5 °C, which is worse than ±0.1 °C, defined in ISO 9886 standard. However the sensor is relatively easy to use and its precision is guaranteed across a wide temperature range and thus it was selected for the prototype. In addition to temperature sensors, the shirt has three relative humidity sensors. Relative humidity is measured to detect sweating activity. The placement of temperature and relative humidity sensors is presented in the Figure 21.

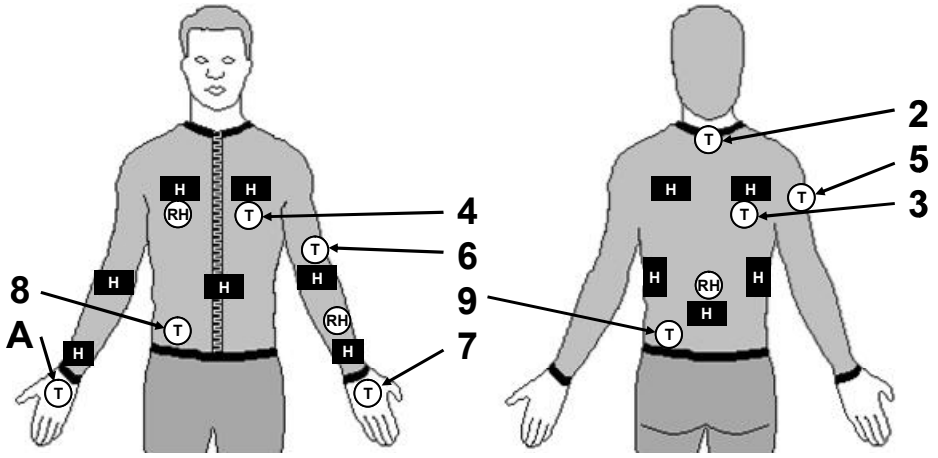

Figure 21. Placement of temperature sensors (T), relative humidity sensors (RH) and heating elements (H) on the temperature measurement and heating garment.

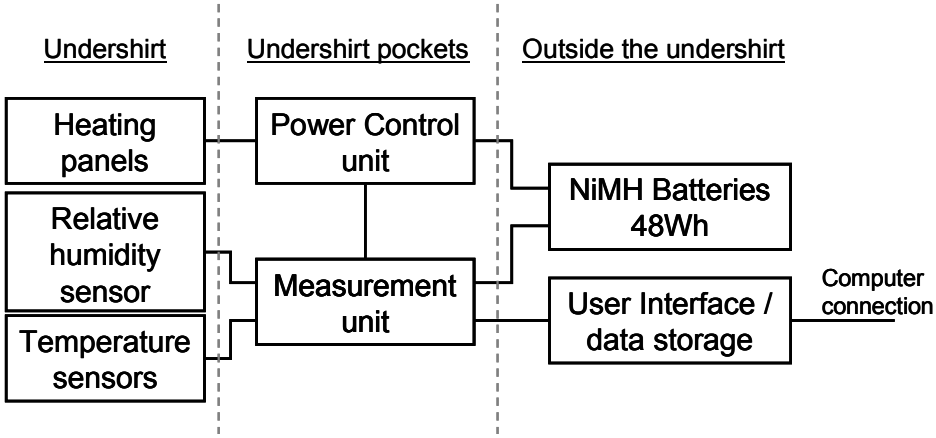

Figure 22. Block diagram of temperature measurement and heating shirt.

The electronics of the application consist of several different blocks, as shown in Figure 22. To accelerate the development process, two main tasks of the system, measuring and heating control, are implemented on separate units designed in parallel. To interface with the user and for measurement data storage, a commercial PDA device, the Palm Pilot III, has been used. After a measurement or test session, the temperature and humidity measurements, together with power consumption data, are transferred to a computer and analyzed with a spread sheet program. The heating functionality of the garment has also been designed to operate without a user interface. However, in such an operating mode, measurements values are used only as controlling parameters without being stored. Figure 23 presents the first version of the heating shirt.

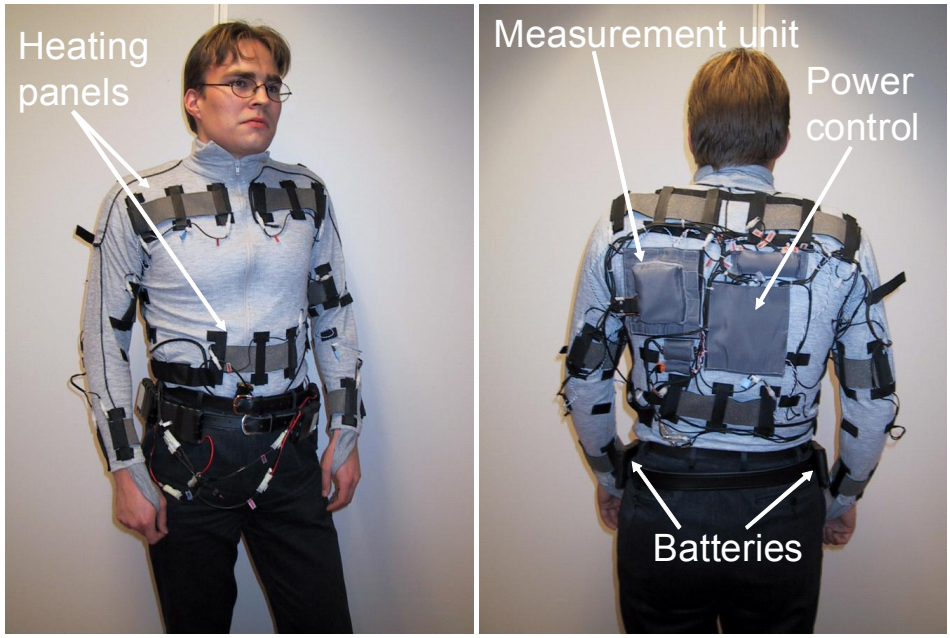

Figure 23. First version of the heating garment prototype. [Rant_01, Rant2_01]

The power source of the measurement and heating system is a set of nickel metal hydride batteries. During one test session the subject had four sets of five battery-cell battery packs. Since the weight of one battery pack is approximately 300 grams, the total weight of batteries is more than one kilogram. Although batteries are the heaviest part of the prototype, this does not pose a problem since they are attached to the belt which distributes the weight evenly around the hips and the centre of gravity is along the body's vertical axis.

As mentioned above, the temperature measurement values are utilized for controlling the heating panels. Using the user interface, two target temperatures can be set, one for the user's arms and the other for the rest of the upper body. The power control unit controls the amount of current flowing through the heating panels according to the difference between the target temperature and skin temperature measured with DS1820. For further analysis, the user interface PDA-device calculates two weighted temperature mean values during the test. The weighting coefficients for the average measurement are presented in Table 8. The first average value is adjusted for indicating the thermal comfort in the upper body so that the sensors near the body core have the highest coefficients and the lower coefficients are assigned for the sensors in the limbs. The second average value, i.e. average of the torso, is simply an evenly weighted average of the four sensors located near the body core.

Table 8. Multiplication coefficients utilized in skin temperature calculations.

Sensor	Upper body Average	Average of torso
2		
3	0.324	0.25
4	0.324	0.25
5	0.130	
6	0.130	
7	0.093	
8		0.25
9		0.25
A		

Figure 24 presents three average torso temperatures measured during three tests carried out with the measurement prototype. During the test, the subjects were wearing the heating shirt prototype and a light overcoat. The other clothes were selected by the subject. During the first fifteen minutes of every test, the subject walked a predefined route with the heating function turned OFF. The heating was then turned ON and the subject followed the route again. When the status of the heating changed, the subjects were allowed to adjust the desired target temperature values. These values are also presented in Figure 24. As the temperature curves show, the mean skin temperature of each subject either drops or remains constant when the heating is OFF. After the heating is turned ON, the skin temperature starts to rise and finally settles at a constant level. However, for both female subjects the desired target value is never reached during the test, whereas for the male subjects the target value is reached. This may be explained by several factors. The male subject was the main designer of the heating shirt and is seen

in Figure 23 presenting the shirt, which fits him almost perfectly. Therefore both the temperature sensors and the heating panels have good contact with the skin. Both female subjects are smaller than the male subject and the heating shirt is rather too large for them, with the result that there is poorer contact between the temperature sensors and the skin. Therefore, the temperature sensors are more likely to measure the temperature of the microclimate under the clothing than actual skin temperature. Due to the low thermal conductivity of air, the temperature of the microclimate is less than the temperature of the skin.

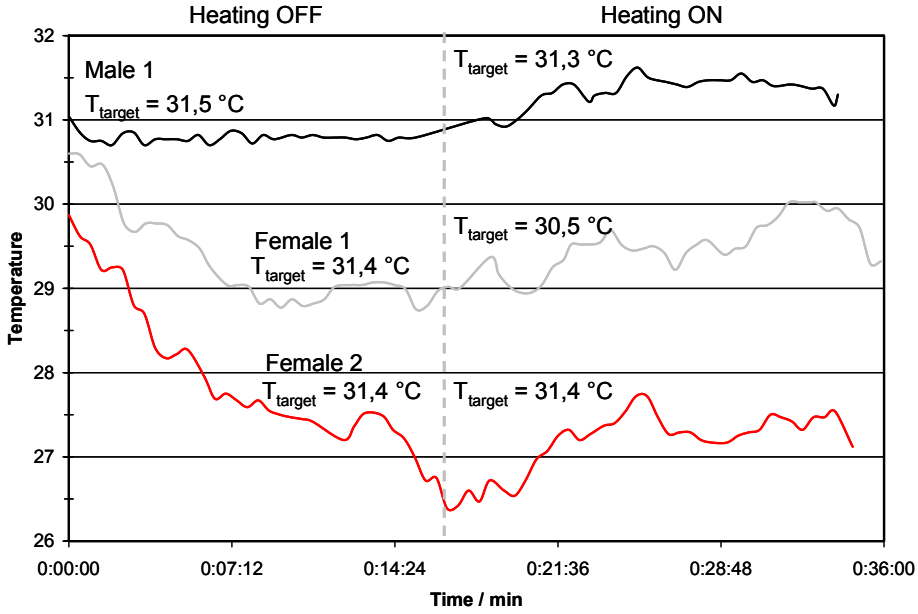

Figure 24. Average temperatures of users' torso measured with the heating shirt prototype one. During the first fifteen minutes, test subjects walked a predefined route with the heating turned OFF. Next the heating is switched ON and the same route is followed. The figure also presents the target temperatures of the heating system during the tests.

On the basis of tests carried out with the first heating shirt prototype, it seems that test subjects had overly high expectations from the suit. Probably due to the rather technical appearance of the shirt, the test subjects expected the heating system to be as efficient as that of a car seat. As presented in [Rant_01], during most of the test measurements the heating functionality was efficient enough to compensate for the heat loss when switched ON. However, the heating panels did not deliver enough power to increase the user's mean skin temperature, which usually decreased during the first fifteen to twenty minutes of the tests because the heating functionality had been turned OFF.

As Figure 23 shows, the first prototype of the heating shirt is not very "wearable". It was calculated that the shirt contained more than ten meters of different wires. The wires increased the overall weight of the system, which was 990 grams excluding batteries and the user interface. Moreover, placement of the electronic modules near the lower back was rather unsatisfactory since it made the garment uncomfortable in certain postures such as sitting on a chair with a backrest.

Because of these shortcomings, another version of the heating shirt was implemented. This outfit consists of two different garments, an undershirt and a covering jacket. Both garments are presented in Figure 25 [Rant2_01]. In this second prototype the functionality of the system is shared between the garments. The undershirt contains all the measurement electronics because it is located near the user's skin and the covering jacket contains the heating function. A block diagram of the system is presented in Figure 26.

Figure 25. Second version of the heating garment prototype. On the left, the undershirt which contains all the sensors and measurement electronics. On the right, the inner covering jacket containing the heating panels and power control electronics. [Rant2_01]

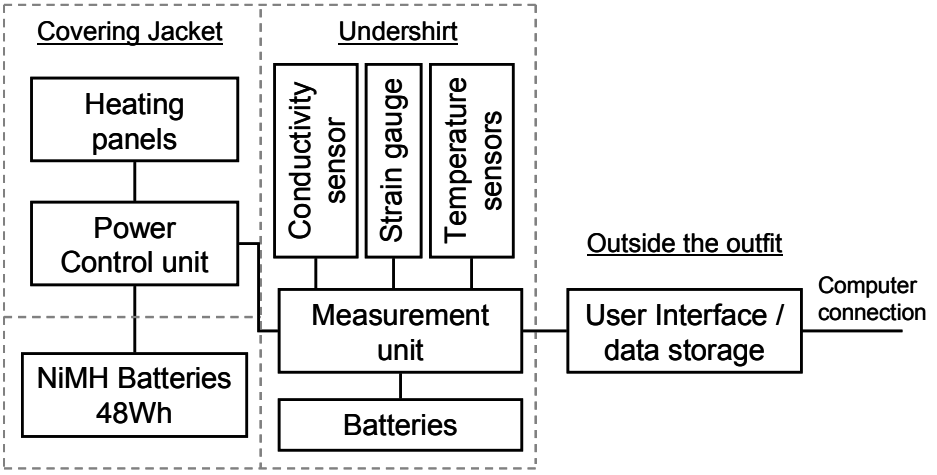

Figure 26. Block diagram of the second version of the heating outfit

From the measurements performed with the first prototype, it became clear that the relative humidity sensor serves very little use, either in controlling the heating power or in the analysis of thermal comfort. The accuracy of the humidity sensor unit (HU10) is ±5%RH and all the variations during the measurement sessions were within this range and so the output of the humidity measurement can be regarded as constant.

In the second version of the heating outfit, the humidity sensors are removed and two new sensors are added. The first new sensor is a conductivity sensor, located in the undershirt so that it is in contact with the user's chest. The purpose of this sensor is to measure the electrodermal activity of the skin, i.e. resistance, which can be used as an indicator of sweating. The electrodes utilized in the measurement are manufactured from conductive fibers, trademark Aracon®. The other new sensor in the shirt is a strain gauge to monitor respiration rate. This is located around the user's chest and adjusted to a comfortable fit with Velcro.

The power supply system has been redesigned to enable separate usage of the undershirt and the covering jacket so that in the second version both garments have their own batteries. The covering jacket is powered by the same kind of belt-worn battery pack as that used in the first prototype and the undershirt is powered by rechargeable NiMH batteries located in the shirt pocket. This arrangement ensures that the undershirt can continue measuring even when the heating jacket has spent all its energy.

Wiring of the measurement part was also redesigned. The conventional wires utilized to connect the temperature sensor to the measurement unit in the first prototype were replaced with conductive fibers. Because the heating panels require large currents, it was not possible to replace the wires between the heating control unit and heating panels with conductive fibers. However these connections are implemented with flexible silicon coated wires that provide rather more comfort than the conventional plastic-coated wires used in the first prototype. The conductive fibers used in the undershirt are much lighter than metallic wires, but they are also more fragile and lack an insulating coating layer. In order to prevent short-circuits, each wire was threaded into a separate narrow fiber fabric tube, which provides some degree of insulation and also allows the fiber to move freely. A problem with the fibers was observed in the attachment of the fibers. The fiber itself is relatively strong, but when several fibers are attached together or a fiber is attached to an electrical circuit board, the point of attachment is much weaker than the actual fiber [Hänn_04].

The second prototype was only tested indoors but still proved to be fully operational. However, as expected, the joints in the conductive fibers and the connection points between the fibers and printed circuit boards are both rather fragile. Numerous fibers snapped off when the under shirt was being put on. The point of breakage was usually next to a knot and not in a straight fiber.

4.2 Electrical Bioimpedance Measurement Suit

Dehydration of 3 % induces increased heart rate and depressed sweating sensitivity [ISO7933] and this can adversely affect the performance of a worker in a warm environment. Therefore continuous monitoring of hydration status is a desirable

application that could improve the safety of workers in warm or hot environments, such as firefighters. The electrical bioimpedance measurement suit is a smart clothing prototype designed to measure the user's hydration status, i.e. the amount of water in the body [P5, Hänn_07]. All the electronics required for measuring bioimpedance have been embedded in the cell suit, presented in Figure 27.

4.2.1 EBI Suit Structure and Operation

The hardware of the measurement system consists of several different functional blocks, as shown in Figure 28. The signal generator, in the upper part of the figure, generates a sinusoidal constant amplitude voltage signal. This voltage is converted to a constant amplitude current with a voltage-to-current converter. As the figure shows, the measurement system has an inbuilt reference resistor R_{ref}, the purpose of which is to provide stable reference impedance to withstand changes in temperature. Before performing a tissue impedance measurement, the measurement system is calibrated by measuring the resistance value of R_{ref}. The system contains four digitally controlled analogue switches for switching between the reference impedance and the tissue being measured. The EBI measurement is performed with two instrumentation amplifiers (IA), two peak detectors, and a phase detector. IAs measure current and voltage signals, whose amplitude is identified by a peak detector and the phase angle with the phase detector. All analogue signals acquired are converted into digital form by the micro-controller's internal analogue-to-digital converter. During a measurement session, data is stored in an EEPROM, after which the data is transferred to a personal computer and analyzed in a spreadsheet program.

Figure 27. A bioimpedance measurement suit. Electronics required in the measurement are integrated into the back of the jacket. The right sleeve and right trouser leg of the jacket contain a snap-in connector for the electrode.

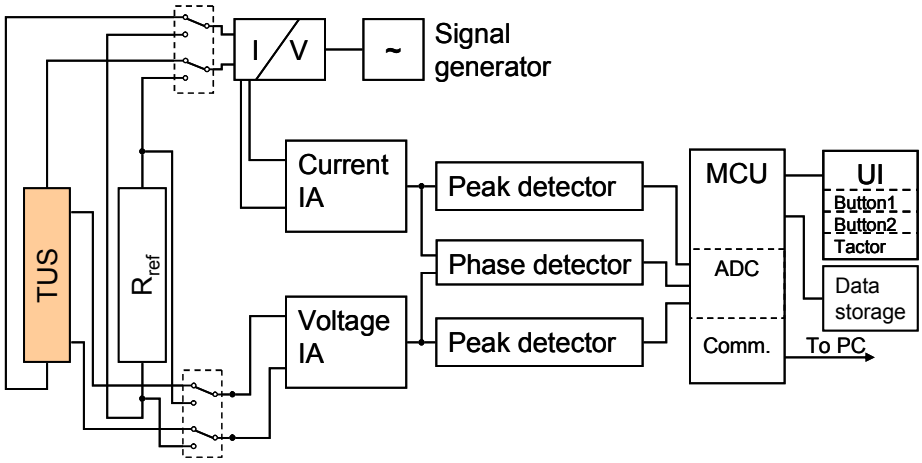

Figure 28. Block diagram of electronics in the bioimpedance measurement suit.

The user interface of the measurement system is designed to be as simple as possible. The UI consists of three buttons and one vibration motor as a feedback device. Button functions switch on the measurement system's operating voltage and also start and stop the measurements. The main power switch is located on the hem of the jacket and the ON and OFF buttons are located on the right sleeve. The rest of the system configuration is achieved through a serial connection from a personal computer. The feedback signals produced by the vibration motor are designed to be simple and clear. Start up of the system is announced by two long vibrations signals. Starting and stopping the measurements are signaled by three short and three long pulses, respectively. If an error is detected during the measurements, the user is notified by seven short vibration pulses. An important user interface signal is a short vibration pulse, repeated every three minutes, to indicate that the measurement procedure is functioning normally. This signal, or lack of it, informs the user whether the measurement session can continue or has to be stopped. The user interface was found to be generally intuitive and easy to use, even in urban areas where noise and lighting can make the utilization of sound and vision UI's difficult.

The system measures EBI of the human body at two frequencies, 5 kHz and 50 kHz. The excitation current used is 500 μA RMS, which should be low enough to comply with the safety guidelines in IEC-60601 [Grim_00]. Impedance at both frequencies is measured three times a minute. In order to minimize disturbances caused by movement every measurement result is an average of two hundred analogue to digital conversions. The interval between consecutive conversions is set to be 30 ms and thus impedance measurement on one frequency lasts 200 * 30 ms = 6 s. This was found to be sufficient time for removing motion artifacts caused by walking or cycling.

To implement a clothing-like measurement system, textile electrodes are utilized instead of conventional Ag/AgCl gel-paste electrodes. Two custom-made electrodes are presented in Figure 29. The textile electrodes are manufactured from conductive yarn and attached to an elastic strap, which enables easy fastening to limbs of various sizes. The connection to the measurement electronics is implemented with snap-in fasteners located on the back of the electrodes. The electrode bands are tightened around a limb

with Velcro-tapes sewn onto the elastic strap. The size of the contact surface in an electrode is 40 x 40 mm.

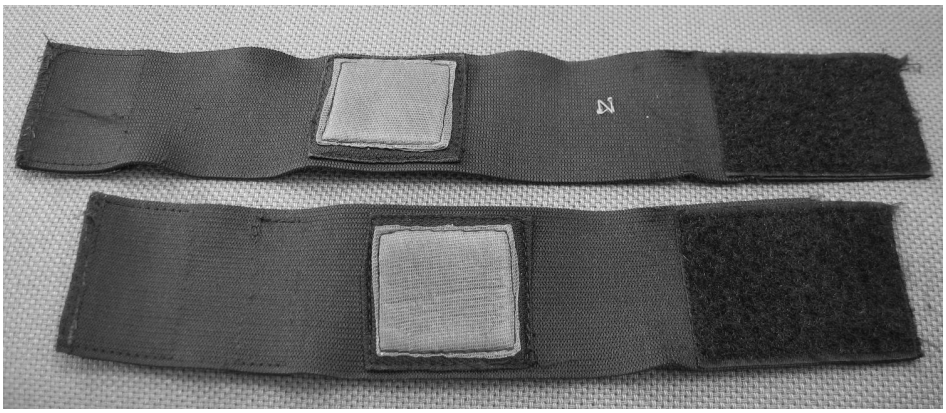

Figure 29. Textile electrodes used in the bioimpedance suit. Electrodes are 40 x 40 mm and are attached to the body with elastic straps fastened with Velcro.

4.2.2 Total Body Water Measurements

Figure 30 shows two sets of measurements performed with the bioimpedance measurement suit. The measurements were taken while the test subject was exercising on a stationary bicycle. Both exercise sessions lasted for an hour. In the first session the subject has not consumed any liquids during the exercise. During the second session the subject has been drinking tap water at regular six minute intervals. The TBW signals in Figure 30 are calculated from the whole body EBI values measured at 50 kHz, using the total body water equation defined for males by Kushner et al. [Kush_86] presented earlier in section 3.4.4 in (21). As can be seen from Figure 30, the absolute value of the TWB is relatively low, only about 22 liters. In an adult male the amount of body water is about 50-70% of body weight [Nien_93]. The test subject's weight was about 95 kg, which yields about 47.5 – 66.5 kg (liters) of water. This is partly explained by the measurement frequency of 50 kHz, which might be a little too low for measuring total body water, as presented by Jaffrin et al. [Jaff_08]. The low measurement frequency might not penetrate the cell membranes and therefore may understate the amount of ICW. In Figure 30 the measured TBW curves start at different levels. This can be due to several factors, the two most likely of which are that testing was performed on different days with varying amounts of water in the subject's body, and also placement of the electrodes. Even though the electrodes were carefully placed at predefined sites on the right wrist and right ankle, the distance between the electrodes is unlikely to remain constant in every test. This causes the measured impedance values to vary and thus the TBW values also differ from each other.

The upper curve in Figure 30 has clearly visible spikes with a constant interval. Because there is a six minute interval between the spikes, it can be assumed that they are caused by the action of drinking the water. As equations (21) and (22) show, the TBW is inversely proportional to the measured resistance, therefore during these spikes the measured resistance has decreased. The resistance might have decreased because the

amount of water in the stomach increases. Another possibility is that, at the moment of drinking, the user's hands have accidentally touched each other. This causes a decrease in impedance since the hands are electrically connected in parallel. However, it can be clearly seen that in the test during which the water has been consumed, the TWB curve is almost vertical, whereas in the test during which no water was consumed the TBW curve slightly decreases. However, the decrease is smaller than 1 ml. This might be caused by a physiological body phenomenon, which occurs during training. Jürimäe et al. have measured athletes before and after endurance rowing exercise and also during recovery time [Jüri_00]. During exercise, no change was observed in TBW, ECW, and ICW even though body weight decreased significantly. Changes in the mentioned parameters were observed during recovery and it can be seen that there is a greater decrease in ECW volume than in ICW volume.

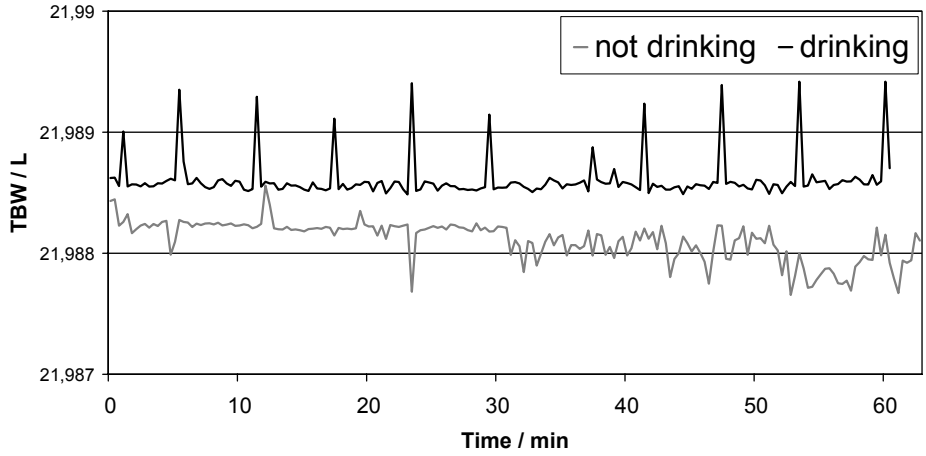

Figure 30. Amount of water in the body calculated from a bioimpedance signal, measured at frequency of 50 kHz with Kushner et al. equation. Upper curve represents a test during which the subject has been drinking tap water during the exercise and the lower curve represents a test during which no liquids were consumed.

The purpose of the bioimpedance measurement suite is to enable monitoring of impedance and, especially, TBW during normal daily activity and exercise. However the lack of a verification method of TBW measurement absolute value, meant that only the behavior of the TBW signal was inspected. The results are plotted with an equation (23) which is deduced from equations (21) and (22). In (21) and (22) the subject's height and weight are considered to be constants and result in (23). In equation (23) the k is a scaling constant with a given value of 10000

$$TBW = \frac{k}{R_{segm}}. \tag{23}$$

The operation of the EBI suit has been verified in numerous tests carried out by members of our research group. During testing, the suit performed as intended and Figure 31 presents some TWB signals acquired from the tests. The measurement signals

are not calibrated to show the absolute value of the TBW, but rather to present the trend in the TWB during a test session. The test (a) was carried out by a 27-year-old male and tests (b) – (f) by a 25-year-old male. Signal (a) was acquired from a running test which lasted approximately one hour. During this test TBW values are actually increasing, even though the test subject did not consume any liquids. The same trend can be seen in signal (b), which was measured during a cycling fitness exercise. The total body water value in this exercise remains relatively constant, even though the test subject was sweating and did not consume any liquids during the test. The measured TBW value is also relatively constant in test signal (c), which was acquired during a test similar to that in signal (b), though here the test subject has been drinking water at regular intervals. In the walking test, (d), the TBW value decreases even though the test subject has been drinking water at six-minute intervals.

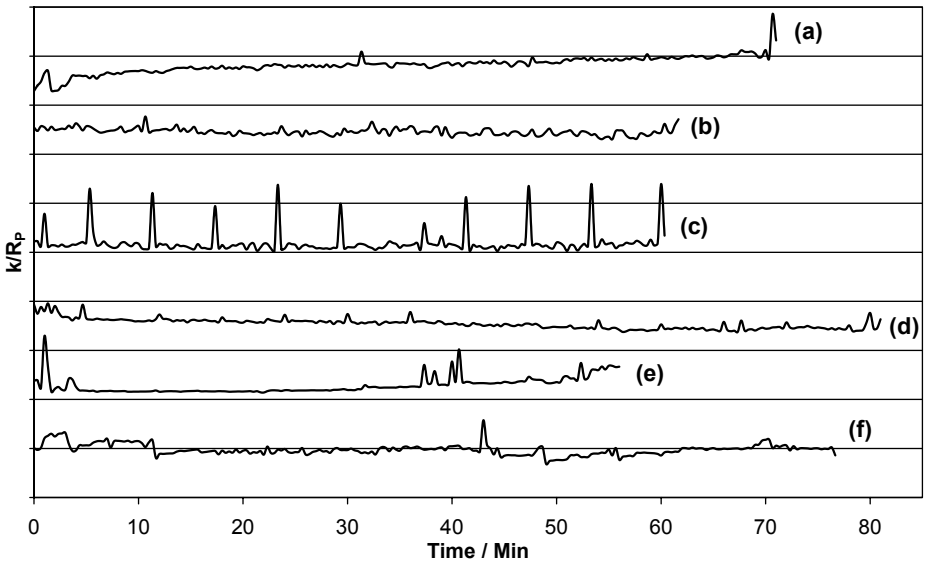

Figure 31. Measurements implemented with the bioimpedance measurement suit. (a) running and not drinking, (b) fitness cycling and not drinking, (c) fitness cycling and drinking, (d) walking and drinking water, (e) and (f) sitting in a sauna and not drinking. Signals are not calibrated to show absolute TBW values, but only to present the trend of TWB during tests.

4.2.3 Skin Temperature Effect in EBI Measurement

The behavior of the TBW signals in Figure 31 can be partly explained by the temperature changes in the test subject's skin. Kyle et al. [Kyle2_04] have reported that immediately after exercise there is a decrease in both the resistance and reactance part of bioimpedance measurements. The same phenomenon can also be seen in the signal plotted in Figure 31. However, Kyle et al. report that impedance values return to their normal state one hour after exercise. In the measurements performed with the EBI suit, no post-exercise changes in the impedance value can be seen because all measurements ceased immediately after the exercise. Cornish et al. [Corn_98] and Beckmann et al. [Beck_09] explain the decrease in impedance during exercise in terms of the effect of sweating and temperature increase. Cornish et al. have demonstrated that skin

impedance can decrease as much as 35 % if skin temperature increases from 20 °C to 40 °C. Beckman et al. have shown that consecutive BIS measurements can be compared only if the skin temperature in every measurement is equal. Furthermore, Cai et al. [Cai_00] report that total body impedance (TBI) decreases when the ambient temperature increases. They attribute the decrease in TBI to changes in blood volume distribution. If body temperature increases, blood circulation shifts from the central to the peripheral blood vessels since the body periphery promotes heat dissipation. Because the extremities form the major part of total body impedance and because the resistivity of blood is less than that of muscle tissue [Fost_96], increased blood volume in the extremities decreases overall body impedance and thus produces a false signal of increase in TBW value.

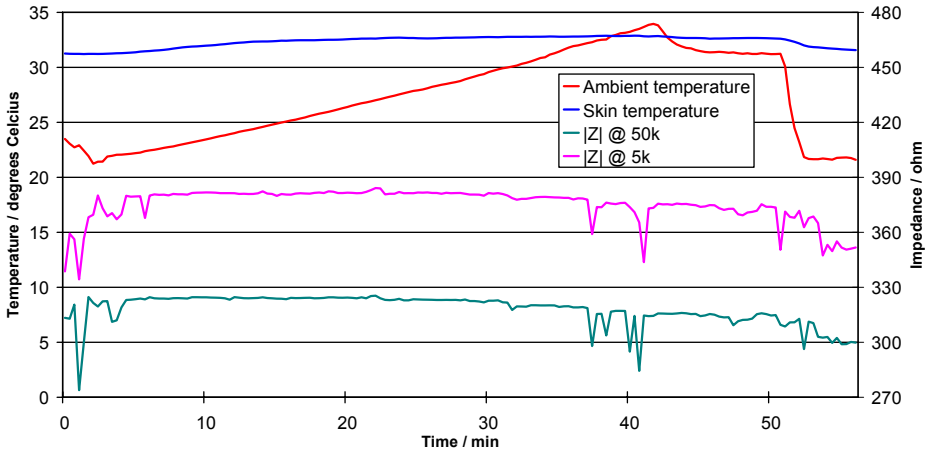

Figure 32. Hand-to-foot body impedance, skin temperature beneath the electrodes and ambient temperature, measured in a Finnish sauna.

To study how ambient temperature affects the bioimpedance measurement, tests were conducted in a Finnish sauna. An example of such measurements is presented in Figure 32. In fact the figure presents the measurement (e) from Figure 31 with additional temperature information. Temperature values are measured with digital temperature sensors (DS1820, Maxim Integrated Products, California USA). Four sensors are placed beneath an elastic strap next to textile electrodes utilized in the measurement. One of the temperature sensors measures the ambient temperature. At the beginning of the measurement session, the sauna stove has been turned ON and the temperature starts to increase. When the ambient temperature reaches approximately 34 °C the stove is turned OFF and the sauna starts to cool down. Figure 32 shows the absolute impedance measured at frequencies 5 kHz and 50 KHz. It can be seen that both impedance values decrease during the measurement session and that the fall is slightly more in the 5 kHz signal (approximately 25 Ω at 50 kHz and 30 Ω at 5 kHz). This supports the findings of Cai et al. [Cai_00] and partly explains the behavior of TBW values in other test measurements.

In Figure 31, signals (a) – (c) are measured during fairly strenuous exercise, running and fitness cycling. During these activities the skin temperature is much more likely to increase due to sweating and physical activity, which decreases the measured

bioimpedance value and increases the calculated bioimpedance value. However, test (d) is conducted during walking and thus there is less sweating than in the other measurements. As a result, the effect of blood shift in measurement (d) is less than in measurements (a) – (c). Due to this, the TBW signal (d) in Figure 31 decreases while the others increase or remain almost constant.

4.3 Portable Physiological Measurement Devices

In the Wisepla (Short-range wireless sensor platform for ambulatory and implantable applications) project [Wisepla] several physiological measurement device prototypes were designed and implemented. The objective of the project was to develop a physiological measurement device platform which could be utilized in a wide range of monitoring applications. One of the design goals of the platform was to enable long-term physiological measurement in a non-clinical environment (e.g. 24-hour home monitoring).

4.3.1 The First Measurement Device

The first prototype [P1, Sepp_06] was designed and implemented in a collaborative project between the Department of Electronics and the Department of Biomedical Engineering at Tampere University of Technology. The operating principle of the device is to measure ECG and bioimpedance signals and transmit the results to a computer via a radio link. An acceleration sensor has also been installed on the implemented PCB but time constraints prevented its functionality being implemented in the software. The block diagram of the measurement system's portable device is presented in Figure 33 and the measurement system in Figure 34. As can be seen in the block diagram, there is some duplication of electronics since both the measurement module and the module for radio and the power supply each include a microcontroller. This is due to parallel implementation of both modules in the different departments.

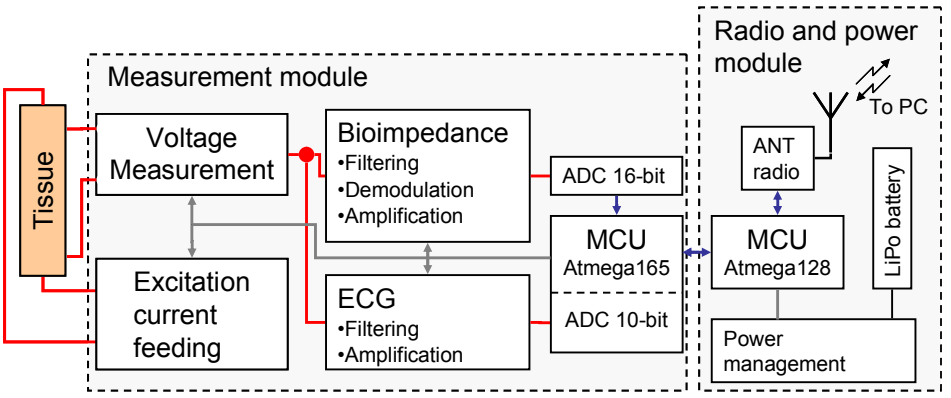

Figure 33. Block diagram of the first measurement device prototype implemented in the Wisepla project.

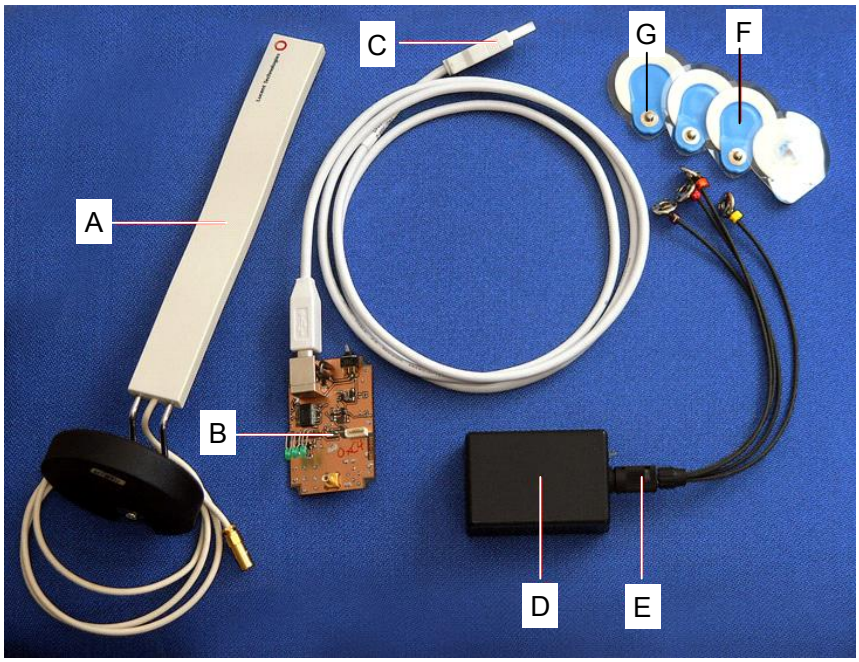

Figure 34. The first portable physiological measurement device system, designed and implemented in the Wisepla project. (A) base station antenna, adapted from an former WLAN base station, (B) base station radio transceiver PCB, (C) USB (Universal Serial Bus) cable for connecting the base station to computers USB port, (D) the portable physiological measurement device, (E) cables for attaching electrodes (F) and snap-on button on electrodes (G). Reproduced from [P2, Sepp_06]

As explained in Section 3.4, an excitation current is needed to measure bioimpedance. In the first prototype of the measurement device, the excitation signal was produced by a programmable waveform generator AD9833 integrated circuit, manufactured by Analog Devices. The AD9833 circuit is based on Direct Digital Synthesis (DDS) and it can produce sinusoidal, triangular and square wave output signals with a maximum frequency of 25 MHz. The constant amplitude voltage signal produced by the AD9833 is converted to an excitation current with a non-inverting operational amplifier amplification circuit. An advantage of the programmable waveform generator is that the measurement frequency can be changed with software and this allows measurement of different tissue zones. For example, the lower frequencies can be used to measure the outer cell environment and the higher frequencies can measure both the outer and inner cell environments of the human body. A drawback of AD9833 is a relatively high power consumption of 20 mW with a 3 V supply voltage.

Both ECG activity and thoracic bioimpedance are measured with the same electrodes, which are connected to the measurement device by means of snap-on buttons. The buttons are used as connectors since they provide an easy, reusable and relatively reliable connection method. The first part of the voltage measurement block is a passive first order high pass filter with a cut-off frequency of 94.6 Hz. The purpose of this filter is to provide a direct current (DC) -block and to set a bias voltage for an INA331 instrumentation amplifier. Because the main purpose of the device was to measure

bioimpedance, the corner frequency of this filter was set relatively high, thereby reducing any voltage impact of the ECG activity. However this was later found to be a limiting factor. After the differential voltage measurement, the bioimpedance and ECG voltage signals are separated with first order passive filters. To remove the high frequency bioimpedance-voltage component from the ECG, the voltage measurement is low-pass filtered with a low-pass filter with a corner frequency of 360 Hz. Similarly, in order to remove the ECG potential from the bioimpedance-voltage measurement, the sensed voltage is high-pass filtered with a high pass filter with a corner frequency of 79.5 kHz. After the filtering stage, only the bioimpedance-voltage component remains and this is demodulated with a peak detection circuit. This is high-pass filtered again to remove the signal's DC-component. Finally, both voltage measurement signals are amplified and low-pass filtered with anti-aliasing filters.

Since the bioimpedance measurement part of the device is intended for measuring volume changes occurring during respiration, a design decision was made to measure only dynamic changes in the bioimpedance instead of the absolute value. The dynamic changes in the bioimpedance value are usually very small compared with the absolute impedance value and so the absolute value component cannot be amplified as much as the dynamic signal without causing signal saturation on the measuring amplifiers.

The bioimpedance signal is converted into digital form with a 16-bit ADC and the ECG signal with Atmega165P's internal 10-bit ADC. The operation principle of the first measurement device is to transmit the measurement data to a personal computer via a radio link. The link has been implemented with an ANT-radio that transmits with a theoretical maximum transmission rate of 20 kbit/s. However, the actual data transmission rate achieved in this application is significantly slower, some 4 kbit/s. As a result the maximum total sample rate is limited to 250 Hz. For example, if the ECG is sampled with 150 Hz, the sample rate of the bioimpedance can be a maximum of 100 Hz. In addition, a design error in the antenna of the portable measurement device restricts the radio link range to a maximum distance of five meters.

The portable part of the measurement system is contained in an off-the-shelf casing, measuring 44.5 x 63.5 x 25 mm. The total weight of the module is 66 g, including the measurement wires. The operating voltage for the measurement module is supplied from a commercially available cell phone battery with a nominal voltage of 3.7 V and a supply capacity of 750 mAh. Average current consumption of the module is approximately 31 mA, which provides a theoretical continuous operating time of (750 mAh / 31 mA) = 24 h.

The first measurement device was utilized in measurements performed by Seppä et al. [Sepp_07]. Here the test subjects exercised on a bicycle ergometer with electrodes spaced evenly along a 12 cm-long horizontal plane on the left side of the torso. A total of seven subjects were measured and the results are presented and analyzed in [Sepp_07]. A sample measurement is presented in Figure 35. The upper curve is the bioimpedance signal measured from the subject's upper body and the signal in the lower part of the figure is the ECG. The signals are synchronized and scaled for visualization purposes in Matlab and so the numerical values on the y-axis are irrelevant. The larger fluctuations in the impedance signal are caused by respiration activity and the smaller ones are the result of changes caused by cardiac activity. As mentioned earlier, the high-

pass filter at the input of the voltage measurement block attenuates the low frequencies of the ECG biopotential signal. As a result only the highest frequency contents, like the R-peaks, are visible in the signal. Since the sampling rate of the ECG signal is relatively low, some irregularity is also visible in the R-peak amplitudes.

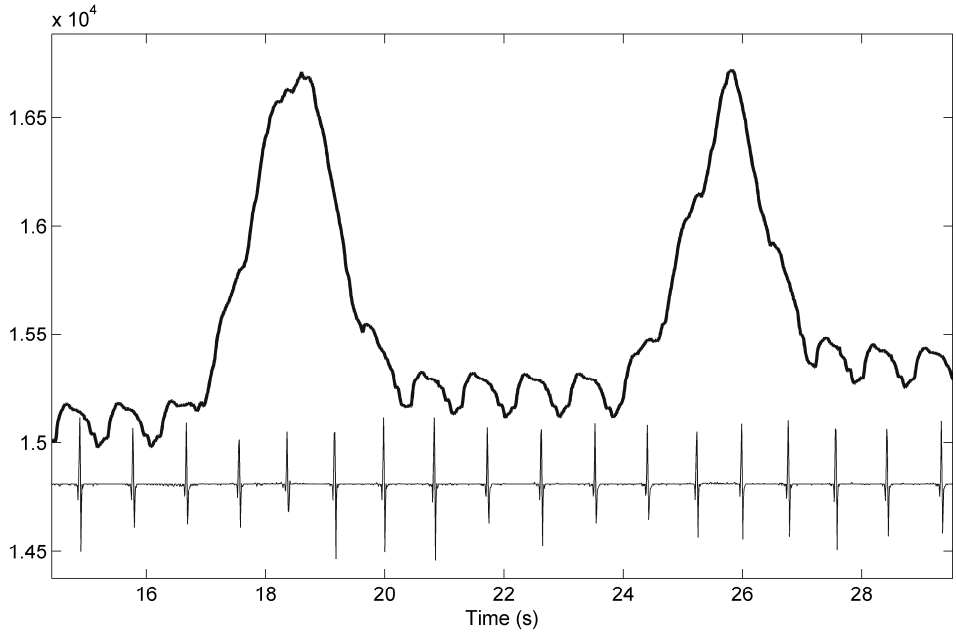

Figure 35. Sample signals measured with the first measurement device prototype. Upper signal is the measured bioimpedance and the lower one is an ECG. Signals are scaled in Matlab and so the values on the y-axis do not correlate with the actual signal values. [P2, Sepp_06]

4.3.2 The Second and the Third Prototype

Because the radio link in the first measurement prototype seriously restricted usability of the device, another approach was adopted in the second and third prototypes. In these devices the radio is eliminated from the design and replaced with a mass memory: a memory card in this case. In the second prototype a multimedia card is utilized and in the third prototype the multimedia card is replaced with a physically smaller micro secure digital card. The operating principle of these devices is to function as autonomous data loggers which are only configured before the measurement session through a wired connection. The devices then measure physiological signals continuously until the measurements are complete or the battery is flat. After the measurement session, the measurement data are transferred to a computer for further analysis. There is no longer the earlier duplication of electronics and the second and the third measurement devices each contain only one microcontroller to handle all the processes of the device.

The analogue electronics in the second prototype have also been improved on those in the first device. The main improvement is the addition of separate instrumentation amplifiers for bioimpedance and ECG signals. This decreases the crosstalk between

signals and also improves the quality of the ECG signals because there is no longer any attenuation in the ECG signal, as there was in the first measurement device. This is achieved by shifting the cut-off frequency of the first high-pass filter from 94.6 Hz to 0.1 Hz. During the initial measurements performed with the second measurement device, it was found that the properties of the instrumentation amplifier (INA331 manufactured by Texas Instruments), were not ideally suited for high frequency bioimpedance measurements. Though the bandwidth of the INA331 is sufficient at 2 MHz, the common mode rejection ratio (CMRR) is not very high. At the highest frequency utilized in the bioimpedance measurement, 100 kHz, the CMRR of INA331 is only 25 dB. This low CMRR value of the amplifier stems from the two amplifier topology implemented in the INA331. Because the paths of signals in inverting and non-inverting inputs are not identical, a signal delay becomes significant at higher frequencies and reduces the CMRR [Fran_02].

To improve the CMRR and decrease distortion artifacts in the measurement signals, a survey was made of commercially available instrumentation amplifiers. This showed that in all instrumentation amplifiers with high bandwidth, the CMRR is usually rather low. It was therefore decided to implement the instrumentation amplifier for the bioimpedance measurement with three separate operational amplifiers and to trim the circuit manually for high CMRR. This approach is clearly unsuited to mass production techniques, but it is acceptable in a prototype implementation.

Another problem detected in the first and the second prototypes was voltage saturation, caused by the stimulating current used to perform the bioimpedance measurements when the value of the polarization impedance of the electrodes is large. After investigation, the cause of this problem was found to be the non-ideal properties of the current feeding operational amplifier. The current feeding electronic circuit utilized in the first measurement device is presented in Figure 36. The tissue under study is connected to form part of the feedback loop of the amplifier and the amount of current flowing through the resistor is defined with the resistance of the resistor R_{set}. The saturation problem is caused by the input offset voltage, U_{offset}, of the operational amplifier. The DC-level of the constant amplitude voltage signal in the operational amplifier's positive input is near the voltage $\frac{1}{2}V_{CC}$. Due to non-zero voltage U_{offset}, a small DC-current flows through resistor R_{set}. This current also flows through the electrodes and the tissue. If the value of the electrode polarization impedance is very large at DC (e.g. several mega Ohms), the DC voltage in the output of the operational amplifier differs from the desired value $\frac{1}{2}V_{CC}$, and may even saturate to supply voltages. This problem was overcome by means of an additional feedback loop, as shown in Figure 37

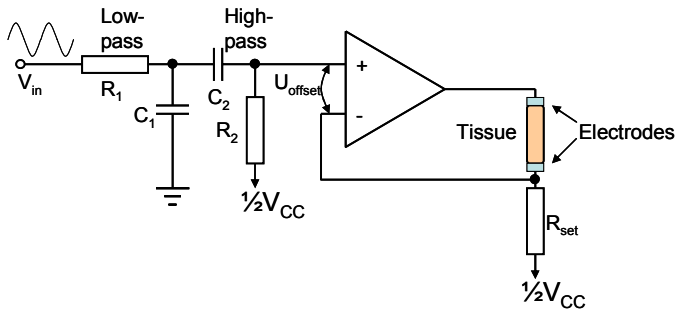

Figure 36. Excitation current amplifier utilized in the first measurement device. The tissue under study is connected to form part of the amplifier's feedback loop and amplitude of the excitation current is defined by the resistor R_{set}.

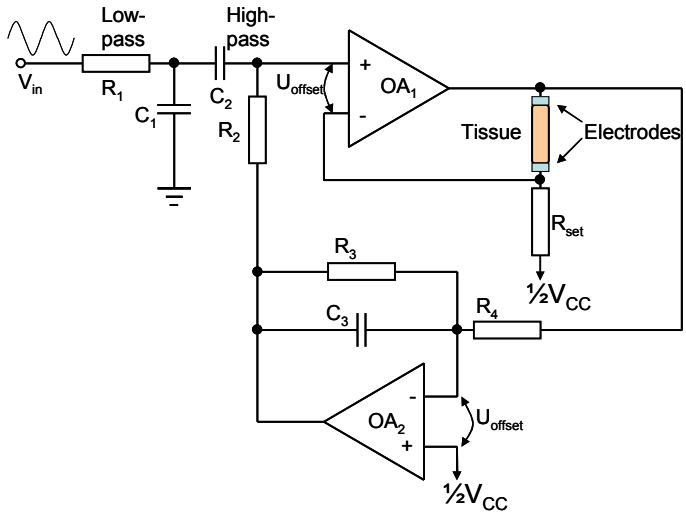

Figure 37. Improved excitation current feeding amplifier. The second operational amplifier OA_2 forms an integrator or a low pass filter that modifies DC-level of the input voltages so that the DC-level in the output is $½V_{CC}$.

The improved excitation current amplifier presented in Figure 37 has an additional feedback loop implemented with the operational amplifier OA_2. This amplifier with resistors R_3 and R_4 and capacitor C_3 forms an inverting low pass filter with a cut-off frequency set to approximately 150 Hz. At high frequencies the circuit attenuates the input signal and at low frequencies below the cut-off frequency, the amplification is approximately ten. Because the filter is an inverting type, a positive offset voltage in the output of the OA_1 causes the voltage in OA_2 output and in the OA_1 non-inverting input to decrease and vice versa. Eventually the circuit stabilizes to a state in which the DC-level in the OA_1 output is almost equal to $½V_{CC}$. Small inaccuracies in this voltage are caused by the input offset voltage of OA_2 and input bias current of OA_1. With this current feeding topology, problems are avoided with large values of electrode polarization impedance at DC frequencies. However such a circuit may easily become unstable if operating conditions are not carefully determined. For example, in order to

guarantee a stable operation when the gain in the feedback loop is ten and the R_{set} is 1.5 kΩ, the impedance of the working load, including tissue and electrodes, must be at least 50 Ω. Smaller impedances can be measured if the gain in the feedback loop is decreased. For example, with a gain of three, the minimum measurable value for the tissue impedance is approximately fifteen ohms.

The most visible difference between the first, second and third prototype is the encapsulation. The second device is housed in a custom-made container manufactured from acrylic plastic with a computer numerical control (CNC) –cutter. The main purpose here is to improve the robustness of the device. However, as the impact tolerance of the device increases, so too does the size and the weight. The second and third measurement devices are presented in Figure 38.

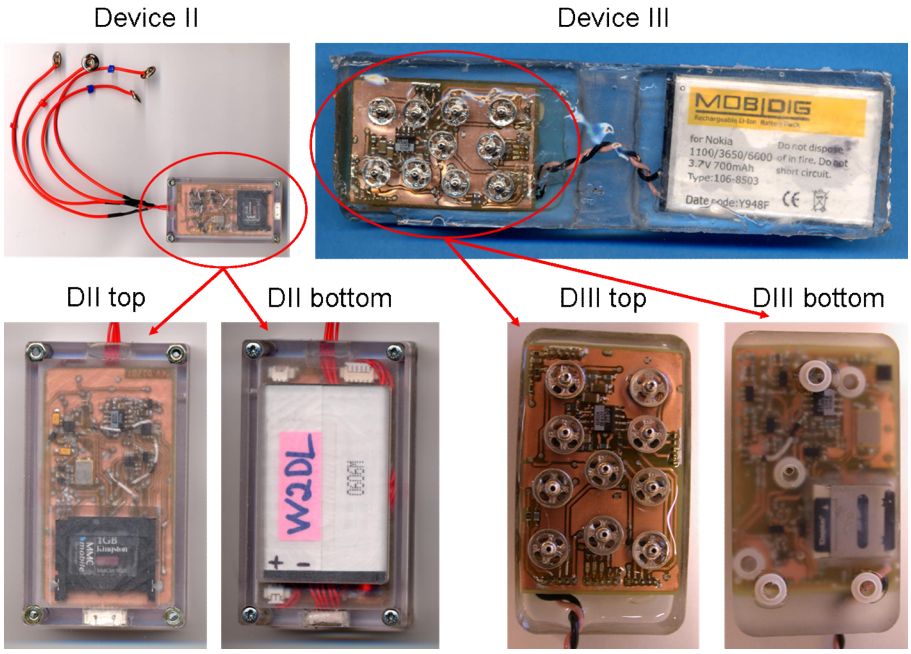

Figure 38. Portable measurement device prototypes II and III. Prototype II is housed in a custom-made casing manufactured from acrylic-plastic with a CNC cutter machine. The PCBs of the third prototype are encapsulated, first into epoxy and then into silicone, together with the rechargeable battery.

The main reason for encapsulation of the third prototype device was to ensure the device was waterproof, making it wearable in wet conditions such as a bathroom shower. Waterproof capability is achieved with layers of epoxy and silicone. First, the memory card holder was sealed with a high viscosity silicone so that the epoxy casting over the PCB does not insulate the spring loaded contacts inside the holder. A second layer of silicone is cast over the epoxy. The silicone serves as an elastic surface, which is more comfortable for the user than a hard epoxy surface. The cell phone battery utilized to provide the power supply for the measurement device has not been cast in epoxy, but only in silicone. The purpose of this arrangement is to enable battery replacement, if needed. The encapsulation of the third measurement device provides

greater resistance to impact than that used with the second device, but unfortunately it is also bulkier and heavier.

The electrode and communications connections in the third prototype are implemented with the snap-on buttons that are soldered to pin headers so that connectors protrude five millimeters above the PCB surface. The space between the connectors and the PCB is filled with epoxy and silicone layers.

Several test measurements were carried out with the second prototype to verify that it was fully functional. However, no extensive testing was performed. During the tests, it was found that the bioimpedance measurements are very sensitive to motion artifacts, as shown by the results reported in publication [P3]. No testing was performed using the third measurement device because of a failure during the coating process. The device was verified to be operational before the coating and between the epoxy and silicone casting. However, after the silicone casting it was discovered that the memory card of the device was not functioning and because it is almost impossible to remove the epoxy layer, the failure was not repaired.

A problem detected with the second measurement device was the data transmission rate. In order to save energy for performing the actual measurements, a low power microcontroller was selected as the core of the device. This poses a problem when the data is copied from the device to a computer after a measurement session. The initial intention was to transfer data from a memory card to a computer through a Universal Serial Bus (USB) connection. This requires the microcontroller to first read the data from memory card and then send them to a personal computer. However, due to the low processing power of the microcontroller, this data transfer takes almost as much time as the measurement session itself. To speed up the data transfer, the second measurement device was screwed open after each measurement session and the data was read from the measurement card with an external memory card reader.

4.3.3 The Fifth Portable Measurement Device

The fourth prototype was simply an evaluation board designed to test the new microcontroller utilized in the fifth, and the final, measurement device. Several decisions were tested on this evaluation board, including co-operation of the ANT radio and the micro SD memory card. After successful testing, the fifth version of the portable physiological measurement device was designed and implemented. The block diagram of the device is presented in Figure 39.

The fifth measurement device combines the best parts of the previous devices with a number of additional improvements. This device contains a memory-card for long-term measurements and a radio link for short-term measurements with a reduced sample rate. The operation principle of the device is to measure physiological signals automatically and to store unconditioned measurement signals to the memory card. Before a measurement session begins, the quality of the measurement signals can be inspected through a radio link. At the end of each measurement session, the data on the memory card are transferred to a computer with a memory card reader for further measurement analysis with Matlab or other software applications.

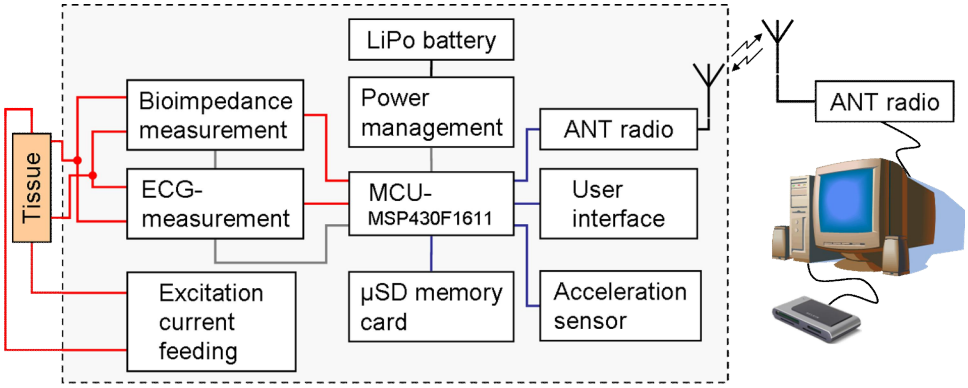

Figure 39. Block diagram of the fifth measurement device prototype developed in the Wisepla project.

One improvement from prototypes one to three is a redesigned constant amplitude voltage generator. In all the previous measurement devices, the voltage signal has been generated with a DDS-based programmable waveform generator. As mentioned earlier, a drawback of this circuit is its high power consumption. In the measurements performed with prototypes one and two, it was found that for the respiration measurement, a programmable excitation current frequency does not provide any additional benefits, provided the frequency is sufficiently high, for example, 100 kHz or higher. Because of this a voltage generator was designed with a constant frequency and low power consumption. The oscillation circuit is based on equal component Sallen-Key low-pass filter topology [Fran_02] and it is presented in Figure 40. The operating principle of the circuit is to set the amplification with the resistors R_2 and R_3 to be high enough to cause the circuit to be unstable. This instability causes the circuit to oscillate and produces a sinusoidal voltage signal with increasing amplitude. When the amplitude in the circuit output is high enough, the diodes D_1 and D_2 start to conduct and connect the resistor R_4 in parallel with the resistor R_2 ,which decreases amplification, decreasing the voltage amplitude in the output and causing the circuit to be stable again. Finally, the circuit stabilizes to produce a constant amplitude sinusoidal voltage signal whose frequency is defined by the ratio of components R_1 and C_1. The current consumption of the circuit is highly dependent on the type of operational amplifier used. In the fifth measurement device the oscillation circuit was implemented with the LMV721 integrated circuit with a supply current of approximately 1 mA, manufactured by National Semiconductors. If the supply voltage is 3.3 V, this gives a power consumption of 3.3 mW, which is considerably less than the 20 mW required by the AD9833 DDS circuit used previously.

As Figure 39 shows, in addition to the other measurement devices, the fifth device includes an acceleration sensor. The sensor is the SCA3000-E04, manufactured by VTI Technologies Oy and can measure acceleration along three axes in the range of ±6 g. The inclusion of the sensor in this design is to gain information on user activities and movement, and thus help in determining whether a high heart or respiration rate is the result of physical activity or by a fit, such as a heart attack.

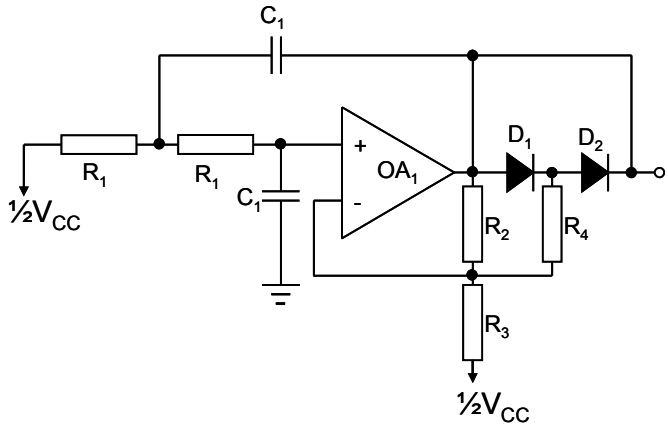

Figure 40. Constant amplitude and frequency voltage generator.

The fifth measurement device is housed in a commercially available plastic container, manufactured from acrylonitrile butadiene styrene plastic. The size of the device is 51 x 83 x 15 mm and the weight is 48 g. The printed circuit board and the housed device are presented in Figure 41.

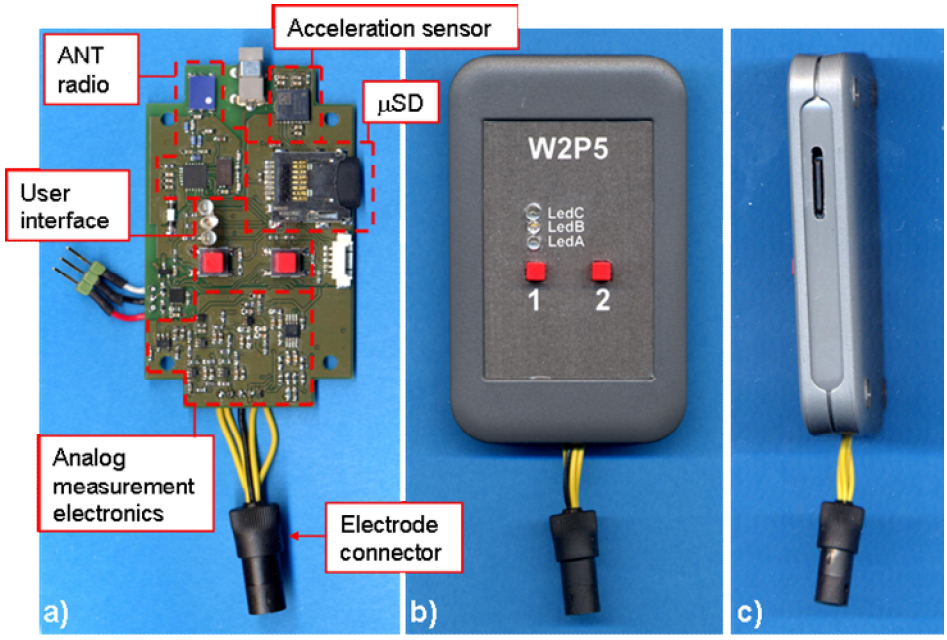

Figure 41. The final prototype of the measurement device designed and implemented in the Wisepla project: a) an assembled printed circuit board; b) top side of the device; c) right side of the device. Device measures 51 x 83 x 15 mm and weighs 48 g

A validation test and potential scenarios of use for the implemented measurement device are presented in publication [P4]. Figure 42 presents a thirty second snapshot of measurements taken during a 45-minute walking test. The measurement sample rates

during the test were set to 512 Hz for the ECG, 128 Hz for the bioimpedance and 64 Hz for every acceleration axis. All signals are handled and filtered in Matlab. The top part of Figure 42 presents a measured ECG signal and heart rate calculated from ECG. The heart rate detection algorithm is very simple. First, the ECG signal is averaged with a central moving average filter of five samples. Next, the signal is differentiated, which amplifies the fastest changes, i.e. high frequencies such as R-peaks. After differentiation, the R-peak's position is detected by thresholding with an auto-adjusted reference level defined as two thirds of the difference between the average and the maximum value inside a three second window. To reduce the amount of false R-peak detection, it is assumed that the heart rate cannot exceed three hundred beats per minute.

The middle chart in Figure 42 presents the thoracic bioimpedance signal measured around the user's chest. The bioimpedance values plotted on the figure do not represent the absolute true bioimpedance, but the dynamic changes in the bioimpedance absolute value, as mentioned earlier. The bioimpedance signal in Figure 42 is actually the voltage signal measured by the ADC, prior to any estimation of impedance. Since the bioimpedance signal contains motion artifacts, the measured signal has been averaged with a 128 sample moving average filter. This corresponds to a one second window, which has been found to be wide enough for averaging out motion artifacts caused by user activity such as by walking. The filtered bioimpedance signal correlates well with the respiration activity, as can be seen when compared to the heart rate signal, also in Figure 42. In [P4] the bioimpedance signal measured with the fifth prototype is compared to a respiration signal measured with a pneumotachograph connected to a Biopack measurement system. It was found that both signals correlate relatively well when the test subject is motionless. If the test subject is moving, motion artifacts cause disturbances to the impedance signal. However, according to preliminary tests, [Sepp_08] respiration rate at least can still be accurately measured.

The bottom part of Figure 42 presents an acceleration signal derived from acceleration signals of three axes. First, an absolute value of the total acceleration is calculated with the equation $A_{tot} = \sqrt{X^2 + Y^2 + Z^2}$. The Earth's gravity is then removed by subtracting the value of one g. The acceleration signal obtained is then averaged with a moving average filter of 16 samples, which corresponds to an averaging window of a quarter of a second. The processed acceleration signal seems to correlate well with the test subject's walking phase. The signal could be utilized for various purposes such as calculating the number of steps taken during a walk or, if the average step length is known, walking speed and walking distance could also be approximated. As demonstrated in [P4], the acceleration signals can be also used to detect the user's basic body positions such as sitting, standing or lying down.

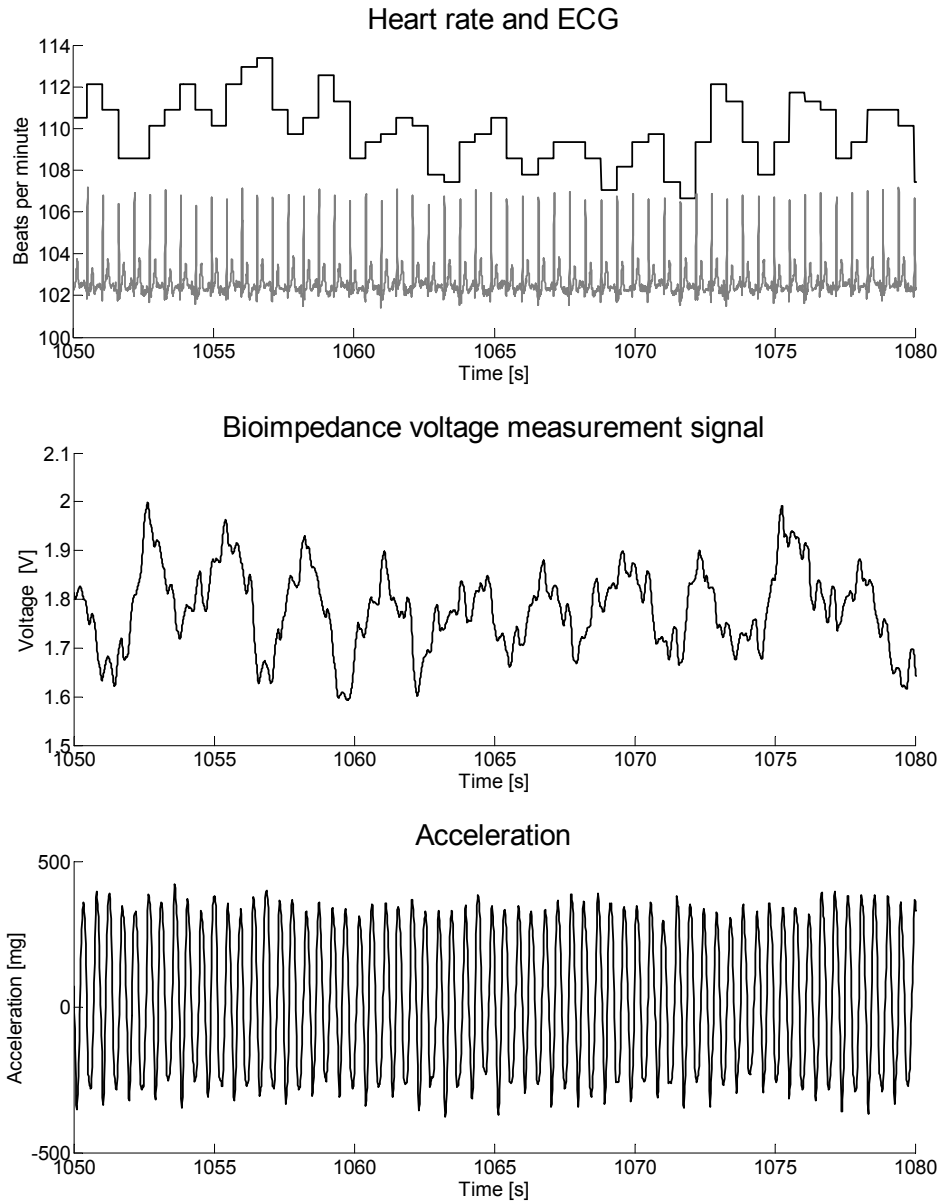

Figure 42. Signals measured with the fifth measurement device. (Top) a heart rate signal calculated from the ECG signal. (Middle) The bioimpedance signal measured around the chest. (Bottom) acceleration signal with the Earth's gravitation effect removed, presented in milli-g.

4.3.4 Conclusion of Portable Measurement Device Implementation

Table 9 summarizes the main properties of the four portable physiological measurement devices presented in this chapter. As the table shows, the fifth version of the device combines all the properties of the previous versions. The fifth device is also the smallest

and lightest. In addition, it can perform more measurements than the other devices and it has lower current consumption than the first device. Although the current consumption of devices two and three were not measured, it is reasonable to assume similar consumption to the first device because of similarities in circuit topology. A drawback of the fifth device is that the housing is not waterproof. However, as noted earlier, the third device is the only one with waterproof encapsulation and this increases the weight considerably.

Table 9. Properties of implemented portable measurement devices

	Device I	**Device II**	**Device III**	**Device V**
Dimension in mm length/width/height	44.5/63.5/25	79/45/20	134/40/16	51/83/15
Volume in cm^3	70.6	71	85.8	63.5
Weight in g	66	84	102	48
Average current consumption in mA	31	-	-	15
Encapsulation	Commercial plastic enclosure	Custom made acrylic plastic enclosure	Molded into epoxy and silicone	Commercial plastic enclosure
Radio link	✓			✓
Memory card		✓	✓	✓
Bioimpedance	✓	✓	✓	✓
ECG	✓	✓	✓	✓
Acceleration				✓

5 Summary of Publications

This thesis consists of nine publications based on the author's work between 2003 and 2010. The work deals with the design of wearable and portable physiological measurement devices and related research into technologies enabling different modules of such devices. The present chapter provides a summary of each publication and a description of the author's contribution. Publications [P1] – [P9] have not been used elsewhere as a part of a doctoral thesis.

The publications can be divided into two groups. The first five publications [P1] – [P5] discuss the implementation of physiological measurement devices and smart clothing prototypes. The last four publications [P6] – [P9] deal with the technologies required for the implementation of wearable and portable devices in general, and for monitoring devices with long term operation, in particular.

Publication [P1] presents the first version of the measurement platform intended for measuring the dynamic bioimpedance signal and ECG of the patient. Of special interest is the device's power consumption; even in continuous measurement mode, a single cell phone battery can power up the device for one full day. Due its small size, the device is inconspicuous under the garment. One major drawback is the restricted range of the implemented radio link. This prototype represents the first stage in the process of developing a compact flexible electronics platform for portable and physiological measurements.

In [P1] the author designed the overall concept of the measurement system together with Ville-Pekka Seppä, M.Sc. Seppä designed and implemented the analogue measurement part of the portable measurement device and the author designed and implemented the radio link as well as the user interface program running on a personal computer. The author wrote the publication and Seppä reviewed the text. Professors Jukka Vanhala and Jari Hyttinen supervised the project.

Publication [P2] presents the next evaluation version of the portable bioimpedance and ECG measurement device presented in [P1]. This version overcomes the drawbacks of the first prototype, such as short radio link range, low sampling rates and crosstalk between ECG and bioimpedance channels.

In [P2] the author designed the measurement device in collaboration with the project group. The analog front-end, designed by Ville-Pekka Seppä, M.Sc. and presented in publication [P1], was used again in this second device. The actual implementation of the device was carried out by the author, as was the writing of the manuscript. Professors Jukka Vanhala and Jari Hyttinen supervised the project.

Publication [P3] describes the development process of the portable physiological signal recorder. In addition to [P1] and [P2], the third evolution of the measurement device is presented. The publication discusses the challenges of designing a portable

measurement device and highlights the importance of watertight coating materials in the design process, since these increase the overall weight of the device. The paper also presents the issues involved in the use of textile electrodes in bioimpedance measurement.

The author was responsible for implementation of the third measurement device presented in [P3] and writing the manuscript. Jaana Hännikäinen, Ph.D. assisted in structuring and reviewing the contents and text. Professor Jukka Vanhala supervised the work.

Publication [P4] concludes the development process of the portable physiological signal recorder presented earlier in publications [P1] – [P3]. This publication presents the fifth version of the measurement device. This is smaller and lighter than the earlier prototypes. [P4] also presents the evaluation measurements of the recording device and demonstrates that it can function effectively and continuously for a full 24 hours.

In [P4], the author was responsible for the design and implementation of the measurement system, together with programming of the user interface program. The measurement device utilizes the basic measurement setup designed initially by Ville-Pekka Seppä, M.Sc. and further developed by the author. Seppä and the author collaborated on arranging the evaluation measurements and Seppä edited the measurements results. The author wrote the manuscript of the paper and Professors Jukka Vanhala and Jari Hyttinen supervised the project.

Publication [P5] presents the implementation of a bioimpedance measurement system, integrated into a shell suit. [P5] presents one of the first attempts to utilize fabric electrodes for bioimpedance measurement of a moving subject. The main purpose of the system is to obtain bioimpedance values that can later be examined to estimate conditions such as total body water. However, a number of research issues were not fully addressed in this publication, such as the functionality of the textile electrodes in mobile measurement applications and the suitability of bioimpedance technology for assessing the hydration status of mobile users.

In [P5], the author defined the functionality of the overall system together with the other members of the research team. The measurement modules utilized in the system were designed and implemented by Kari Kukkonen, M.Sc. The author designed and implemented the user interface, integrating the electronics into the measurement suit and also the user interface program running on a personal computer. Tiina Järvinen, M.Sc. helped with the sewing tasks and also in performing the test. The publication was written by the author and reviewed by Jaana Hännikäinen, M.Sc. and Kari Kukkonen, M.Sc. Professor Jukka Vanhala supervised the project.

Publication [P6] deals with the behavior of textile electrodes in bioimpedance measurements. The bioimpedance measurement suit presented in publication [P5] was utilized as an evaluation platform for the electrodes. To assess the behavior of textile electrodes, it is necessary to compare their performance with that of commercial Ag/AgCl electrodes. Both types of electrode are tested during light office work and walking. The results show that textile electrodes attach more firmly to the skin than gel-paste electrodes. This was because the textile electrodes were attached with an elastic

strap and the gel-paste electrodes only with glue. When the attachment of gel-paste electrodes was improved with an additional rubber band, both electrodes performed equally well, thus confirming that textile electrodes are suitable for use in bioimpedance measurement on moving subjects.

For [P6] the author designed the evaluation measurements protocol in collaboration with the project group. The measurement results were analyzed by the author and Jaana Hännikäinen, M.Sc. Katja Vähäkuopus designed the garment that was used for the measurement electronics during the test. The publication manuscript was written by the author and Jaana Hännikäinen, M.Sc. Professor Jukka Vanhala supervised the work.

Publication [P7] presents a simple measurement system which can be utilized for measuring the instruction-level energy consumption of a microcontroller. [P7] presents instruction-level measurements and methods for reducing microcontroller energy consumption through optimizing software running in the particular controller. The results contained in the publication show that energy-aware software optimization can achieve energy savings of up to 10 % in current consumption.

In [P7] the author implemented the system for measuring the microcontroller's current consumption and undertook the measurements. The measurement results were analyzed by Kimmo Surakka, M.Sc. and the author. The author wrote the manuscript and Kimmo Surakka revised the text. Professors Jukka Vanhala and Hannu-Matti Järvinen supervised the project.

Publication [P8] discusses instruction-level energy optimization in the compiler backend. [P8] utilizes the measurement results presented in publication [P7] and evaluates the suitability for implementing it in the compiler backend. The publication reports that many of the performance optimization methods currently implemented in compilers are also energy optimization methods. This is because they decrease the execution time of programs and thereby reduce average current consumption. In addition, some of the energy optimization techniques presented in [P8] are unsuitable for implementation in the compiler backed, but require compatibility between different stages in the compilation process. As a result, energy aware compiler backend is not implemented.

[P8] was written by Kimmo Surakka, M.Sc. The author implemented the measurements for the target microcontroller and the results were analyzed by Kimmo Surakka, M.Sc., together with the author. Professors Tommi Mikkonen, Hannu-Matti Järvinen and Jukka Vanhala reviewed the text and supervised the work.

Publication [P9] is based on the author's Master of Science thesis work. It presents the testing and measuring of four different short-range radio transceiver integrated circuits. On the basis of the measurements, one transceiver circuit was selected for implementation of a data link in a smart clothing application. This publication addresses the important issue that long data transfer wires in smart clothing and portable measurement applications hamper the application's usability. Measurements also show that large differences exist in the energy consumption and efficiency of different transceiver ICs. [P9] also shows that radio ICs are a fast-developing domain and that, unsurprisingly, newer circuits perform better than older ones.

In [P9] the author was responsible for specifying the area of research in co-operation with the research group. The author also implemented the required electronic instrumentation and performed the measurements. The publication was written by the author and the group members reviewed the manuscript.

6 Discussion and Conclusions

This thesis begins by presenting a definition of the general architecture for a portable measurement device. The functional blocks required on the signal path in the device are as follows: sensing front-end, signal conditioning, data storing, and user interface and/or communication. The sensing and signal conditioning blocks in a measurement system or in a measurement device are application dependent and no general architecture for them can be presented. As a result, this work does not consider these blocks at a general level. Chapter 4 presents examples of sensing blocks implemented for electrical bioimpedance measurement. The measurement device prototypes developed during the work are also introduced.

The data storing and communication or user interface blocks are also application dependent. Technologies for implementing these blocks were presented. However, because the requirements for the blocks vary greatly from one application to another, there is no technology that would stand out as being uniquely better than the others. For example, in communication, Bluetooth provides a high data rate but it also requires a lot of energy, whereas Zigbee requires less energy but provides a slower data rate. However, the design decision and technology selections for the particular functional blocks, made during the implementation of prototype measurement devices, were introduced in the Chapter 4.

An energy storage and power supply module is required to support all the other functional blocks. In most current portable devices, energy is supplied by primary or secondary batteries and thus the properties of the most common rechargeable battery technologies were discussed. A brief review is given of a fuel cell technology as one possibility for energy storage in future devices, as well as a description of some methods for energy scavenging and harvesting. It was noted that these new technologies are not yet sufficiently developed for use in portable applications. Energy available from harvesting or scavenging is somewhat limited and fuel cell technology suffers from problems with fuel distribution.

An important design consideration in portable devices is energy consumption. In order to provide long term continuous operating times and/or to use small energy storages, energy consumption should be as low as possible. Energy consumption-aware design can and must be done at every stage in the development of portable devices. If not, savings achieved at one level are easily wasted at another. In the present work, energy consumption has been studied from the perspective of consumption caused by the software running in the measurement device. It was demonstrated that with optimization of the instructions at the assembler level, energy savings of a few per cent can be achieved. To maximize the benefit of such an energy-optimization approach, its automation in a software compiler is recommended. For instance, the software in current cell phones is so large that it must be implemented with high level programming languages such as C++. Utilization of such languages conceals the low level operations of the hardware behind multiple layers of software and prevents the programmer

optimizing the energy consumption of the implemented software. A compiler with embedded energy-consumption optimization technology would allow the software programmer to write platform-independent code but still produce energy consumption-efficient software. However, the fact remains that energy consumption optimization at the instruction level can easily be discarded if the high level architecture of the software is not carefully designed.

Chapter 3 of this dissertation presents basic information on the physiological signals recorded by the measurement devices that were described in Chapter 4. These measurements relate to temperature, acceleration, bioimpedance, and ECG. Though the list of the measurements presented is by no means exhaustive, the chapter sets out only to provide background information for Chapter 4. It is probable that these types of measurement are also the most common signals to be monitored by portable monitoring systems. As such, they represent part of the basic knowledge for every designer of instrumentation for physiological measurement.

Chapter 4 discusses the measurement devices implemented at the Department of Electronics in Tampere University of Technology. These devices include two smart clothing prototypes, one for measuring the user's thermal comfort and the other for measuring the user's hydration status. The chapter also describes the development of a system targeting the implementation of a portable measurement device. All the implemented measurement devices are prototypes and as such are not suitable for commercial serial production without further development. For example, the sensing modules for bioimpedance measurement require manual tuning to achieve high quality measurement signals. Such tuning is not practical in serial production and so the devices would need to be redesigned for commercial use.

This work is intended to serve as a source of reference for the designer of portable physiological measurement devices. The purpose has not been to present all possible measurement details or all the measurement sensors and measurement conditioning circuits required for the implementation of the physiological measurement devices. Instead the purpose has been to provide an overview of the implementation blocks and technologies currently available. Having read this material, the reader should have gained an understanding of the field as well as the sources of further information.

References

[Adam_06] Adams, J.T., An introduction to IEEE STD 802.15.4, Aerospace Conference, 2006 IEEE, pp. 8.

[adiStar] Homepage of adiStar fusion textiles and shoes, available [online] http://www.adidas-polar.com, visited 16.8.2008.

[ADS1298] Datasheet for ADS1298, available [online] http://www.ti.com/lit/gpn/ads1298, visited 24.5.2010.

[ANT] Homepage of ANT technology, available [online] http://www.thisisant.com/, visited 17.5.2010.

[AT25DF641] AT25DF641 flash memory datasheet, available [online] http://www.atmel.com/dyn/resources/prod_documents/doc3680.pdf, visited 28.5.2010.

[AT90S8515] AT90S8515 microcontroller's datasheet, available [online] http://www.atmel.com/atmel/acrobat/doc0841.pdf, visited 6.4.2010.

[Atmega8515] AT90S8515 microcontroller's datasheet, available [online] www.atmel.com/atmel/acrobat/doc2512.pdf, visited 7.4.2010.

[Atmel] Atmel semiconductors, company homepage available [online] http://www.atmel.com visited 30.3.2010.

[Awad_99] Awad, E., and Asada, H.H., The Doppler Necklace: a wearable and noninvasive ultrasound sensor for continuous monitoring of blood flow in the common carotid artery, Proceedings of the First Joint, 21st Annual Conference of Engineering in Medicine and Biology and the Annual Fall Meeting of the Biomedical Engineering Society, BMES/EMBS, 1999. vol.2, pp.795.

[Aziz_06] Aziz, O. Lo, B. Darzi, A. and Yang, G-Z. . (2006). Introduction. In: Yang, G-Z. Body Sensor Networks. London: Springer –Verlag. 1-34.

[Bach_03] Bachmann, E.R., Xiaoping Y., and McGhee, R.B., Sourceless tracking of human posture using small inertial/magnetic sensors, Computational Proceedings of the IEEE International Symposium on Intelligence in Robotics and Automation, July 16-20, 2003. vol.2, pp. 822-829.

[Bake_05] Baker, N., ZigBee and Bluetooth strengths and weaknesses for industrial applications, Computing & Control Engineering Journal, vol.16, no.2, pp. 20- 25, April-May 2005.

[Bake_89] Baker, L.E., Principles of the impedance technique, IEEE Engineering in Medicine and Biology Magazine, vol.8, no.1, pp.11-15, Mar 1989.

[Beck_07] Beckmann, L., van Riesen, D., and Leonhardt, S., Optimal electrode placement and frequency range selection for the detection of lung water using Bioimpedance Spectroscopy, 29th Annual International Conference of the IEEE Engineering in Medicine and Biology Society, EMBS, August 22-26, 2007 pp.2685-2688.

[Beck_09] Beckmann, L., Hahne, S., Medrano, G., Kim, S. Walter, M., and Leonhardt, S., Monitoring change of body fluids during physical exercise using bioimpedance spectroscopy, Annual International Conference of the IEEE on Engineering in Medicine and Biology Society, EMBC, September 3-6, 2009, pp.4465-4468.

[Bez_03] Bez, R., Camerlenghi, E., Modelli, A., and Visconti, A., Introduction to flash memory, Proceedings of the IEEE, vol. 91, no. 4, pp. 489-502, April 2003.

[Blach_99] J., Blacher, R., Asmar, S., Djane, G. M., London, and M. E. Safar, Aortic Pulse Wave Velocity as a Marker of Cardiovascular Risk in Hypertensive Patients, Hypertension, Vol. 33, No. 5. pp. 1111-1117, May 1999.

[Bogo_09] Bogonez-Franco, P., Bragos, R., Bayes-Genis, A., Rosell-Ferrer, J., Implantable bioimpedance monitor using ZigBee, Proceedings of the Annual International Conference of the IEEE Engineering in Medicine and Biology Society, 2009. EMBC 2009, pp.4868-4871, 3-6 Sept. 2009

[Brew_08] Brewer, J., Gill, M., Introduction to Nonvolatile Memory, chapter on: Nonvolatile Memory Technologies with Emphasis on Flash: A Comprehensive Guide to Understanding and Using Flash Memory Devices, Pages: 1 -18, IEEE, 2008.

[BTSIG] Homepage of the Bluetooth special Interest Group, BT SIG, available [online] http://www.bluetooth.com, visited 20.5.2010.

[Byun_03] Byun, Y.H., Youn, D.Y., Lee, M.G., Kim, K.S., Song, C.H., Soo C. K., Deok, W. K., and Song, C.G., A new approach for detection of leg movement using bio-impedance technique, Proceedings of the 25th Annual International Conference of the IEEE Engineering in Medicine and Biology Society, EMBC 17-21 September 2003, vol.4, pp. 3122- 3125.

[Cai_07] Cai, Y., Jenstrup, M., Ide, K., Perko, M., and Secher, N. H., Influence of temperature on the distribution of blood in humans as assessed by electrical impedance, European Journal of Applied Physiology, Volume 81, 5, 4–3 – 448, 2000-02-07.

[CFR] Homepage of Electronic code of federal regulations, available [online] http://ecfr.gpoaccess.gov, visited 18.5.2010.

[Chak_99] Chakrabarti C., and Gaitonde D., Instruction Level Power Model of Microcontrollers, proceedings of the International Symposium on Circuits and Systems 1999, ISCAS'99, May 30 – June 2, 1999, Orlando, Florida, USA, pp. 76-79.

[Cho_09] Cho, M-C., Kim, J-Y., and Cho, S-H., A bio-impedance measurement system for portable monitoring of heart rate and pulse wave velocity using small body area, IEEE International Symposium on Circuits and Systems, ISCAS, May 24-27, 2009. pp.3106-3109.

[Corn_98] Cornish, B.H., Thomas, B.J., and Ward, L.C., Effect of temperature and sweating on bioimpedance measurements, Proceedings of International Symposium on In Vivo Body Comparison Studies Applied Radiation and Isotopes, Volume 49, Issues 5-6, May-June 1998, Pages 475-476.

[Cox_02] Cox-Riejven, P.L.M., van Kreel, B., and Soeters, P.B., Bio-electrical impedance spectroscopy: Alternatives for the conventional hand-to-foot measurements, Clinical Nutrition, Volume 21, Issue 2, April 2002, Pages 127-133.

[Dens_08] Densmore, D., and Davare, A., A Platform-Based Design Methodology for the Electronic System Level, VDM Verlag Dr. Müller Aktiengesellschaft & Co. KG, 2008, 384 pages.

[Deve_16] Van Deventer, H.R., US Patent 1184056, Self-contained generating and lighting unit, May 23, 1916.

[Dunn_06] Dunne, L.E., Walsh, P., Smyth, B., and Caulfield, B., Design and Evaluation of a Wearable Optical Sensor for Monitoring Seated Spinal Posture, the 10th IEEE International Symposium on Wearable Computers, October 11-14, 2006, pp.65-68.

[Dvor_08] Dvorak, J.L., Moving Wearables into the Mainstream Taming the Borg. New York: Springer Science+Business Media, LLC. 392, 2008.

[Eart_07] Earthman, C., Traughber, D., Dobratz, J., and Howell, W., Bioimpedance spectroscopy for Clinical Assessment of Fluid Distribution and Body Cell Mass, Nutrition in Clinical Practice, Vol. 22, No. 4, 2007 pp. 389 – 405.

[ECO] Homepage of European Communication Office, available [online] http://www.ero.dk/, visited 17.5.2010.

[Edwa_00] Edwardson, M., Talaie, V., Clark, C., Antinoro, R., Risse, A., Gonzalez, J., Weisberger, C., and Feldman, C.L., A bioelectrical impedance analysis device for improved management of congestive heart failure, Computers in Cardiology, September 24 – 27, 2000 pp. 9-12.

[Fink_03] Finkenzeller, K., RFID handbook, 2nd edition. John Wiley and Sons, 2003.

[Fost_96] Foster, K.R., and Lukaski, H.C., Whole-body impedance – what does it measure?, American Journal of Clinical Nutrition, September 1996, Vol. 64, pp. 3–8 – 396.

[Fran_02] Franco, S., Design with Operational Amplifiers and Analog Integrated Circuits, 3rd edition, New York: The McGraw-Hill Companies. 658 pages, 2002.

[Freeplay] Homepage of Freeplay consumer electronics company, available [online] http://www.freeplayenergy.com/, visited 24.6.2010

[Garmin] Homepage of Garmin, available [online] http://www.garmin.com, visited 21.5.2010.

[Gedd_89] Geddes, L.A., Baker, L.E., Principles of Applied Biomedical Instrumentation, 3rd edition, New York, Chichester, Brisbane, Toronto, Singapore, John Wiley & Sons. 961 pp.

[Gonz_08] Gonzalez-Landaeta, R. Casas, O. and Pallas-Areny, R., Heart Rate Detection From Plantar Bioimpedance Measurements, IEEE Transactions on Biomedical Engineering, vol. 55, no. 3, pp.1163-1167, March 2008.

[Grim_00] Grimnes, S., and Martinsen, Ø.G., Bioimpedance and Bioelectricity Basics, London, United Kingdom, Academic press, 360 pages, 2000.

[Gudi_99] Gudivaka, R., Schoeller, D.A., Kushner, R.F., and Bolt, M.J.G., Single- and multifrequency models for bioelectrical impedance analysis of body water compartments, Journal of Applied Physiology Vol. 87, Issue 3: 1087-1096, 1999.

[Halt_07] Halter, R.J., Hartov, A., Heaney, J.A., Paulsen, K.D., and Schned, A.R., Electrical Impedance Spectroscopy of the Human Prostate, IEEE Transactions on Biomedical Engineering, vol. 54, no. 7, pp.1321-1327, July 2007.

[Harm_08] Harms, H., Amft, O., Tröster, G., and Roggen, D. SMASH: a distributed sensing and processing garment for the classification of upper body postures. Proceedings of the 3rd international Conference on Body Area Networks, ICST, Tempe, Arizona, March 13 – 17, 2008.

[Hein_06] Heinisuo, S., and Vanhala, J., Wireless Platform for Multi-Channel Analog Measurements, the 28th Annual International Conference of the IEEE Engineering in Medicine and Biology Society, EMBS '06, August 30 – September 3, 2006, pp.5908-5911.

[Hänn_04] Hännikäinen, J., Järvinen, T., Vuorela, T., Vähäkuopus, K., and Vanhala, J., Conductive fibers in smart clothing applications. Proceedings of the Fifth International Conference on Machine Automation ICMA2004, November 24 (Wed) – 26 (Fri), 2004, Osaka, Japan, pp. 227 – 232.

[Hänn_07] Hännikäinen, J., Vuorela, T., and Vanhala, J., Physiological Measurements in Smart Clothing: A case Study of Total Body Water Estimation with Bioimpedance. Transactions of the Institute of Measurement and Control, Vol. 29, No. 3-4, pp. 337-354, 2007

[Hänn_09] Hänninen, V., "Kaksi Uutta Bluetoothia Nopeampi ja Niukempi", Prosessori, 6-7, 2009, pp. 32 – 33.

[Intel_04] Intel white paper, Enhanced Intel SpeedStep Technology for the Intel Pentium M Processor, March 2004, available [online] ftp://download.intel.com/design/network/papers/30117401.pdf

[ISO7933] International standard ISO 7933:2004 Analytical Determination and Interpretation of Heat Stress Using Calculation of the Predicted Heat Strain.

[ISO9886] International standard ISO 9886:2004 Evaluation of Thermal Strain by Physiological Measurement.

[IsoK_05] Iso-Ketola P., Karinsalo T., Myry M., Hahto L., Karhu H., Malmivaara M., and Vanhala J., A mobile device as user interface for wearable applications. Third International Conference on Pervasive Computing, PERVASIVE 2005, Munich, Germany, May 2005, pp. 5-9.

[Jaeg_95] Jaeger, R.J., Szidon, J.P., and Doucette, P.J., Instrumentation for measuring frequency of cough, the 17th IEEE Annual Conference on Engineering in Medicine and Biology Society, September 20-23, 1995, vol. 2, pp.1645-1646.

[Jaff_08] Jaffrin, M.Y., Morel, H., Body fluid volumes measurements by impedance: A review of bioimpedance spectroscopy (BIS) and bioimpedance analysis (BIA) methods, Medical Engineering & Physics, Volume 30, Issue 10, Special issue to commemorate the 30th anniversary of Medical Engineering & Physics – December 2008, Pages 1257-1269.

[Jüri_00] Jürimae, J., and Jürimae, T., Changes in Body Fluids during Endurance Rowing Training, Annals of the New York Academy of Sciences, 2000, May, Vol. 904, pp. 353-358.

[Khal_95] Khaled, M.A., Khatun, M., Haque, M., Kabir, I., and Mahalanabis, D., Single, dual and multi-frequency bioimpedance to measure human body composition, Proceedings of the First Regional IEEE Conference on Engineering in Medicine and Biology Society and the 14th Conference of the Biomedical Engineering Society of India, February 15-18, 1995 pp.1/87-1/88.

[Kim_99] Kim, S., and Kim, J., Opcode encoding for low-power instruction fetch, Electronics Letters , vol. 35, no. 13, June 24, 1999, pp.1064-1065.

[Kish_07] Kishimoto, Y., Kutsuna, Y., and Oguri, K., Detecting Motion Artifact ECG Noise During Sleeping by Means of a Tri-axis Accelerometer, Proceedings of the 29th Annual International Conference of the IEEE Engineering in Medicine and Biology Society, EMBS 2007, August 22-27, 2007, pp.2669-2672.

[Klei_05] Kleiger R. E., Stein P. K., and Bigger J.T. Jr., Heart Rate Variability: Measurement and Clinical Utility, The Annals of Noninvasive Electrocardiology, vol. 10, no. 1, pp. 88-101, 2005.

[Knaa_10] Knaappila, A., Fuel Cells in Electronics, Master of Science Thesis, Tampere University of Technology, Faculty of Computing and Electrical Engineering, 2010, 66 pages.

[Korh_03] Korhonen I., Pärkkä J., Van Gils M., Health monitoring in the home of the future, IEEE Magazine on Engineering in Medicine and Biology, vol.22, no.3, pp. 66-73, May-June 2003.

[Kubi_70] Kubicek, W. G., Patterson, R. P., and Witsoe, D. A., Impedance Cardiography as a noninvasive Method of Monitoring Cardiac Function and Other Parameters of the Cardiovascular System, Annals of the New York Academy of Sciences, Vol. 170, Issue 2, pp. 724-732, 1970.

[Kukk_01] Kukkonen, K., Vuorela, T., Rantanen, J., Ryynänen, J., Siili, A., & Vanhala, J., 2001. The design and implementation of electrically heated clothing. The Fifth International Symposium on Wearable Computers, 8-9 October 2001, Zürich, Switzerland, pp. 180-181.

[Kush_86] Kushner, R.F., and Schoeller, D.A., Estimation of total body water by bioelectrical impedance analysis, American Journal of Clinical Nutrition, Vol 44, 417-424, 1986.

[Kyle_04] Kyle, U.G., Bosaeus, I., De Lorenzo, A.D., Deurenberg, P., Elia, M., Gomez, J.M., Heitmann, B.L., Kent-Smith, L., Melchior, J.C., Pirlich, M., Scharfetter, H., Schols, A.M.W.J., and Pichard, C., Composition of the ESPEN Working Group, Bioelectrical impedance analysis–part I: review of principles and methods, Clinical Nutrition, Volume 23, Issue 5, October 2004, Pages 1226-1243.

[Kyle2_04] Kyle, U.G. Bosaeus, I., De Lorenzo, A.D., Deurenberg, P., Elia, M., Gomez, J.M., Heitmann, B.L., Kent-Smith, L., Melchior, J.C., Pirlich, M., Scharfetter, H., Schols, A.M.W.J., and Pichard, C., Bioelectrical impedance analysis – part II: utilization in clinical practice, Clinical Nutrition, Volume 23, Issue 6, December 2004, Pages 1430-1453.

[Kymi_98] Kymissis, J., Kendall, C., Paradiso, J., Gershenfeld, N., Parasitic power harvesting in shoes, Digest of Papers. On Second International Symposium on Wearable Computers, pp.132-139, 19-20 Oct 1998.

[Lahi_02] Lahiri, K., Raghunathan, A., Dey, S., and Panigrahi, D., Battery-driven system design: a new frontier in low power design, Proceedings of the 7th Asia and South Pacific Design Automation Conference and the 15th International Conference on VLSI Design, ASP-DAC, 2002, pp.261-267.

[Lee_01] Lee, S., Ermedahl, A., and Min, S.L., An Accurate Instruction-Level Energy Consumption Model for Embedded RISC Processors. In Proceedings of the ACM SIGPLAN Workshop on Languages, Compilers and Tools For Embedded Systems, LCTES '01, Snow Bird, Utah, US, 2001.

[Lee_03] Lee, S.M., Kwon, S.Y., Cho, B.H., Kim, I.Y., and Kim, S.I., A new PDA based body fat measurement system, IEEE EMBS Asian-Pacific Conference on Biomedical Engineering, October 20-22, 2003, pp. 44- 45.

[Lee_07] Lee, J.S., Su, Y.W., Shen, C.C., A Comparative Study of Wireless Protocols: Bluetooth, UWB, ZigBee, and Wi-Fi, proceedings of the 33rd Annual Conference of the IEEE Industrial Electronics Society, IECON 2007, November, 5-8, 2007, pp.46-51.

[Li_08] Zhangyong Li, Zhonghua He, Wei Wang, and Chaoshi Ren, Measurement system for electrical impedance and EGG, Proceedings of the International Conference on Information Technology and Applications in Biomedicine, 2008. ITAB 2008., pp.495-498, 30-31 May 2008.

[Ling_99] Lingwood, B.E., Colditz, P.B., and Ward, L.C., Biomedical applications of electrical impedance analysis, Proceedings of the Fifth International Symposium on Signal Processing and Its Applications, ISSPA '99, 1999, vol.1, pp.367-370.

[Loza_97] Lozano, A., Electrode errors in bioimpedance measurement systems for long-term applications, Proceedings of the Sixteenth Southern Biomedical Engineering Conference, April, 3-6, 1997, pp.3-6.

[Luka_85] Lukaski, H.C., Johnson, P.E., Bolonchuk, W.W., and Lykken, G.I., Assessment of fat-free mass using bioelectrical impedance measurements of the human body, American Journal of Clinical Nutrition, Vol. 41, pp. 810-817.

[Luo_05] Luo, R., Luo, H., Yang, H., and Xie, Y., An instruction-level analytical power model for designing the low power systems on a chip, the 6th International Conference On ASIC, ASICON 2005, October 24, 2005 vol.2, pp.1094-1097.

[Maci_02] Macii, A., Benini, L., and Poncino, M., Memory Desing Techniques for Low Energy Embedded Systems, Kluwer Academic Publisher, Boston, 144 pages, 2002.

[Maje_08] Majer, L., and Stopjakova, V., Portable Measurement Equipment for Continuous Biomedical Monitoring using Microelectrodes, 11th IEEE Workshop on Design and Diagnostics of Electronic Circuits and Systems, DDECS 2008, April 16-18, 2008, pp.1-4.

[Mali_96] Malik, M., Bigger, J.T., Camm, A.J., Kleiger, R.E., Malliani, A., Moss, A.J., and Schwartz P.J., Heart rate variability: Standards of measurement, physiological interpretation, and clinical use, European Heart Journal 1996 Vol. 17, No. 3, pp. 354-381.

[Malm_95] Malmivuo, J., and Plonsey, R., Bioelectromagnetism. New York: Oxford University Press, 1995, 482 pp.

[Marq_09] Marquez, J.C., Seoane, F., Valimaki, E., Lindecrantz, K., Textile electrodes in electrical bioimpedance measurements – a comparison with conventional Ag/AgCl electrodes, Proceedings of the Annual International Conference of the IEEE on Engineering in Medicine and Biology Society, 2009. EMBC 2009. pp.4816-4819, 3-6 Sept. 2009.

[Matt_07] Mattmann, C., Amft, O., Harms, H., Troster, G., and Clemens, F., Recognizing Upper Body Postures using Textile Strain Sensors, the 11th IEEE International Symposium on Wearable Computers, October, 11-13, 2007, pp.29-36.

[Medr_07] Medrano, G., Ubl, A., Zimmermann, N., Gries, T., and Leonhardt, S., Skin Electrode Impedance of Textile Electrodes for Bioimpedance Spectroscopy, proceedings of the 13th International Conference on Electrical Bioimpedance and the 8th Conference on Electrical Impedance Tomography, ICEBI 2007, August 29th – September 2nd 2007, Graz, Austria.

[Meht_97] Mehta, R., Owens, R.M., Irwin, M.J., Chen, R., and Ghosh, D., Techniques for low energy software, Proceedings of International Symposium on Low Power Electronics and Design, August 18-20, 1997, pp. 72- 75.

[Merr_90] Merri, M., Farden, D.C., Mottley, J.G., and Titlebaum, E.L., Sampling frequency of the electrocardiogram for spectral analysis of the heart rate variability, IEEE Transactions on Biomedical Engineering, Vol.37, No.1, pp.99-106, January 1990.

[Mund_05] Mundt, C.W., Montgomery, K.N., Udoh, U.E., Barker, V.N., Thonier, G.C., Tellier, A.M., Ricks, R.D., Darling, R.B., Cagle, Y.D., Cabrol, N.A., Ruoss, S.J., Swain, J.L., Hines, J.W., and Kovacs, G.T.A., A multiparameter wearable physiologic monitoring system for space and terrestrial applications, IEEE Transactions on Information Technology in Biomedicine, vol.9, no.3, pp.382-391, September, 2005.

[Mura_07] Murakami, K., and Uchiyama, T., Bioelectrical Impedance Measurement of Subcutaneous Fat Thickness Using Apparent Resistivity, the 6th International Special Topic Conference on Information Technology Applications in Biomedicine, ITAB 2007, November 8-11, pp.210-212.

[Naim_09] Naima, R., and Canny, J., The Berkeley Tricorder: Ambulatory Health Monitoring, Sixth International Workshop on Wearable and Implantable Body Sensor Networks, BSN, June 3-5, 2009, pp.53-58.

[Naka_01] Nakamura, T., and Yamamoto, Y., Evaluation system of physical exercise ability using bio-electrical impedance, Proceedings of IEEE International Symposium on Industrial Electronics, ISIE 2001, vol.3, pp.2053-2058.

[Neef_09] Neef, H.J., International overview of hydrogen and fuel cell research, the 6th World Energy System Conference; Advances in Energy Studies, 5th workshop on Advances, Innovation and Visions in Energy and Energy-related Environmental and Socio-Economic Issues, WESC 2006, Volume 34, Issue 3, March 2009, Pages 327-333.

[Neum_95] Neuman, M. R. Biopotential Electrodes, chapter in book Medical Instrumentation Application and Design, 2nd edition 1995, New Ypork, Chichester, Brisbane, Toronto, Singapore John Wiley & Sons inc, 814 pp.

[Neuv_04] Neuvo, Y. Cellular phones as embedded systems, Digest of Technical Papers of IEEE International Solid-State Circuits Conference, ISSCC. 2004, February 15-19, pp. 32- 37.

[Nien_93] Niensstedt, W., Hänninen, O., Arstila, A., and Bjorkqvist, S.E., Ihmisen fysiologia ja anatomia. 9th ed. Werner Söderström osakeyhtiö, Porvoo, 635 pp. 1993.

[Niko_02] Nikolaidis, S., Kavvadias, N., Neofotistos, P., Kosmatopoulos, K., Laopoulos, T., and Bisdounis, L., Instrumentation Set-up for Instruction Level Power Modeling, Integrated Circuit Design. Power and Timing Modeling, Optimization and Simulation, Volume 2451/2002, pages 263-290, Springer Berlin / Heidelberg.

[Niko_03] Nikolaidis, S., Kavvadias, N., Laopoulos, T., Bisdounis, L., and Blionas, S., Instruction Level Energy Modeling for Pipelined Processors, Lecture Notes in Computer Science, Integrated Circuit and System Design, Volume 2799/2003, September 17, 2003, pages 279-288 Springer Berlin / Heidelberg.

[Niko_05] Nikolaidis, S., Chatzigeorgiou, A., and Laopoulos, T., Developing an environment for embedded software energy estimation, Selected Papers Presented at IDAACS 2003 Computer Standards & Interfaces, Volume 28, Issue 2, December 2005, Pages 150-158.

[Nopp_97] Nopp, P., Harris, N., Zhao, T., and Brown, B., Model for the dielectric properties of human lung tissue against frequency and air content, Medical and Biological Engineering and Computing, Vol. 35, Num. 6, pp. 695 – 702, 1997.

[Obri_88] O'Brien, J.F., Bernard, T.E., and Kenney, W.L., Personal monitor to protect workers from heat stress, Conference Record for 1988 IEEE Fourth Conference on Human Factors and Power Plants, June 5-9, 1988, pp.529-531.

[Oliv_03] Oliver, J., Mocanu, O., Ferrer, C., Energy awareness through software optimization as a performance estimate case study of the MC68HC908GP32 microcontroller, proceedings of the 4th International Workshop on Microprocessor Test and Verification: Common Challenges and Solutions, May 29-30, 2003, pp. 111- 116.

[Omron] Homepage of Omron healthcare products, available [online] http://omronhealthcare.com, visited 25.3.2010.

[Opencores] Opencores, integrated circuit models, available [online] http://www.opencores.org, visited 31.3.2010.

[Panf_06] Panfili, G., Piccini, L., Maggi, L., Parini, S., and Andreoni, G., A wearable device for continuous monitoring of heart mechanical function based on Impedance CardioGraphy, proceedings of the 28th Annual International Conference of the IEEE Engineering in Medicine and Biology Society, EMBS '06, August 30 – September 3, 2006, pp.5968-5971.

[Para_05] Paradiso, J.A., and Starner, T., Energy scavenging for mobile and wireless electronics, IEEE Pervasive Computing, vol. 4, no. 1, pp. 18- 27, January-March, 2005.

[Para_06] Paradiso, J.A., Systems for human-powered mobile computing, the 43rd ACM/IEEE Design Automation Conference, 2006, pp.645-650.

[Patt_89] Patterson, R.P., Fundamentals of impedance cardiography, IEEE Engineering in Medicine and Biology Magazine, vol. 8, no. 1, March 1989, pp. 35-38.

[Patt_10] Patterson, R. P., Impedance cardiography: What is the source of the signal, Journal of Physics: Conference Series, Vol. 224, Num. 1., 2010.

[Picc_94] Piccoli, A., Rossi, B., Pillon, L., and Bucciante, G., A new method for monitoring body fluid variation by bioimpedance analysis: The RXc graph, Kidney International, Vol. 46,Issue 2, 1994, pp. 534 – 539.

[Picc_95] Piccoli, A., Nigrelli, S., Caberlotto, A., Bottazzo, S., Rossi, B., Pillon, L., and Maggiore, Q., Bivariate normal values of the bioelectrical impedance vector in adult and elderly populations, American Journal on Clinical Nutrition, vol. 61, No. 2, pp. 269-270, 1995.

[Pinn_94] Pinna, G.D., Maestri, R., Di Cesare, A., Colombo R., and Minuco, G., The accuracy of power-spectrum analysis of heart-rate variability from annotated RR lists generated by Holter systems, Physiological Meas., Vol. 15, No. 2, pp. 163-79, 1994.

[Pola_07] Pola, T., and Vanhala, J., Textile Electrodes in ECG Measurement, the 3rd International Conference on Intelligent Sensors, Sensor Networks and Information, ISSNIP 2007, December 3-6 pp. 635-639.

[Polar] Homepage of Polar heart rate monitors, available [online] http://www.polar.fi, visited 25.3.2010.

[Popa_06] Popa, M., Sirbu, D., Curseu, D., and Ionutas, A., The Measurement of Body Composition by bioelectrical Impedance, IEEE International Conference on Automation, Quality and Testing, Robotics, May 25-28, 2006, vol.2, pp.437-440.

[Pulk_05] Pulkkinen, A., Saalasti, S., and Rusko, H. Energy expenditure can be accurately estimated from HR without individual laboratory calibration. ACSM Congress, Nashville, June 1-4, 2005.

[Puur_06] Puurtinen, M.M., Komulainen, S.M., Kauppinen, P.K., Malmivuo, J.A.V., and Hyttinen, J.A.K., Measurement of noise and impedance of dry and wet textile electrodes, and textile electrodes with hydrogel, the 28th Annual International Conference of the IEEE Engineering in Medicine and Biology Society, EMBS '06, August 30 - September 3, 2006, pp.6012-6015.

[Ragh_05] Raghunathan, V., Kansal, A., Hsu, J., Friedman, J., and Srivastava, M., Design considerations for solar energy harvesting wireless embedded systems, Fourth International Symposium on Information Processing in Sensor Networks, IPSN 2005. April 15, 2005, pp. 457-462.

[Rant_01] Rantanen, J., Ryynänen, O., Kukkonen, K., Vuorela, T., Siili, A. & Vanhala, J. 2001. Electrically heated clothing. World Multiconference on Systemics, Cybernetics and Informatics, Mobile/Wireless Computing, Proceedings, July 22-25, 2001, Orlando, Florida, USA, pp. 490-495.

[Rant2_01] Rantanen, J., Vuorela, T., Kukkonen, K., Ryynänen, O., Siili, A. & Vanhala, J. 2001. Improving human thermal comfort with smart clothing. 2001 IEEE International Conference on Systems, Man and Cybernetics, e-Systems and e-Man for Cybernetics in Cyberspace, Tucson, Arizona, October 7-10, 2001, pp. 795-800.

[Rosa_09] Rosati R., Evaluation of Remote Monitoring in Home Health Care, Proceedings of International Conference on eHealth, Telemedicine, and Social Medicine, eTELEMED '09, February 1-7, 2009, pp.151-153.

[Rome_09] Romero, E., Warrington, R.O., Neuman, M.R., Body motion for powering biomedical devices, Annual International Conference of the IEEE on Engineering in Medicine and Biology Society, 2009. EMBC 2009, pp.2752-2755, 3-6 Sept. 2009.

[Round_04] Roundy, S., Steingart, D., Frechette, L., Wright, P., and, Rabaey, J., Power Sources for Wireless Sensor Networks, proceedings of 1st European workshop on Wireless Sensor Networks, ESWN'04, Berlin, Germany, pp. 1-17.

[Rusk_03] Rusko, H.K., Pulkkinen, A., Saalasti, S., Hynynen, E. and Kettunen, J., Pre-prediction of EPOC: A tool for monitoring fatigue accumulation during exercise?, ACSM Congress, San Francisco, May 28-31, 2003.

[Russ_98] Russell, J.T., and Jacome, M.F., Software power estimation and optimization for high performance, 32-bit embedded processors, Proceedings of International Conference on Computer Design: VLSI in Computers and Processors, ICCD '98, October 5-7, 1998, pp.328-333.

[Sang_08] Sanghyun K., Dongwan R., and Changseok, B., Implementation of Smart Headband for the Wearable Healthcare, Digest of Technical Papers. International Conference on Consumer Electronics, ICCE 2008, January 9-13, 2008, pp.1-2.

[Sche_03] Scheffler M., Hirt E., and Caduff A., Wrist-Wearable Medical Devices: Technologies and Applications. Medical Device Technology, September 2003, Vol. 14 Issue 7, p. 26, 5 pages.

[Schm_89] Schmidt, R.F., and Thews, G., Human Physiology. 2nd ed. Berlin Heidelberg: Springer-Verlag, 1989, 825 pp.

[Schm_04] Schmitz, M., Al-Hashimi, B., and Eles, P., System-Level design Techniques for Energy-Efficient embedded Systems, Luwer Academic Publishers, 2004, 211 pages.

[SDCARD] Homepage of SD association, available [online] http://www.sdcard.org/home/, visited 31.5.2010.

[SDIO_07] SD Specifications Part E1 SDIO Simplified Specification, version 2.00, available [online] http://www.sdcard.org/developers/tech/sdio/sdio_spec/, visited 31.5.2010.

[SDSpec_06] SD Specifications Part 1 Physical Layer Simplified Specification, version 2.00, available [online] http://www.sdcard.org/developers/tech/sdcard/pls/, visited 31.5.2010.

[SDT] Homepage of Swim Distance Tracker. http://uintimatkamittari.fi/, visited 25.3.2010.

[Seiko] Homepage of Seiko kinetic watches, available [online] http://www.seikowatches.com/technology/kinetic/index.html, visited 7.5.2010.

[SenseWear] Homepage of SenseWear, available [online] http://www.sensewear.com/, visited 25.3.2010.

[Sepp_06] Seppä, V.P., Master of Science Thesis, Bioimpedance in a wireless wearable device, Tampere University of Technology, Department of electrical engineering, June 2007, 66 pages.

[Sepp_07] Seppä, V.P., Väisänen, J., Kauppinen, P., Malmivuo, J., and Hyttinen, J., Measuring Respirational Parameters with a Wearable Bioimpedance Device, Proceedings of the 13th International Confrence on Electrical Bioimpedance, ICEBI 2007, 29th Aug - 2nd Sept, Graz, Austria, pp. 663-666.

[Sepp_08] Seppä, V.P., Lahtinen, O., Väisänen, J., and Hyttinen, J., Assessment of breathing parameters during running with a wearable bioimpedance device, in IFMBE Proceedings, vol. 22, pp. 1088-1091, Springer, 2008

[Sepp_09] Seppä, V.P., Viik, J., Naveed, A., Väisänen, J., and Hyttinen, J., Signal waveform agreement between spirometer and impedance pneumography of six chest band electrode configurations, in IFMBE Proceedings, vol. 25 of VII, pp. 689-692, Springer, 2009.

[Sepp_10] Seppa, V.P., Viik, J., Hyttinen, J., Assessment of Pulmonary Flow Using Impedance Pneumography, IEEE Transactions on Biomedical Engineering, vol.57, no.9, pp.2277-2285, Sept. 2010

[Snel_09] Snellman, H., Polttokennoa sovitetaan hybridiautoon, Prosessori, no. 8, 2009, pp. 26-29.

[Sokw_98] Sokwoo R., Yang B.H., Chang K., and Asada H.H., The ring sensor: a new ambulatory wearable sensor for twenty-four hour patient monitoring, Proceedings of the 20th Annual International Conference of the IEEE Engineering in Medicine and Biology Society, 29 Oct-1 Nov, 1998, vol.4, pp.1906-1909.

[Star_03] Starner, T.E., Powerful change part 1: batteries and possible alternatives for the mobile market, IEEE Pervasive Computing magazine, October-December, 2003, vol. 2, no. 4, pp. 86- 88.

[Star_04] Starner, T., and Paradiso, J.A., Human Generated Power for Mobile Electronics, chapter 45 in Low-Power Electronics Design, C. Piquet, editor, CRC Press, 2004, pp 1-35.

[Star_96] Starner, T., Human-powered wearable computing, IBM Systems Journal, 1996, vol. 35, no. 3, pp. 618-629.

[Steg_05] Steg, H., Strese, H., Hull, J., and Schmidt, S., Europe is facing a demographic challenge Ambient Assisted Living offers solutions, September, 2005, 85 pages, available [online] http://www.aal169.org/Published/Final%20Version.pdf, visited 11.6.2010

[Stoj_09] Stojcev, M.K., Kosanovic, M.R., and Golubovic, L.R., Power management and energy harvesting techniques for wireless sensor nodes, the 9th International Conference on Telecommunication in Modern Satellite, Cable, and Broadcasting Services, TELSIKS '09, October 7-9, 2009, pp.65-72

[Su_94] Su, C.L., Tsui, C.Y., and Despain, A.M., Saving power in the control path of embedded processors, IEEE Design & Test of Computers, Winter 1994, vol. 11, no. 4, pp.24-31.

[Suunto] Homepage of Suunto wrist computers, available [online] http://www.suunto.com, visited 25.3.2010.

[Team] Homepage of Team Group Incorporated, available [online] http://www.teamgroup.com.tw, 31.5.2010.

[Tekes] Homepage of Tekes Fuel Cell program, available [online] http://akseli.tekes.fi/opencms/opencms/OhjelmaPortaali/ohjelmat/Polttokennot/en/etusivu.html, visited 1.6.2010.

[Texas] Texas Instruments, company homepage, available [online] http://www.ti.com/, visited 31.3.2010.

[Tilastokeskus] Tilastokeskus, Statistics Finland, available [online] http://www.stat.fi/til/vaenn/2007/vaenn_2007_2007-05-31_tie_001.html, visited 25.3.2010.

[Tiwa_94] Tiwari, V., Malik, S., and Wolfe, A., Power Analysis Of Embedded Software: A First Step Towards Software Power Minimization, IEEE Transactions on Very Large Scale Integration (VLSI) Systems, December, 1994, Vol. 2, No. 4, pp. 437 – 445.

[Tiwa2_94] Tiwari, V., Malik, S., and Wolfe, A., Compilation techniques for low energy: an overview, Digest of Technical Papers, IEEE Symposium on Low Power Electronics, October 10-12, 1994, pp.38-39

[Togn_06] Tognetti, A. Lorussi, F., Tesconi, M., Bartalesi, R., Zupone, G., and De Rossi, D., Wearable kinesthetic systems for capturing and classifying body posture and gesture, the 27th Annual International Conference of the Engineering in Medicine and Biology Society, IEEE-EMBS 2005. January 17-18, 2006, pp.1012-1015

[Wireless] Wireless project homepage, available [online] http://www.ele.tut.fi/tule/, visited 7.5.2010.

[Wisepla] Homepage of the Wisepla project available [online] http://www.mit.tut.fi/wisepla/wisepla_intro.htm, visited 23.3.2010.

[Vivago] Vivago –well being products, company homepage, available [online] http://www.istsec.fi/en.php, visited 16.4.2009.

[vonB_03] von Buren, T., Lukowicz, P., and Troster, G., Kinetic energy powered computing - an experimental feasibility study, Proceedings of the Seventh IEEE International Symposium on Wearable Computers, ISWC'03, October 18-21, White Plains, New York, United States, pp. 22- 24.

[Vond_06] Vondra, V., Halamek, J., Viscor, I., and Jurak, P., Two-Channel Bioimpedance Monitor for Impedance Cardiography, the 28th Annual International Conference of the IEEE Engineering in Medicine and Biology Society, EMBS '06, August 30 – September 3, 2006, pp.6061-6063.

[Yang_05] Yang, Y., and Wang, J., A Design of Bioimpedance Spectrometer for Early Detection of Pressure Ulcer, the 27th Annual International Conference of the Engineering in Medicine and Biology Society, IEEE-EMBS 2005, January 17-18, 2006, pp. 6602-6604.

[Yang_06] Yang, G-Z editor, Body Sensor Networks. 1st edition. London: Springer-Verlag. 2006, 493 pp.

[ZigBee] Homepage of the ZigBee Alliance, available [online] http://www.zigbee.org, visited 20.5.2010

[ZOE] ZOE, Non-invasive Thoracic Fluid Status Monitor, available [online] http://www.omnimedicalsupply.com/zoe.htm 25.8.2010

Publications

Publication [P1]

Timo Vuorela, Ville-Pekka Seppä, Jukka Vanhala and Jari Hyttinen. Wireless Measurement System for Bioimpedance and ECG. Proceedings of the 13th International Conference on Electrical Bioimpedance and 8th Conference on Electrical Impedance Tomography, IFMBE, August 29 – September 9, 2007, Graz, Austria, Vol. 17, pp. 248-251.

Publication [P2]

Timo Vuorela, Ville-Pekka Seppä, Jukka Vanhala, and Jari Hyttinen. Two portable long-term measurement devices for ECG and bioimpedance. Proceedings of the 2nd International Conference on Pervasive Computing Technologies for Healthcare 2008, Pervasive Health 2008, January 30 – February 1, 2008, Tampere, Finland, 4 pages.

Publication [P3]

Timo Vuorela, Jaana Hännikäinen, and Jukka Vanhala. Plaster like Physiological Signal Recorder – Design Process, Lessons Learned. Proceedings of the Ambience 08 Smart Textiles – Technology and Design. June 2 – 3, 2008, Borås, Sweden, pp. 89-96.

Publication [P4]

Timo Vuorela, Ville-Pekka Seppä, Jukka Vanhala, and Jari Hyttinen Design and Implementation of a Portable Long-Term Physiological Signal Recorder, IEEE Transactions on Information Technology in Biomedicine, vol.14, no.3, pp.718-725, May 2010.

Publication [P5]

Timo Vuorela, Kari Kukkonen, Jaana Rantanen, Tiina Järvinen, & Jukka Vanhala, Bioimpedance Measurement System for Smart Clothing. Proceedings of the Seventh International Symposium on Wearable Computers ISWC 2003, 21-23 October, White Plains, New York, USA. pp. 98 – 107.

Publication [P6]

Timo Vuorela, Jaana Hännikäinen, Katja Vähäkuopus, and Jukka Vanhala. Textile Electrode Usage in a Bioimpedance Measurement. Proceedings of the first international scientific conference on Intelligent Ambience and Well-Being, Ambience05. ISBN: 952-15-1429-9. Tampere, Finland, September 19(Mon) – 20(Tue), 2005, pp. 147 – 154.

Publication [P7]

Timo Vuorela, Kimmo Surakka, Jukka Vanhala, and Hannu-Matti Järvinen. Instruction Level Energy Measurement of General-purpose Microprocessor: A Case Study AT90S8515 and Atmega8515. Proceedings of the sixth International Conference on Machine Automation, ICMA 2006, Seinäjoki, Finland, June 7-8, 2006, 9 pages.

Publication [P8]

Kimmo Surakka, Tommi Mikkonen, Hannu-Matti Järvinen, Timo Vuorela and Jukka Vanhala. "Towards Compiler Backend Optimization for Low Energy Consumption at Instruction Level", Proceedings of the Estonian Academy of Sciences, Engineering, Special issue on Programming Languages and Software Tools, 11/4 December 2005. Pp. 347-357.

Publication [P9]

Timo Vuorela, Kari Kukkonen, Jaana Rantanen, Tero Alho, Tiina Järvinen, Jukka Vanhala, 2003. RF Data Link for a Smart Clothing Application. Adjunct Workshop Proceedings of 3rd International Workshop on Smart Appliances and Wearable Computing. Held at IEEE 23rd International Conference on Distributed Computing Systems. Providence Rhode Island, USA, May 19 – 22, pp. 7 – 12.